NAVAL POSTGRADUATE SCHOOL
Monterey, California

THESIS

LIFT ENHANCEMENT USING CLOSE-COUPLED CANARD/WING VORTEX INTERACTION

by

John M. Kersh, Jr.

December, 1990

Thesis Advisor: Richard M. Howard

REPORT DOCUMENTATION PAGE

Form Approved OMB No. 0704-0188

1a REPORT SECURITY CLASSIFICATION: UNCLASSIFIED	1b RESTRICTIVE MARKINGS
2a SECURITY CLASSIFICATION AUTHORITY	3 DISTRIBUTION / AVAILABILITY OF REPORT: Approved for public release; distribution is unlimited
2b DECLASSIFICATION / DOWNGRADING SCHEDULE	
4 PERFORMING ORGANIZATION REPORT NUMBER(S)	5 MONITORING ORGANIZATION REPORT NUMBER(S)
6a NAME OF PERFORMING ORGANIZATION: Naval Postgraduate School; 6b OFFICE SYMBOL (If applicable): Code AA	7a NAME OF MONITORING ORGANIZATION: Naval Postgraduate School
6c ADDRESS (City, State, and ZIP Code): Monterey, Ca. 93943-5000	7b ADDRESS (City, State, and ZIP Code): Monterey, Ca. 93943-5000
8a NAME OF FUNDING / SPONSORING ORGANIZATION; 8b OFFICE SYMBOL (If applicable)	9 PROCUREMENT INSTRUMENT IDENTIFICATION NUMBER
8c ADDRESS (City, State, and ZIP Code)	10 SOURCE OF FUNDING NUMBERS: PROGRAM ELEMENT NO; PROJECT NO; TASK NO; WORK UNIT ACCESSION NO

11 TITLE (Include Security Classification)

LIFT ENHANCEMENT USING CLOSE-COUPLED CANARD/WING VORTEX INTERACTION

12 PERSONAL AUTHOR(S)
Kersh, John McKay

13a TYPE OF REPORT	13b TIME COVERED	14 DATE OF REPORT (Year, Month, Day)	15 PAGE COUNT
Master's Thesis	FROM _____ TO _____	1990, December	139

16 SUPPLEMENTARY NOTATION
The views expressed in this thesis are those of the author and do not reflect the official policy or position of the Department of Defense or the U.S. Government

FIELD	GROUP	SUB-GROUP

18 SUBJECT TERMS (Continue on reverse if necessary and identify by block number)
Canard, Close-Coupled Canard, High Angle of Attack Aerodynamics, Vortex Interaction

19 ABSTRACT (Continue on reverse if necessary and identify by block number)

A wind-tunnel study to find the lift and drag characteristics of a low-aspect-ratio wing/body configuration from an angle of attack (AOA) of -8 to 50 degrees was conducted. A further study to find the comparative lift enhancement using the same wing/body with a close-coupled canard for wing/body angles of attack of 10, 22, 34, 40, and 48 degrees and canard deflection angles from -25 to 25 degrees was carried out. It was found that a properly-located canard enhanced the lift at all tested angles of attack, compared to the baseline wing/body configuration results. The lift enhancement was maximized in the post-stall regimes, reaching values up to 34%. A small improvement in lift-to-drag ratio was noted at all tested angles above 10 degrees angle of attack.

20 DISTRIBUTION / AVAILABILITY OF ABSTRACT: [X] UNCLASSIFIED/UNLIMITED [ ] SAME AS RPT [ ] DTIC USERS	21 ABSTRACT SECURITY CLASSIFICATION: Unclassified
22a NAME OF RESPONSIBLE INDIVIDUAL: Richard M. Howard	22b TELEPHONE (Include Area Code): (408) 646-2870; 22c OFFICE SYMBOL: Code AA/Ho

DD Form 1473, JUN 86 — Previous editions are obsolete. S/N 0102-LF-014-6603

Approved for public release; distribution is unlimited.

Lift Enhancement Using Close-Coupled Canard/Wing Vortex Interaction

by

John M. Kersh, Jr.
Lieutenant, United States Navy
B.A., University of Virginia, 1984

Submitted in partial fulfillment
of the requirements for the degree of

MASTER OF SCIENCE IN AERONAUTICAL ENGINEERING

from the

NAVAL POSTGRADUATE SCHOOL
December 1990

Author: John M. Kersh Jr.
John M. Kersh, Jr.

Approved by: Richard M. Howard
Richard M. Howard, Thesis Advisor

Louis V. Schmidt
Louis V. Schmidt, Second Reader

E. R. Wood
E. Roberts Wood, Chairman
Department of Aeronautics and Astronautics

ABSTRACT

A wind-tunnel study to find the lift and drag characteristics of a low-aspect-ratio wing/body configuration from an angle of attack (AOA) of -8 to 50 degrees was conducted. A further study to find the comparative lift enhancement using the same wing/body with a close-coupled canard for wing/body angles of attack of 10, 22, 34, 40, and 48 degrees and canard deflection angles from -25 to 25 degrees was carried out. It was found that a properly-located canard enhanced the lift at all tested angles of attack, compared to the baseline wing/body configuration results. The lift enhancement was maximized in the post-stall regimes, reaching values up to 34%. A small improvement in lift-to-drag ratio was noted at all tested angles above 10 degrees angle of attack.

TABLE OF CONTENTS

ACKNOWLEDGEMENTS

I would like to thank all the people who helped me during the preparation of this thesis. I am most greatful for Professor Rick Howard's much needed help and guidance. This thesis has been a tremendous opportunity for me to study some of the aspects of high-angle-of-attack aerodynamics and wind-tunnel testing techniques that would not have been possible without Professor Howard as a mentor.

There are a number of other NPS personnel whose assistance is greatly appreciated, in particular Mr. Ron Ramaker and Mr. Don Meeks. Mr. Ron Ramaker did a great job building the close-coupled canard/wing model. Mr. Don Meeks was instrumental in the design of the canard lead screw mechanism. Without Mr. Meeks' tremendous efforts and skill this thesis would have been effected adversely and delayed considerably. I would also like to thank Professor Schmidt for his help and guidance in understanding the reflection-plane balance that he and the late Provost Milton Clauser designed for the low-speed wind tunnel.

DEDICATION

This thesis is dedicated to my wife, Pamela, for without her love and support this thesis would not have been possible.

I. BACKGROUND

A. AIRCRAFT AGILITY

In future air-to-air combat scenarios the aircraft that is the most maneuverable while at the same time controllable will in all likelihood win the engagement. Winning an air-to-air engagement against another agile fighter using all-aspect missiles, such as the AIM-9L, requires the ability to out maneuver the opposition to point and shoot first. [Ref. 1]

In close-in combat with another agile fighter the aircraft that "wins" will have three advantages over its opponent. First, the aircraft will need the ability to "outpoint" its opponent. The aircraft that points at its opponent first has the first opportunity to launch a "fire-and-forget" weapon. Second, the aircraft must have the ability to keep the nose of the aircraft pointed at the opposition for a longer time. The aircraft that can point longer has the capability to maneuver at higher turn rates for longer periods than the opposition. Maintaining nose-point longer than the opposition enables the aircraft to defend itself against aircraft other than the target or to engage multiple targets. Third, the aircraft must have a greater straight-ahead acceleration than the opposition. Greater acceleration gives the ability to escape

the battle or to reengage the opposition to the advantage of the agile aircraft. [Ref. 1]

To outpoint, turn faster, and accelerate faster than an opponent the aircraft must be supermaneuverable. Supermaneuverability is a blend of post-stall maneuvers and the use of sideslipping or direct force control. Post-stall manueuverablity (PST) is the capability to tactically maneuver the aircraft in a controlled fashion beyond the maximum lift angle of attack. Direct force-control maneuver (DFM) is the ability to change the aircraft's yaw and pitch independent of flight path or to maneuver the aircraft at constant fuselage attitude. A PST maneuver sacrifices energy for a positional advantage. A typical PST maneuver involves rapidly pitching the aircraft to a high angle of attack and maintaining this condition for 2 to 3 seconds. The aircraft that maneuvers in the PST regime will complete a tactical maneuver in less time and space than an aircraft not executing a PST maneuver. Unfortunately there are a number of limitations which prevent a conventional aircraft from performing a PST maneuver. [Ref. 2]

At high angles of attack, the flow tends to separate from the wing surface. The center of pressure and neutral point move aft with respect to the center of gravity as the airflow separates from the wing surface at the maximum lift angle of attack. The control surfaces are also losing their effectiveness at the same time. The result is that the

aircraft encounters severe trim and stability problems when it has the greatest control power requirements and is the least controllable. At angles of attack greater than 30 degrees, an additional reaction control system is necessary for pitch and yaw. The deflection of the engine thrust is one of the proposed methods for a reaction control system. In general, at angles of attack greater than 50 degrees, engine thrust vice aerodynamic lift provides the necessary lift and control. [Ref. 2]

A DFM is used to aim the fuselage at the opponent independent of flight path for more precise firing solutions. Studies have shown that for a rear hemisphere attack, an elevation aiming ability of at least 6 degrees and an azimuth aiming ability of about 4 degrees would be advantageous. With conventional aircraft, elevation aiming can be achieved to a limited extent through the use of wing flaps in conjunction with elevator deflection. Azimuth aiming for a conventional aircraft would involve the use of special control surfaces and an associated flight control system. [Ref. 2]

An example of a proposed supermaneuverable aircraft is the X-31. The X-31 aircraft uses a long-coupled canard for controllability with thrust vectoring to be supermaneuverable in the post-stall flight regime. Figure 1 shows the difference between a close- and long-coupled canard. More will be noted on the difference directly. When the angle of attack is increased to the point where the aircraft begins to

stall, computer-controlled thrust vectoring comes into play. The thrust vectoring is provided by three curved paddles that can move into the exhaust stream to deflect the flow. The ability to successfully use thrust vectoring assumes adequate control to prevent spin departure. [Ref. 3]

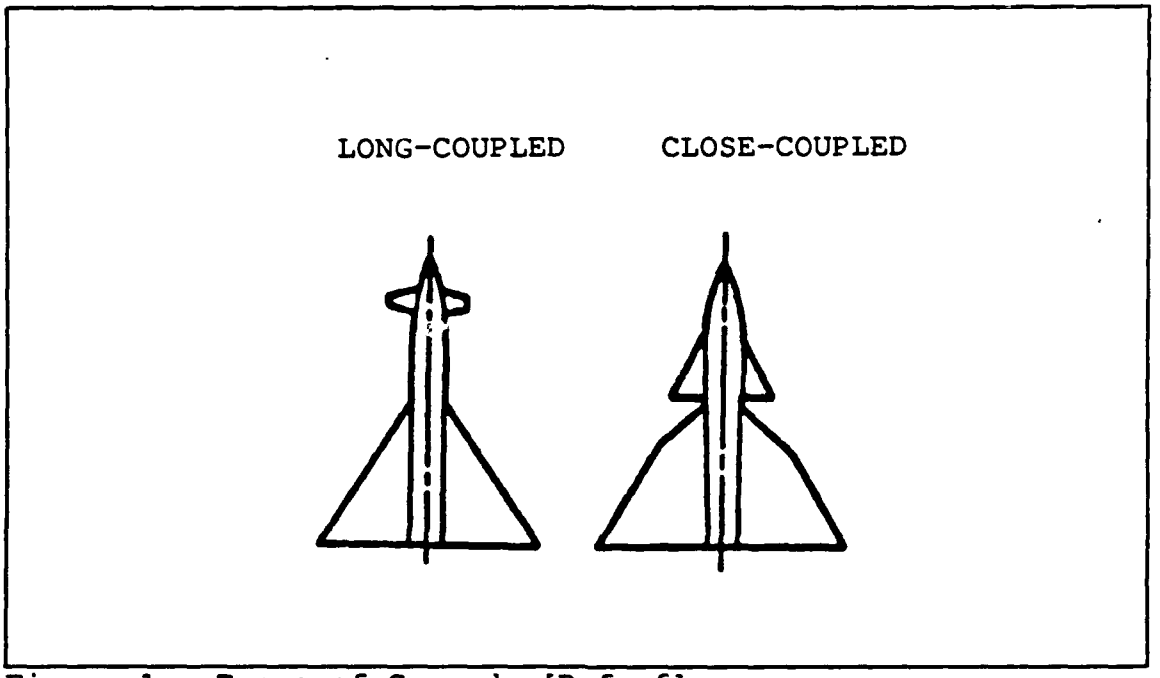

Figure 1. Types of Canards [Ref. 6]

Herbst states, "Unfortunately there is a progressive effect of thrust versus weight on weight and cost and even an asymptotic limit." [Ref. 2] A prohibitive cost limit in the race to achieve greater thrust-to-weight would imply aircraft such as the X-31 that extensively use thrust vectoring may not be built in sufficient numbers to counter the opposition's agile aircraft. Accordingly, other methods of obtaining maneuverability and control in the post-stall regime warrant increased investigation. [Ref. 2]

One such area of increased interest is dynamic stall. Dynamic stall is a complex event where there is a "...dynamic delay of stall on a wing's airfoil experiencing unsteady motion, to angles significantly beyond the static stall angle." [Ref. 4] The delay of stall is usually followed by large changes in lift and pitching moment. Dynamic stall was first observed on helicopter blades. It was found that increased lift could be obtained by rapidly pitching the airfoils. The increased lift was due in part to the vortex formed on the airfoil during the unsteady motion. It was found that the increased lift due to dynamic stall could also be utilized by fighter aircraft when the aircraft was rapidly pitched. This increase in lift due to dynamic stall, as noted, is an unsteady time-dependent phenomenon. At the present time predictable control of this unsteady, separated flow for increased lift has not been achieved. Accordingly, other potential methods for lift enhancement such as the use of a close-coupled canard/wing are receiving increased attention. [Ref. 4]

B. CANARD/WING INTERACTION

Increased agility through the use of a close-coupled canard configuration for enhanced lift has been the subject of growing scientific interest and practical aeronautical application. In the 1960's Behrbohm established that a close-coupled canard with the canard and wing of aspect ratios

between 1 and 3 had an increased coefficient of lift over their non-canard counterparts. The increased maximum C_L in turn contributed to an increase in the angle of attack that could be achieved. The increase in maximum C_L was due to constructive interference between the vortex systems of the wing and canard. It is thought that constructive interference occurs when the downwash from the canard suppresses the flow separation on the wing. The formation of wing leading-edge vortices are delayed until induced downwash of the canard supports flow separation. The longer the flow separation is delayed, the greater the lift enhancement. [Ref. 5]

The translation of theory into reality was realized with the SAAB AJ-37 Viggen aircraft. The Viggen aircraft uses a close-coupled canard that was able to generate a 65 percent greater maximum C_L at approach than a pure delta wing. The Viggen aircraft successfully took advantage of favorable vortex wing-canard interactions to achieve greater lift which allowed the aircraft to lower its landing and takeoff speed for a STOL capability. [Ref. 6] Figure 2 illustrates the canard/wing vortex interaction of the SAAB Viggen [Ref. 7]

The use of a close-coupled canard on the SAAB Viggen also gave the aircraft much greater trim control compared to a tailless delta-winged aircraft such as the Mirage III. The lack of a horizontal tail on aircraft such as the Mirage III requires the use of elevons, which are deflected upward to create a down thrust to rotate the aircraft for landing and

takeoff. The elevons have a much shorter moment arm than a horizontal tail, which in turn requires that the elevons be large to be effective. The elevons exact a weight penalty of as much as two tons, but more importantly decrease the effective lift of the aircraft, just the opposite of what is needed for enhanced takeoff and landing ability. The SAAB Viggen uses a large canard with trailing-edge flaps. During takeoffs and landings the Viggen has lift from the main wing, lift from the canard, plus lift from the downward-depressed main wing elevons. The result is that the Viggen has a much shorter takeoff and landing distance than the Mirage III. [Ref. 7]

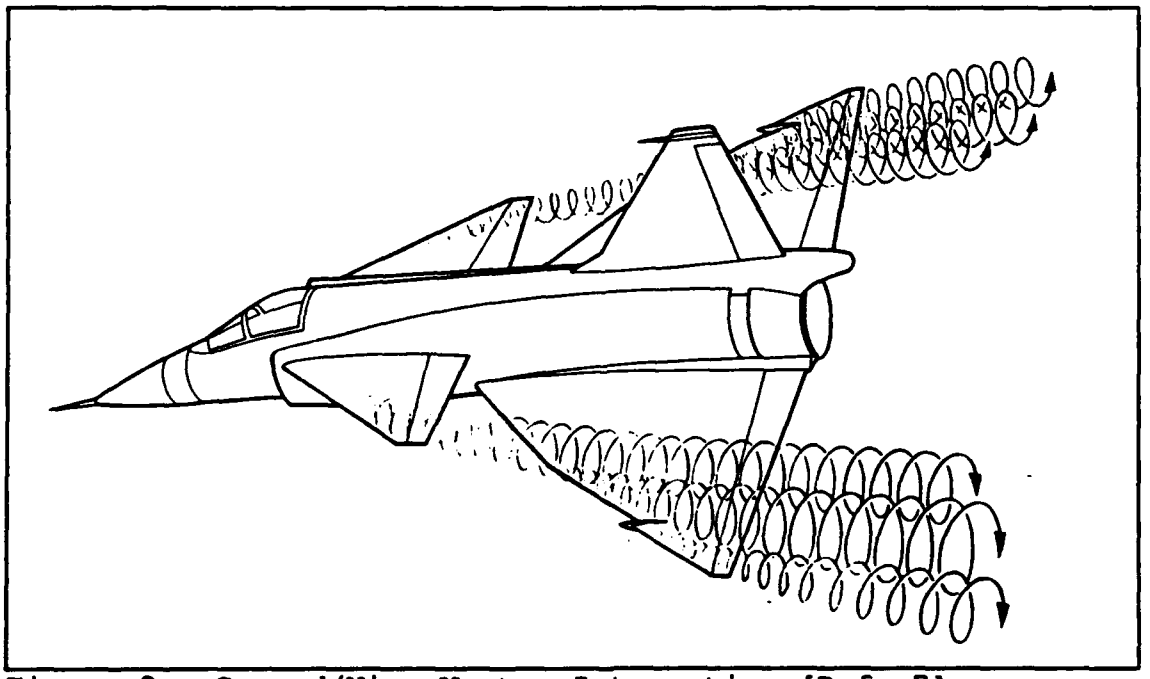

Figure 2. Canard/Wing Vortex Interaction [Ref. 7]

Stoll and Koenig demonstrated that the maximum lift of a close-coupled canard model was 34 percent greater than a non-

canard version of the same model. Furthermore, the increase in lift could not be solely attributed to an increase in wing reference area. The wing reference area of the canard-wing model was only 15 percent greater than that of the wing-alone model. [Ref. 8]

Er-El and Seginer found that a close-coupled canard placed upstream and above a 60-degree swept wing delayed the onset of wing-leading-edge vortex breakdown for an angle-of-attack range from 14 to 24 degrees. But significantly, the use of a close-coupled canard/wing did not always result in improved aerodynamic characteristics. Improved lift was dependent upon proper longitudinal positioning of the canard. Er-El and Seginer did not rigorously establish what this longitudinal position should be, but that was not the objective of their study. [Ref. 9]

Calarese tested a model with the canard placed above the wing and coplanar to the wing. At all angles of attack, the canard mounted above the wing created a more favorable interaction between the leading-edge vortices than the coplanar canard. The use of a canard placed above the wing caused a noticeable improvement in the lift-to-drag ratio for the tested angles of attack of 10, 16, and 19 degrees. The increase in the lift-to-drag ratio was 12 percent greater than the lift-to-drag ratio for the coplanar model. It was surmised that the more favorable lift-to-drag ratio of the model with the canard positioned above the wing was due in

part to the vortex and wakeflow of the canard missing the wing and therefore causing less interference. A more likely explanation is that downwash suppressed the flow separation of the wing and thus improved lift. [Ref. 10]

O'Leary and Weir demonstrated that the maximum C_L using a close-coupled canard was 20 percent greater and at an angle of attack 5 degrees greater than for a non-canard model. At angles of attack from 0 to 36 degrees, the canard had little effect on the slope of the lift versus angle-of-attack curve for canard deflections of 0,-10,-20 degrees. A slightly higher value for maximum C_L was achieved with a canard deflection of -20 degrees than with canard deflections of 0 and -10 degrees. A positive canard deflection of 10 degrees reduced the slope of the lift curve. At a canard deflection of -40 degrees, the maximum C_L was reduced by approximately 20 percent. [Ref. 11]

The research by David W. Lacey at the David W. Taylor Naval Ship Research and Development Center (now the David W. Taylor Research Center) in the 1970's in the area of close-coupled canard/wing interaction was quite comprehensive. Lacey found that the increase in the maximum C_L was mainly a function of the ratio of the canard area to the wing area (S_c/S_w) and the canard placement in both the longitudinal and vertical directions. The longitudinal position was measured from the 0.25 mean aerodynamic chord of the wing to the 0.40 exposed root chord of the canard. For lift enhancement, it

was found that the ratio of the longitudinal canard position to the mean aerodynamic chord of the wing with respect to the centerline of the fuselage, x/c_{mac}, should be between 1.0 to 1.25. If the canard was mounted too far forward, the canard/wing combination would actually generate less lift than what the wing and canard could generate separately. (It should be noted that the long-coupled canard on the X-31 is a control, and not a lifting, device.) It was determined that the canard should be positioned so that the ratio of the vertical distance from the plane of the wing to the mean aerodynamic chord, z/c_{mac}, should be equal to 0.2. The trailing edge of the canard and the leading edge of the wing should never overlap, for a loss of lift results. The combination of a proper selection of vertical and longitudinal position maximized C_L and L/D. Increasing the size of the canard increased lift in a fairly linear fashion up to $S_c/S_w = 0.25$. Beyond 0.25 a sharp drop off in canard/wing lift effectiveness resulted. [Ref. 6]

Lacey tested canards with a leading-edge sweep of 25, 45 and 60 degrees. Maximum lift was developed with the 60-degree swept delta canard. Maximum L/D was developed with the 25-degree high-aspect-ratio canard. A tradeoff study was conducted and found that for maximum lift and L/D the 45-degree canard should be chosen, closely followed by the 60-degree canard. If any of the planforms were properly located they would enhance lift. [Ref. 6]

Lacey noted the SAAB TN 60 report postulated that a highly-swept canard delta wing should be chosen to maximize the synergism between the canard and wing vortices for increased lift. Lacey found that a 45-degree canard with a 25-degree swept wing also greatly enhanced lift, but in this case neither the wing nor the canard generated the strong leading-edge vortices "required" by the SAAB report. Lacey postulated that the canard downwash delayed the leading-edge stall of the wing in a manner similar to that of a leading-edge slot. The canard could be thought of as a large low-drag boundary-layer device. [Ref. 6]

It was shown that, with the canard in a high position above the wing, the overall lift was actually less than the wing/body alone configuration for angles of attack below 18 degrees. The interference that took place between the flowfields of the canard and wing that caused this lift degradation was not very well understood. It was thought that destructive interference occurred when the wash of the canard impinged upon the wing in an upward direction, which then promoted flow separation on the wing and thereby caused a loss of lift. Beyond an 18 degree angle of attack, the wash of the canard impinged upon the wing in a downward direction, and thereby delayed the onset of flow separation on the wing and correspondingly increased the lift. [Ref. 6]

Deflecting the canard in 5-degree increments from -10 to +10 degrees with the model at a fixed angle of attack resulted

in a change of C_L of only 0.08. Positive canard deflections for a main body angle of attack of 5 degrees were found to increase drag and correspondingly decrease the maximum L/D markedly. Slightly negative canard deflections increased the maximum L/D because a 0-degree local angle of attack for the canard minimized induced drag. [Ref. 6]

C. OSCILLATING CANARD

The next area of increased interest for lift enhancement involves interactions between an oscillating close-coupled canard and the main wing flowfield. Thus far few studies have been completed in this area. Huyer and Luttges investigated the flowfield interaction between the unsteady wake of an oscillating canard upstream of a static wing. An NACA 0015 airfoil was used for both the canard and the main wing. The main wing was mounted coplanar to the canard and 0.5 chord lengths downstream. Main wing angles of attack of 10 and 20 degrees were used. The mean canard deflection angle was 15 degrees and the oscillation amplitude was +/- 10 degrees. The canard was oscillated about the quarter chord with periods of 156 and 105 msec. Huyer and Luttges found that the dynamic stall vortex from the oscillating canard energized the boundary layer of the main wing which resulted in flow reattachment at angles of attack far exceeding static stall angles for the main wing. But the amount of enhanced lift was

not well quantified. No comparison was made to a static canard and main wing case. [Ref. 12]

Other studies have considered the flowfield due to an oscillating canard for an X-29 aircraft model, but no lift-enhancement results have been presented. [Ref. 13 and Ref. 14]

D. STATEMENT OF PURPOSE

From the previous work of others it is fairly well understood that locating the canard in an optimum position vertically and longitudinally will generate vortices that will constructively interfere for maximum lift. Studies have not been conducted for main wing/body angles of attack greater than 36 degrees, nor have static canard deflection angle increments of less than 5 degrees been used.

It is known that oscillating a coplanar canard separated from the main wing by 0.5 chords will reattach the flow over the main wing at angles far exceeding the normal stall angle of attack for the main wing alone. The canard, however, was not optimally located vertically and horizontally to maximize lift enhancement, and only two main wing body angles of attack of 10 and 20 degrees were used. Additionally, the lift enhancement with the use of an oscillating canard was not compared to the lift enhancement with a static canard. The objectives of this investigation were to conduct :

(1) A baseline study to find the lift and drag characteristics of a low-aspect-ratio wing/body model from low angles of attack to angles of attack beyond 36 degrees.

(2) A further study to find the comparative lift enhancement using the same wing/body and a close-coupled canard for wing/body angles of attack of 10, 22, 34, 40, and 48 degrees and canard deflection angles -25 to 25 degrees.

Upon completion of the above investigation a follow-on study will be conducted to examine the lift enhancement of an optimally-located oscillating canard for comparison to the results of the static canard/wing configuration.

II. EXPERIMENT AND PROCEDURES

A. OVERVIEW

A close-coupled canard model was designed and constructed at the Naval Postgraduate School. A calibration rig was then designed and constructed to calibrate an existing external strain-gage balance in the NPS low-speed wind tunnel. Data were acquired from the signal conditioning assembly through a digital multimeter, multiplexer and amplifier, and stored on a floppy disk. The results were reduced to lift and drag coefficients.

In a baseline run of the model without the canard, the angle of attack of the wing and body model was varied from -8 to 50 degrees. The lift, drag, C_L, and C_D were then plotted for the baseline run. Results from the baseline run were used to determine the angles of attack of the main body and wing to use for the canard runs. Under similar tunnel conditions as the baseline run, the canard was varied from -25 to +25 degrees deflection for various wing/body angles of attack to determine any lift enhancement through the use of a close-coupled canard.

B. APPARATUS

The primary equipment used was the NPS low-speed wind tunnel, external strain-gage balance and signal conditioning

assembly, balance calibration rig, canard/wing model, data acquisition system, and data reduction software.

1. Wind Tunnel

The Naval Postgraduate School low-speed, single-return wind tunnel is powered by a 100 hp electric motor coupled to a three-blade variable-pitch fan and a four-speed truck transmission. A set of stator blades immediately following the fan assist in straightening the flow. A combination of turning vanes at each corner and two fine-wire-mesh screens at the entrance to the settling chamber help reduce the air flow turbulence further. The settling chamber to test section contraction ratio is about 10:1. [Ref. 15]

The test section of the tunnel operates at approximately atmospheric pressure due to the use of downstream vents. The test section measures 45 by 32 inches. The corner lighting and reflection plane in the tunnel test section reduce the tunnel height from 32 to 28 inches, which results in an effective cross-sectional area of 9.88 square feet. A remotely-controlled turntable mounted flush with the reflection plane allowed the angle of attack of the model to be varied. The temperature of the tunnel air was measured with a dial thermometer mounted on the tunnel wall extending into the settling chamber. Figure 3 shows the NPS low-speed wind tunnel. [Ref. 15]

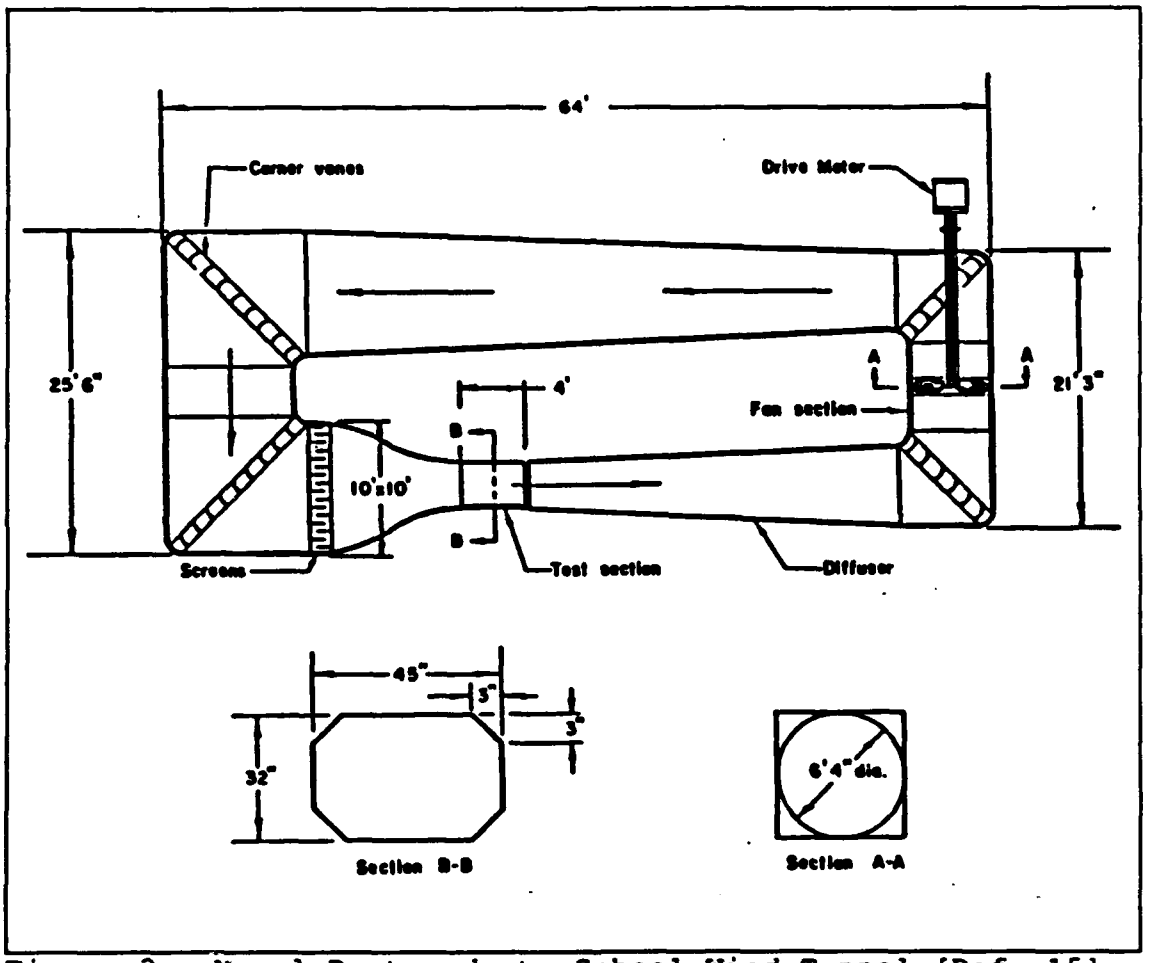

Figure 3. Naval Postgraduate School Wind Tunnel [Ref. 15]

The test-section dynamic pressure, q, was determined by measuring the static pressure difference, Δp, between the test section and the settling chamber using a water manometer. The settling chamber and the test section each have four static pressure taps that are connected to the manometer via a common manifold. The pressure difference measured by the manometer, in centimeters of water, was converted to the test-section dynamic pressure and test-section reference velocity from a previous calibration resulting in equations (1) and (2). [Ref. 16 and Ref. 17]

$$q = 2.047(-.026749 + 1.1149\Delta P) \qquad (1)$$

$$V = \sqrt{\frac{q}{\frac{1}{2}\rho}} \qquad (2)$$

Where:

ρ	air density (slugs/ft^3)
ΔP	manometer reading in cm of H_2O
q	test-section dynamic pressure (lbf/ft^2)
2.047	a constant converting cm of H_2O to lbf/ft^2
1.1149	tunnel calibration factor
-.026749	tunnel calibration intercept
V	reference velocity (ft/sec)

The wind tunnel calibration factor,1.1149, and tunnel calibration intercept, -0.026749, corrected the manometer reading, Δp, to test-section dynamic pressure, q. The

calibration factor was found by plotting the actual dynamic pressure measured by a pitot-static tube mounted in the test section versus the measured pressure difference. The relationship was found to be linear, with the slope of the curve being the tunnel calibration factor. The slope did not pass through the origin, which resulted in there being a tunnel calibration intercept with the y-axis. [Ref. 17]

2. Canard/Wing Model

The canard/wing model was designed as a half-model for compatibility with the existing reflection-plane balance previously installed in the wind tunnel. The half-model was of a generic agile-fighter fuselage with a low-aspect-ratio close-coupled canard and wing. The model was fabricated from mahogany by Naval Postgraduate School personnel. The canard and wing of the model were reinforced with an aluminum core. There were three main sections to the model: the ogive nose, canard, and wing. The ogive nose and wing section were permanently attached to one another by an aluminum base plate. A large removable canard section allowed the canard to be instrumented with an electric motor and controller so the angle of attack of the canard could be varied remotely without shutting down the tunnel. The model mounted flush to the base of the tunnel reflection plane. The model angle of attack was varied using the tunnel turntable. Figure 4 shows a sketch of

the model. See Appendix A for the model design process and the resultant geometric parameters.

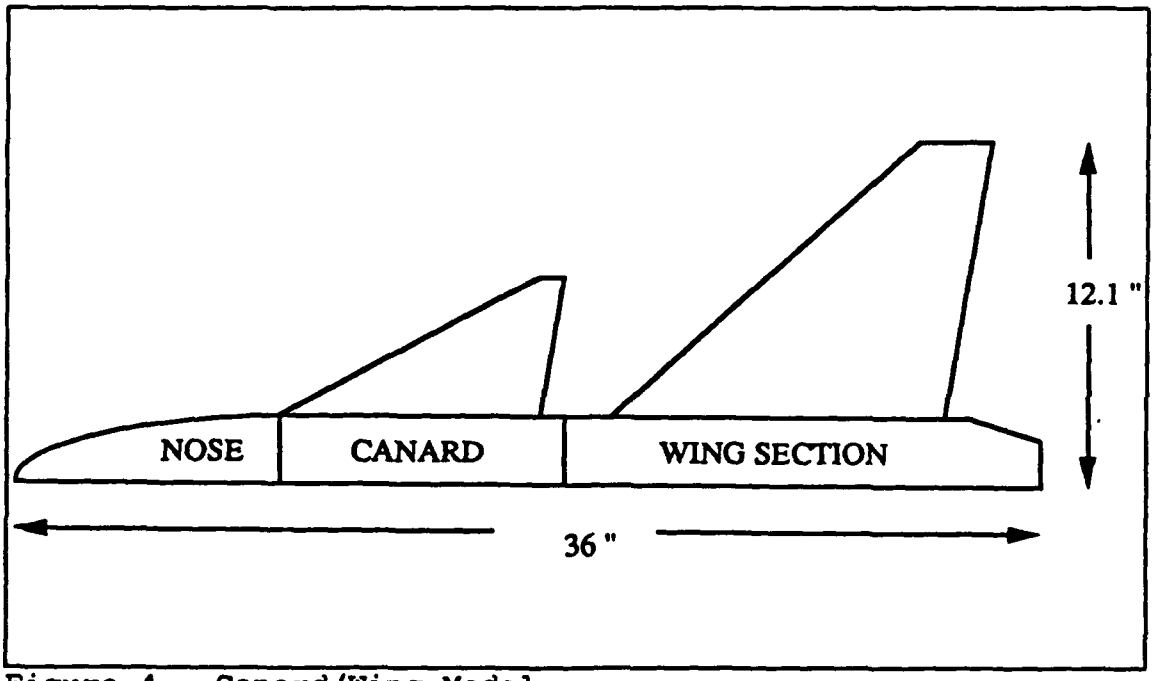

Figure 4. Canard/Wing Model

3. Balance and Turntable

An external strain-gage balance and turntable, shown in Figure 5, was originally designed and built by NPS personnel in 1974 to facilitate the measurement of normal and axial forces and pitching moment in the NPS low-speed wind tunnel. Each external strain-gage bridge had four active legs for automatic temperature compensation. The normal and axial moments were measured by two orthogonal strain-gage bridges cemented on the balance column separated by a vertical distance of 26.5 inches. With the wind tunnel in operation the force on the model created a different moment on the upper

and lower strain-gage bridges. Once the balance was accurately calibrated the voltage output from the lower and upper normal or axial bridges could be converted to moments and subtracted from one another, then divided by the vertical separation of the bridges, to find the normal or axial force. Any inherent moments on the model were removed from the measurements by this process.

Unfortunately, prior to this thesis, the balance had never been calibrated and some of the documentation, such as the gage factor of the strain gages, was unavailable. Drawings of the balance were found which gave the separation distance between the strain gages and indicated that the balance was designed to be capable of measuring forces up to 150 lbs. A balance calibration procedure and associated calibration rig were then developed with the help of NPS personnel and Reference 18. The calibration procedure and associated calibration rig are described in Appendix B.

The balance and turntable were one rigid unit. When the turntable rotated the balance column upon which the strain gages were cemented rotated with it. The turntable was controlled by an electric motor with hard-wired remote. The model was attached to the top of the turntable platter. The angle of attack of the model was varied using the tunnel turntable.

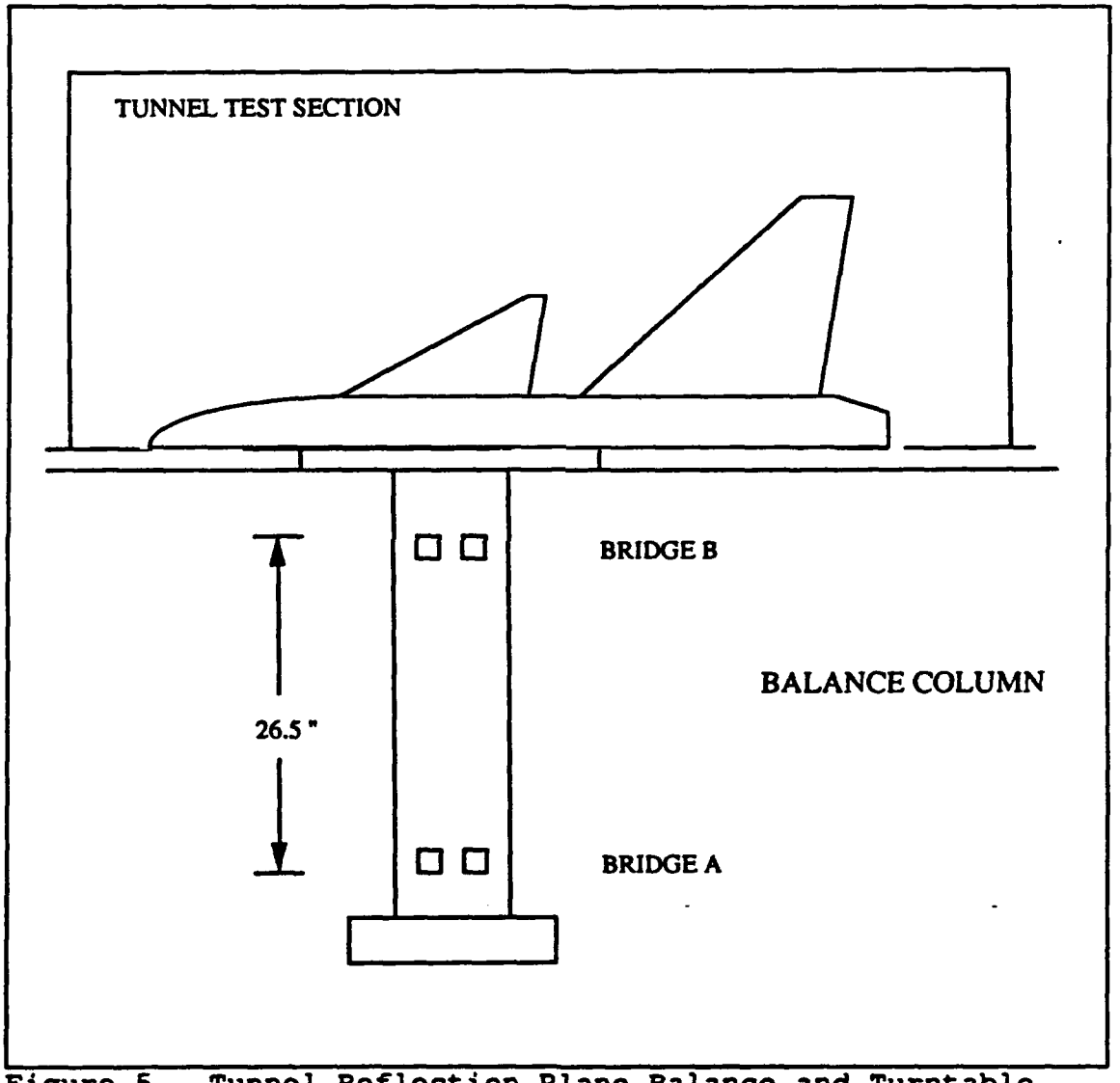

Figure 5. Tunnel Reflection Plane Balance and Turntable

4. Data Acquisition Hardware

Each strain-gage bridge had an individual signal conditioning assembly that supplied the excitation voltage. The signal conditioning assemblies allowed their associated strain-gage bridges to be zeroed and calibrated. Each balance channel from the signal conditioner assembly was passed through a 1000-gain low-noise amplifier. The signal was then routed to the Hewlett-Packard relay multiplexer that sampled each channel sequentially every 0.9 seconds. The sampling period of the multiplexer could be varied, but it was found that a sampling period less than 0.9 seconds caused an unacceptable level of noise in the voltage output. A sampling period greater than 0.9 seconds did not measurably reduce the noise in the voltage output. A Hewlett-Packard digital multimeter then converted the voltage output from each channel from analog to digital. An IBM-AT microcomputer drove the data acquisition software and Hewlett-Packard hardware and stored collected data. A sketch of the data acquisition system is shown in Figure 6. [Ref. 15]

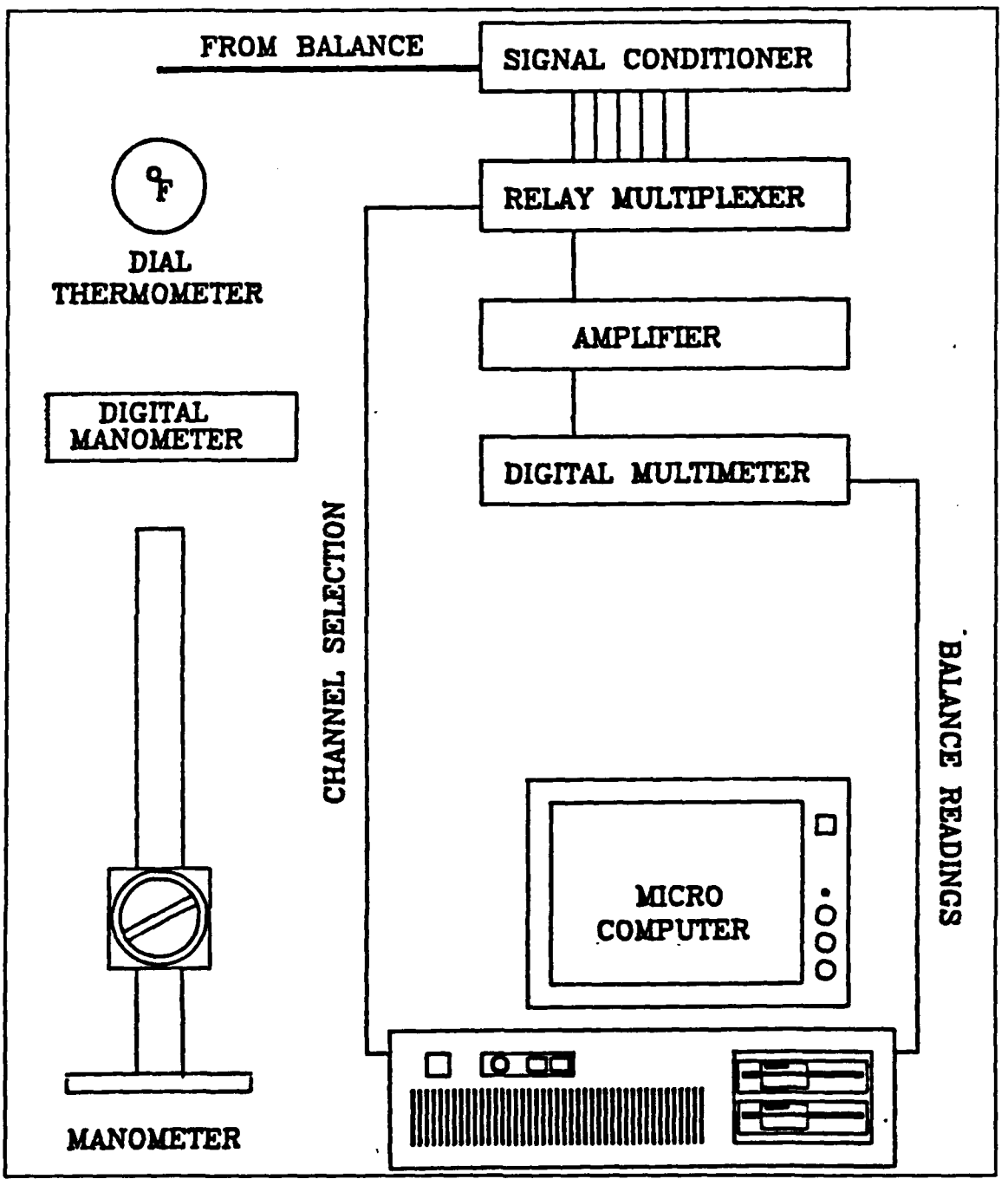

Figure 6. Data Acquisition System [Ref. 15]

5. Data Acquisition Software

The data acquisition software consisted of two BASIC programs. The first program, JMK.BAS, was composed of a shell program to control the Hewlett-Packard instrumentation and a BASIC program to manipulate the output signal from the data acquisition hardware into a usable form. The voltage outputs of each of the balance channels were sampled 10 times and went through a standard deviation rejection routine. Any reading that fell one standard deviation outside was rejected. The remaining voltage readings for each channel were then averaged. At most 4 readings were rejected of the 10 sampled. In general, the rejected channel readings varied from the average channel readings by 1 to 10%. The average channel readings were used to calculate the normal and axial force using equations found in Appendix B. The normal and axial forces at the given angle of attack were used to calculate the lift and drag forces using equations (3) and (4).

$$DRAG = (Axial\ Force)\sin(AOA) - (Normal\ Force)\cos(AOA) \tag{3}$$

$$LIFT = (Axial\ Force)\cos(AOA) + (Normal\ Force)\sin(AOA) \tag{4}$$

The data from the run were stored on the C drive of the IBM microcomputer and on a floppy disk in the A drive. Upon completion of the tunnel run, the program prompted the

user to input the test conditions for the tunnel run which were added to the files on the C and A drives of the microcomputer. The files generated by JMK.BAS were later manipulated by the program CORCOEF.BAS to convert lift and drag forces into C_L and C_D after accounting for test conditions and making necessary corrections for tunnel blockage, balance calibration, and turntable alignment. The data acquisition and manipulation programs are listed in Appendices C and D. [Ref. 15]

C. EXPERIMENTAL CONDITIONS

There are numerous variables which could affect flow separation and vortex formation at high angles of attack. The following parameters were kept as constant as possible:

(1) Test section ΔP = 17 cm of H_2O

(2) Test section velocity = 172 -174 ft/sec

(3) Test section Mach number = 0.17

(4) Reynolds number = 9.5×10^5 based on wing MAC

A strong dependence on test-section temperature was found for one of the balance strain gages. The application of excessive temperature corrections was avoided by keeping the tunnel operating temperature below 74 degrees. If the tunnel temperature rose above this value, the tunnel was shut down and allowed to cool. See the Experimental Corrections section for strain-gage temperature correction procedures.

A 1/8-inch gap existed between the base plate of the model and the reflection plane. The gap was needed to prevent the model from transferring any wind-induced loads to the reflection plane. The 1/8-inch gap was used for both the wing/body and canard/wing/body studies. No correction was applied for the gap; however, the gap should not adversely affect the experimental results since the experiment was attempting to measure the comparative lift enhancement between the two configurations.

The presence of the wind tunnel walls leads to stream-line curvature and downwash errors requiring corrections for angle of attack and induced drag of the model. The solid boundaries form streamlines forced upon the flow which result in the formation of image vortices which should be accounted for in measurements of absolute lift and drag. In the present study, the errors are expected to be small, since the model spans only 37.8% of the test section. Since the study involved a comparison of the lift and drag for the wing/body and canard/wing/body configurations, the lack of application of wall corrections should not adversely impact the results.

The pitching moment of the model was not measured. The goal of this thesis was to measure and compare the enhanced lift between a wing/body and canard/wing/body configuration. As this study was of a basic research phenomenon, no attempt was made to trim the aircraft longitudinally. A strain-gage bridge existed that when calibrated would have allowed the

pitching moment of the model to be measured. If in the future it is desired to measure the pitching moment of the model, then the moment strain-gage bridge can be used.

During wind tunnel operation, the vibration of the tunnel itself could not be controlled. This wind tunnel vibration was transferred to the tunnel balance via the model. The electrical outputs of the strain-gage bridges were averaged over time and then used to find the forces on the model. Because the average values of the electrical outputs were used, any adverse effect due to vibration of the tunnel should have been ameliorated.

The ambient turbulence level of the wind tunnel was about 0.2%. The reference length used to calculate the Reynolds number was the mean aerodynamic chord of the wing taken to the centerline of the fuselage of 9.52 inches.

D. EXPERIMENTAL PROCEDURE

1. Prerun Calibration and Test

The external strain-gage balance was initially calibrated. Appendix B illustrates the procedure that was used to find the coefficients for the calibration matrices. Once the balance was calibrated it was checked prior to each use.

Figure 7 shows a sketch of the calibration rig assembly. First the calibration rig was attached to the balance turntable platter. The stand and cable were lined up

vertically and horizontally with the calibration rig head by the use of a plumb bob and level. Proper wiring between the signal conditioning assembly and the HP digital multimeter was checked. Table 1 shows the channels and their associated strain-gage bridges. The IBM-AT microcomputer was then energized and the HP program PANELS.EXE for the multimeter was called. Relay Mux 1. was entered in the PANELS.EXE program and channel (8) was enabled. The Pacific Amplifier gain switch was turned to zero and the gain output was adjusted via a set screw to +/- 50 μvolts. The gain was increased to 1000 and the gain input adjusted to +/- 500 μvolts. Channels (2) through (5) were read and recorded. In general, the voltage readings from channels (2) to (5) were not zero. The signal conditioner assemblies could have been adjusted so that the outputs from the channels were close to zero. Adjusting the voltage readings of the channels risked unsettling the system or changing the calibration of the balance. It was decided to note the voltage readings from channels (2) through (5) as zero offsets.

Initially no weight was attached to the calibration rig assembly. The IBM BASIC editor was entered and the program JMK.BAS called. The program prompted the user for the angle of attack of the model, the deflection angle of the canard, the temperature, and the zero offset readings of

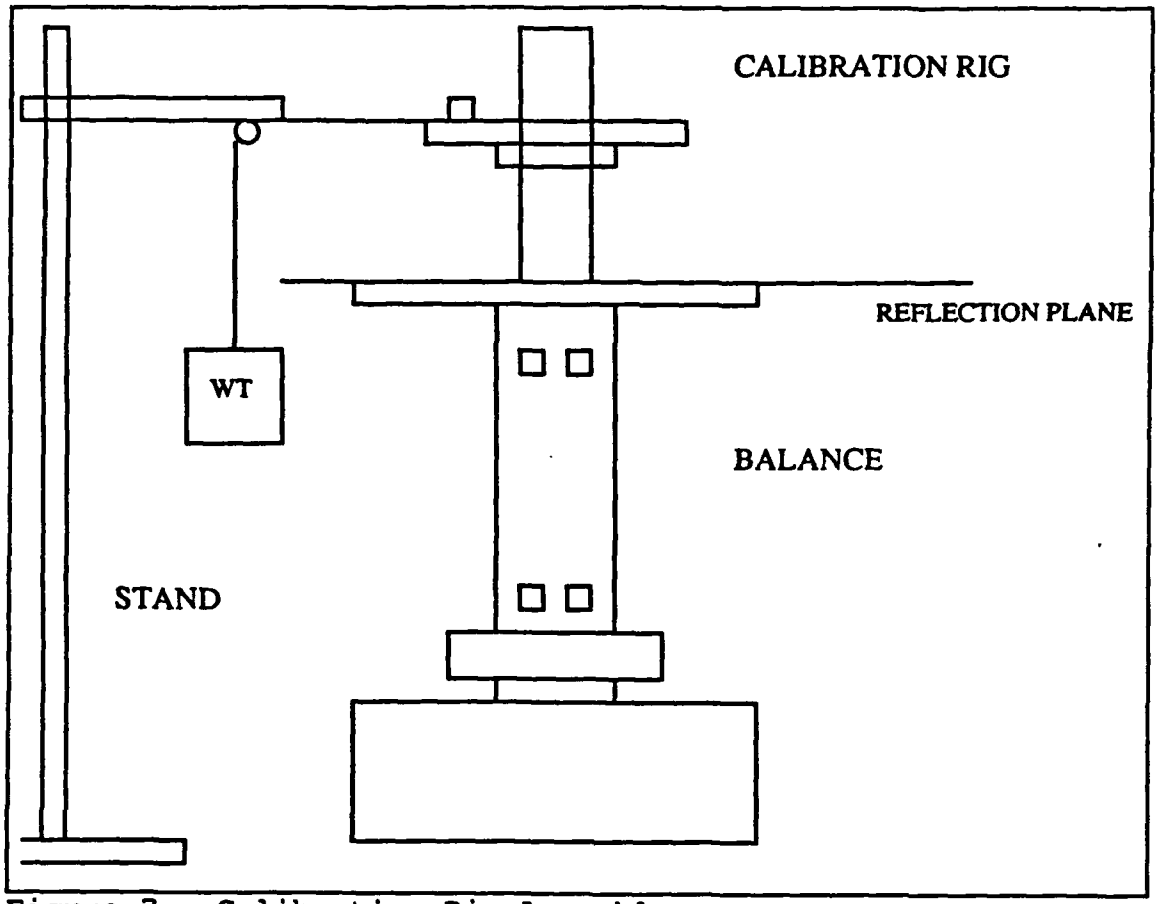

Figure 7. Calibration Rig Assembly

Table 1. Channels and Associated Strain-Gage Bridges

Channel	Strain Gage Bridge
(2)	EAA
(3)	EBA
(4)	EAN
(5)	EBN

channels (2) to (5) found using PANELS.EXE. The requested information was entered and the program started. The displayed axial and normal forces found should be less than .05 lbf. If the resultant normal and axial forces were greater than .05 lbf, then the offset voltages from channels (2) through (5) were checked and reentered. It was not necessary to leave the program JMK.BAS and reenter PANELS.EXE to update the zero offset voltages because the program displayed the average voltage readings for each channel on the monitor. These displayed readings, that with no force on the calibration rig were the zero offsets, were then entered into the computer at the start of the next iteration.

Once the balance was zeroed the turntable was rotated to 0, 90, and 55 degrees. Suspending weights from the calibration rig with the turntable at 0 degrees imparted a pure normal moment to the balance. Rotating the turntable to 90 degrees and suspending weights induced a pure axial moment on the balance. The 55-degree position was used to impart a simultaneous axial and normal moment on the balance. The 55-degree position simulated the approximate resultant force direction on the balance, which was at about 325 degrees, while the tunnel was in operation with the model at high angles of attack. With the turntable rotated to one of the angles of attack the requested information was entered into the computer including the previously determined zero offset for each channel. Successively larger weights were then hung

from the balance calibration rig and the normal and axial forces calculated by the program JMK.BAS. After each weight was hung from the balance the zero offsets of the channels were checked to ensure that they had not drifted. In general, channel (3) drifted 1 or 2 millivolts a minute. If the zero offset for channel (3) was not updated over the course of one hour, error in the balance would change by 2%. The computed values for axial and normal forces were then compared to the actual normal and axial forces induced by the weight on the balance rig and the computed values found during the original calibration procedure. (See Appendix B.) If the computed values for the prerun calibration differed from the original computed calibration values by less than .1 lbf, alignment of the turntable was verified and a known weight was again suspended from the rig. If the difference was still greater than .1 lbf, the balance was recalibrated.

The calibration rig was sized for a maximum anticipated force on the balance of about 25 lbf during tunnel operation. It was found that the balance was actually subjected to axial forces of up to 70 lbf. Due to the limitations of the calibration rig the largest weight that could be hung from the rig was 21 lbf. The response of the strain gages was linear, so the use of lesser weights should still verify the calibration.

2. Data Collection

After a satisfactory prerun calibration the model was mounted on the turntable platter. If the canard was used, the canard remote-control wiring was strung through the turntable platter and balance column. The program PANELS.EXE was then called and the Pacific Amplifier was again zeroed in the same manner as was done during the prerun calibration. The outputs of channels (2) to (5) were recorded for zero offsets.

The program JMK.BAS was called via the BASIC editor and the requested information was entered. The zero offsets for channels (2) to (5) were then updated by letting the program run before the tunnel was started. The only offset that usually changed by a significant amount was for channel (3). Tunnel runs were made changing the turntable angle of attack and/or canard deflection angle as required. The remote control of the canard allowed the canard deflection angle to be varied without actually shutting down the tunnel to reposition the canard.

3. Preliminary Runs

Test runs were made at a number of different tunnel speeds with the wing/body model to verify the operation of the balance. A number of short runs were made during testing of the canard servo motor and eventual canard electric motor with lead screw. As noted in Appendix A, the servo motor was

unable to position and hold the canard in the flow at all but the lowest tunnel speeds, which necessitated the use of an electric motor with lead screw to drive the canard.

It was found that there was a linear dependence of channel (3) upon temperature for temperatures greater than about 74 degrees. In general, no data were used that were taken at a tunnel settling chamber temperature greater than 74 degrees. Once the tunnel reached this temperature the tunnel was shut down to allow it to return to ambient air temperature. At angles of attack of 40 and 48 degrees, the tunnel heated up very rapidly from the typical starting temperature of 67 degrees. The time until the tunnel reached 74 degrees was as little as 15 minutes. The relative slowness of the data acquisition system meant as few as six data points could be collected under such conditions. Accordingly, a compensation routine was incorporated in the program JMK.BAS to correct for the temperature dependence and allow for longer tunnel runs should the need arise in the future. Table 2 and Figure 8 show the linear variation of the channel (3) voltage output with temperature at a constant model angle of attack of 40 degrees, a constant canard deflection angle of -17 degrees, and a ΔP of 17 cm H_2O.

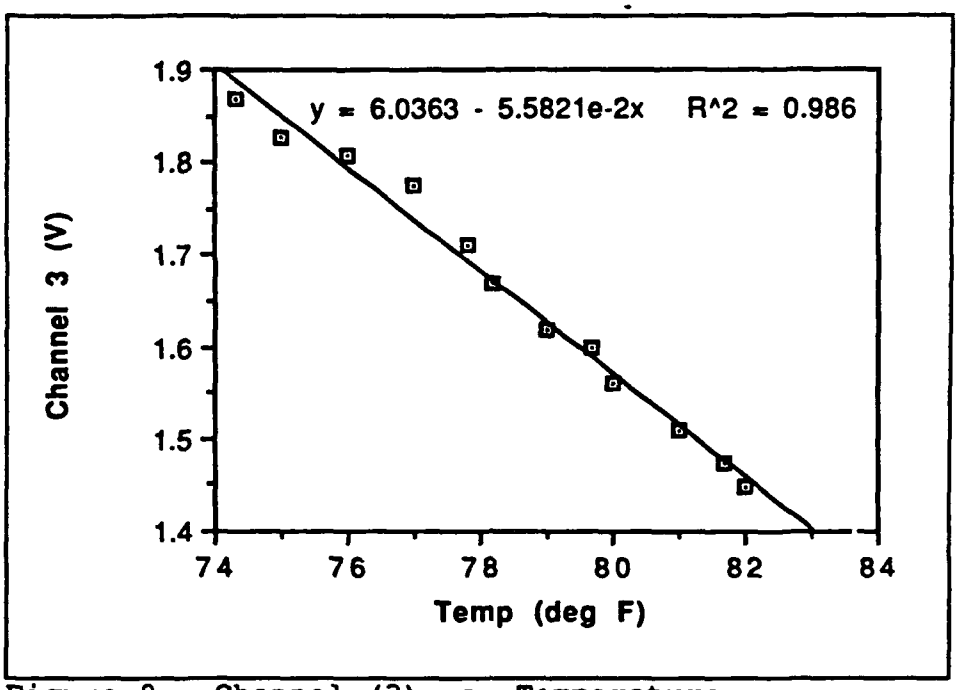

Figure 8. Channel (3) vs. Temperature

Table 2. Channel (3) vs. Temperature

CHANNEL 3 (V)	TEMP (deg F)
1.869	74.3
1.827	75.0
1.808	76.0
1.776	77.0
1.710	77.8
1.669	78.2
1.619	79.0
1.599	79.7
1.559	80.0
1.510	81.0
1.474	81.7
1.449	82.0

E. EXPERIMENTAL CORRECTIONS

The lift and drag coefficients were corrected for model blockage by equations (5) and (6) from References 15 and 18.

$$q = q_M(1 + 2\varepsilon) \tag{5}$$

$$U = U_M(1 + \varepsilon) \tag{6}$$

where:

q	dynamic pressure (lbf/ft^2)
q_M	measured reference q (lbf/ft^2)
U	horizontal velocity (ft/sec)
U_M	measured horizontal velocity (ft/sec)
ε	blockage factor

The blockage correction factor depended upon the angle of attack of the model and, if the canard was in place, the canard deflection angle. For the wing/body case, the blockage correction factor was determined from equation (7) where 0.02098 was the ratio of the cross-sections of the wing/body and the tunnel test section. If the canard was in place, equation (8) was used where 0.00383 was the ratio of the canard cross-sectional area to that of the test section.

$$\varepsilon_{body} = .0298\sin(AOA) \tag{7}$$

$$\varepsilon_{body+canard} = \varepsilon_{body} + .00383\sin(AOA + Canard\ AOA) \qquad (8)$$

During tunnel postrun calibration trials, a calibration error was found in the balance. The balance calibration error was quantified using the calibration rig with the turntable at an angle of attack of 55 degrees. With the turntable at 55 degrees a resultant force direction of 325 degrees could be simulated, which was close to the resultant force direction on the model at high angles of attack. Figure 9 is a plot of the experimental normal force versus actual normal force at an AOA of 55 degrees. Figure 10 is a plot of the experimental axial force versus the actual axial force at an AOA of 55 degrees. The plots indicate an error of +4.5% in the reading of the actual normal force and an error of -3.7% in the reading of the actual axial force. Accordingly, the program CORCOEF.BAS was updated to multiply the normal force output by .955 and the axial force output by 1.037 to compensate for balance calibration error these values were then used to find the corrected lift and drag. Table 3 includes the data used in Figures 9 and 10.

The turntable was found to be misaligned by +2.2 degrees at the end of all the data runs. This necessitated a further correction of the calculated lift and drag forces. The model was mounted on the platter with the turntable at 90 degrees AOA with the result that a -2.2 degree correction was applied

to the AOA of the wing/body. All the corrections were incorporated in the BASIC program CORCOEF.BAS found in Appendix D.

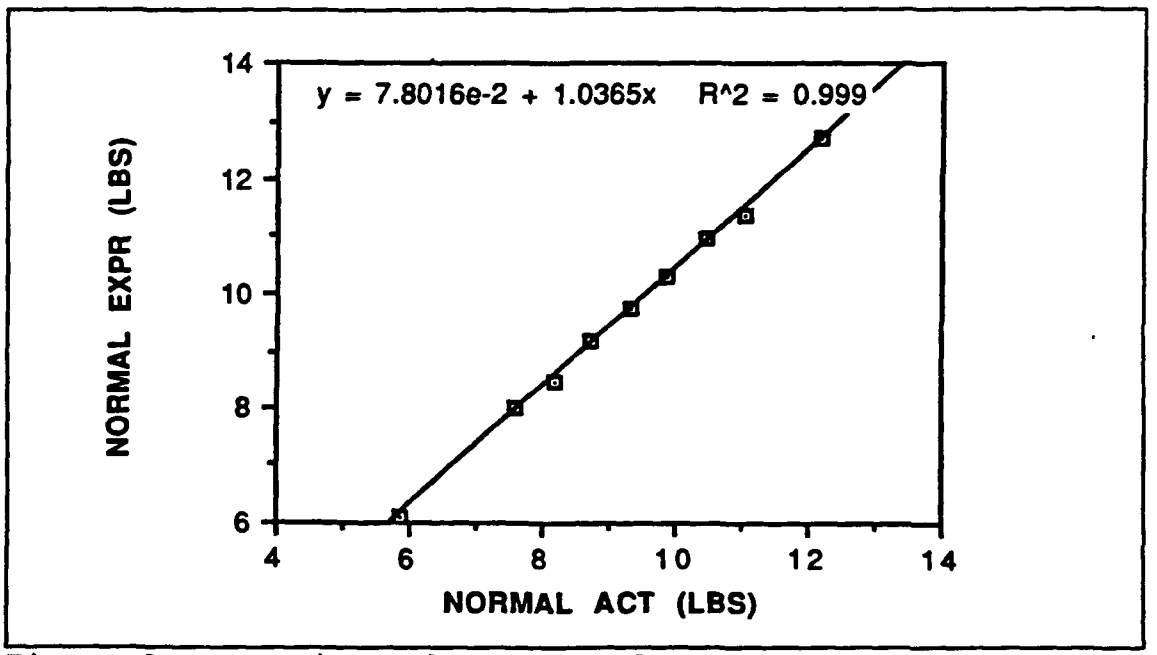

Figure 9. Experimental vs. Actual Normal Force

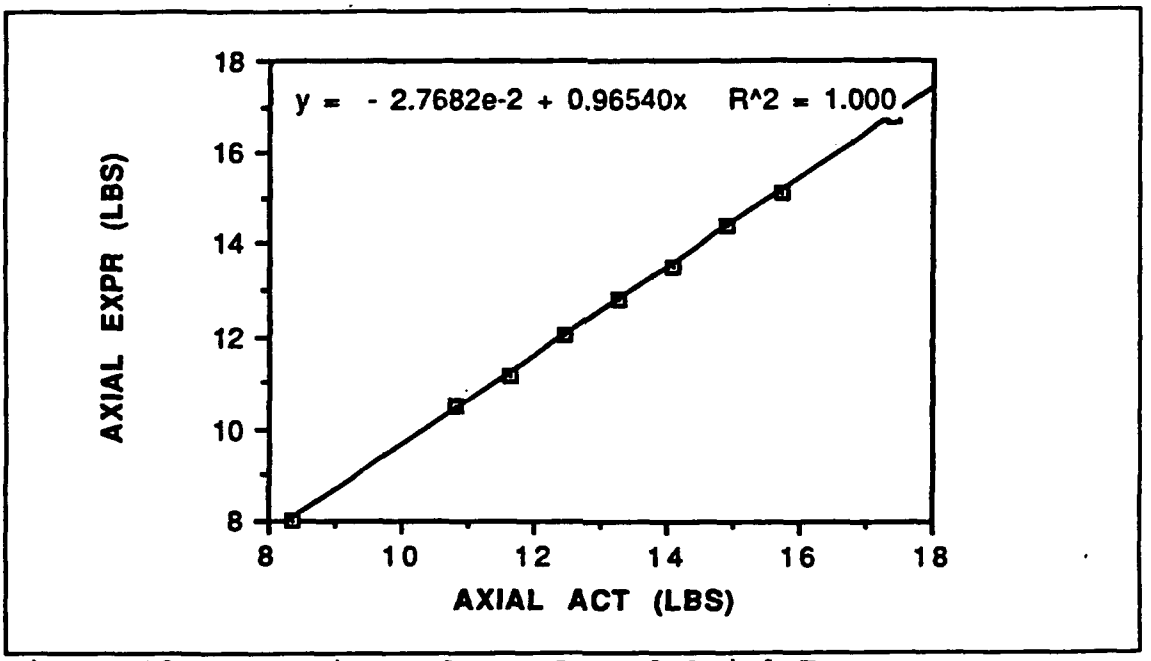

Figure 10. Experimental vs. Actual Axial Force

Table 3. Experimental and Actual Axial and Normal Forces

WEIGHT (LBS)	NORMAL EXPER FORCE (LBS)	NORMAL ACTUAL FORCE (LBS)	AXIAL EXPER FORCE (LBS)	AXIAL ACTUAL FORCE (LBS)
10.2216	6.11	5.86	8.03	8.37
13.2216	8.02	7.58	10.50	10.83
14.2262	8.48	8.16	11.16	11.65
15.2251	9.16	8.73	12.04	12.47
16.2297	9.74	9.31	12.83	13.29
17.2241	10.30	9.88	13.54	14.11
18.2287	10.99	10.46	14.44	14.93
19.2276	11.40	11.03	15.09	15.75
21.2388	12.73	12.18	16.81	17.40

III. RESULTS AND DISCUSSION

The following sections discuss the plots and data from six wind-tunnel runs. The first was a baseline run without the canard, where the angle of attack (AOA) of the wing/body was varied from -8 to 50 degrees in 2-degree increments or less. The following runs were conducted with the canard in place at wing/body angles of attack of 10, 22, 34, 40, and 48 degrees where the canard deflection angle (canard AOA) was varied from -25 to 25 degrees in increments of 5 degrees or less. It should be noted that the term "canard deflection angle" refers to the incidence angle of the canard relative to the fuselage centerline. C_L and C_D refer to the coefficients of lift and drag. Data for C_L versus AOA, C_L versus C_D, and C_L/C_D versus AOA were plotted for the baseline run. Data for C_L versus canard deflection angle and C_L versus C_D were plotted for the five wing/body angles of attack with the canard in place.

The reference area for the C_L and the C_D of the wing/body configuration was the area of the wing taken to the model centerline of 0.685 ft^2. The reference area for the C_L and the C_D of the canard/wing/body configuration was the area of the wing to the centerline plus the exposed area of the canard, which total area equalled 0.815 ft^2. Appendix E includes the data sets used for all plots in the Results/Discussion chapter.

A. BASELINE WING/BODY CONFIGURATION

Figure 11 shows the variation of C_L with AOA. The AOA of the wing/body was varied from -8 to 50 degrees, and C_L varied from .036 to 1.586. The maximum lift occurred at an AOA of 40 degrees.

Wings with aspect ratios less than 5 typically stall at higher angles of attack than higher-aspect-ratio wings. The wing of the model had an aspect ratio of 3. The overall shape of the C_L versus AOA curve is similar to curves for other low-aspect-ratio wing configurations. [Ref. 19]

The C_L versus AOA curve was linear from -8 to 4 degrees with a slope of 0.0577/degree. At angles of attack greater than 4 degrees the slope became slightly non-linear; from 4 to 12 degrees, the C_L was greater than the projected linear slope. This non-linear increase in lift was probably due to the formation of a weak wing-leading-edge vortex. From 12 to 18 degrees, the C_L was less than the projected linear slope. At about 18 degrees the first maximum C_L occurred and the first stall began.

The angle-of-attack increment was decreased to one degree from 17 to 29 degrees so that the nature of this first stall could be better observed. It was established that from 21 to 25 degrees the C_L did not appreciably vary with AOA. The first stall was probably caused by the onset of major flow separation on the outboard wing section. At angles of attack greater than 25 degrees, the C_L again began to increase with

AOA. It is speculated that a strong leading-edge vortex has formed at this high angle of attack, tending to reattach the flow.

From 28 to 32 degrees, the C_L versus AOA curve was again linear with a slope of 0.0473/degree. This slope is not very different from the earlier linear slope from -8 to 4 degrees. At angles of attack greater than about 32 degrees the C_L versus AOA curve again began to decrease as the second stall was initiated. The maximum C_L was 1.586 at an AOA of 40 degrees. The C_L at 40 degrees was 0.53 greater than the C_L during the first stall. The second stall was probably due to the breakdown of the strong wing-leading-edge vortex.

Figure 12 shows the variation of C_L with C_D. The value of C_D at the maximum C_L was 1.262. The value for C_D minimum was 0.034 at a C_L of 0.036. The plot shows typical drag-polar behavior from a C_L of -0.420 to 1.031. From a C_L of 1.031 to 1.059, the first stall occurred and C_D increased from .390 to .512. For a C_L greater than 1.059, lift again increased until the maximum C_L, 1.586, was reached. At a C_D greater than 1.262 the second stall took place where the lift fell off rapidly and the drag increased greatly.

Figure 13 show the variation of C_L/C_D with AOA. The maximum C_L/C_D was 7.15 at an AOA of 6 degrees. This condition is the region in which the lift was enhanced by the weak leading-edge vortex. The minimum post-stall C_L/C_D was 0.92 at 50 degrees. C_L/C_D increased rapidly from -8 to 6 degrees,

changing 12.75 units in 14 degrees. From 6 degrees to 50 degrees C_L/C_D decreased in a smooth non-linear drop-off to 0.92 at an AOA of 50 degrees. Values in the high angle-of-attack regime from 20 to 40 degrees, where an agile-aircraft might be expected to have an excursion, decrease from about 2.8 to 1.3, indicating the significant thrust levels required for supermaneuverability.

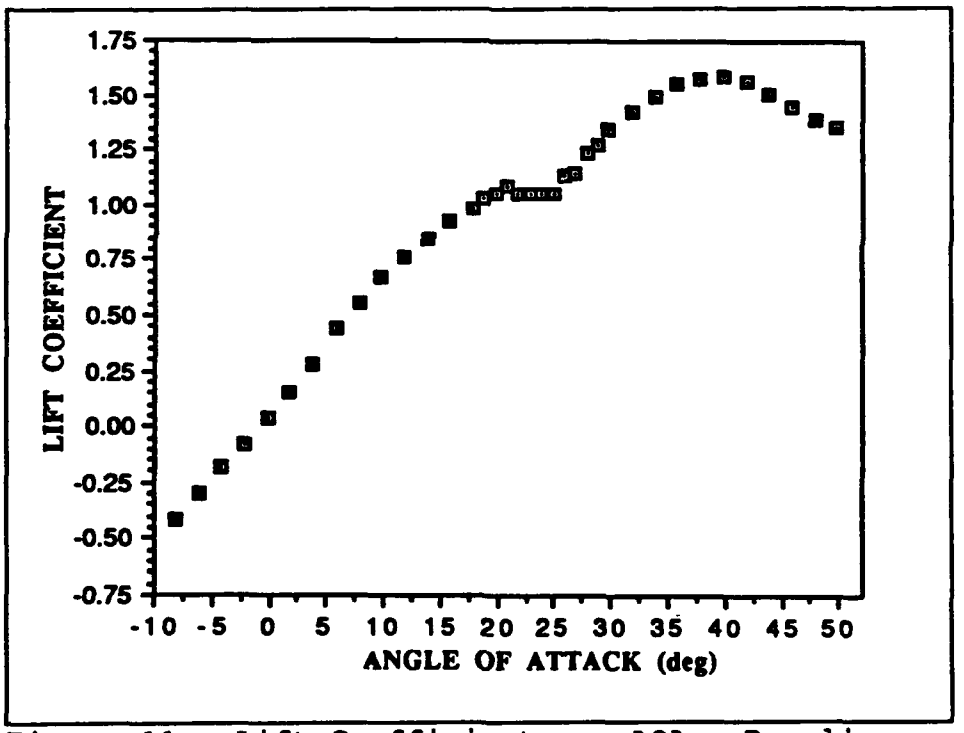

Figure 11. Lift Coefficient vs. AOA; Baseline

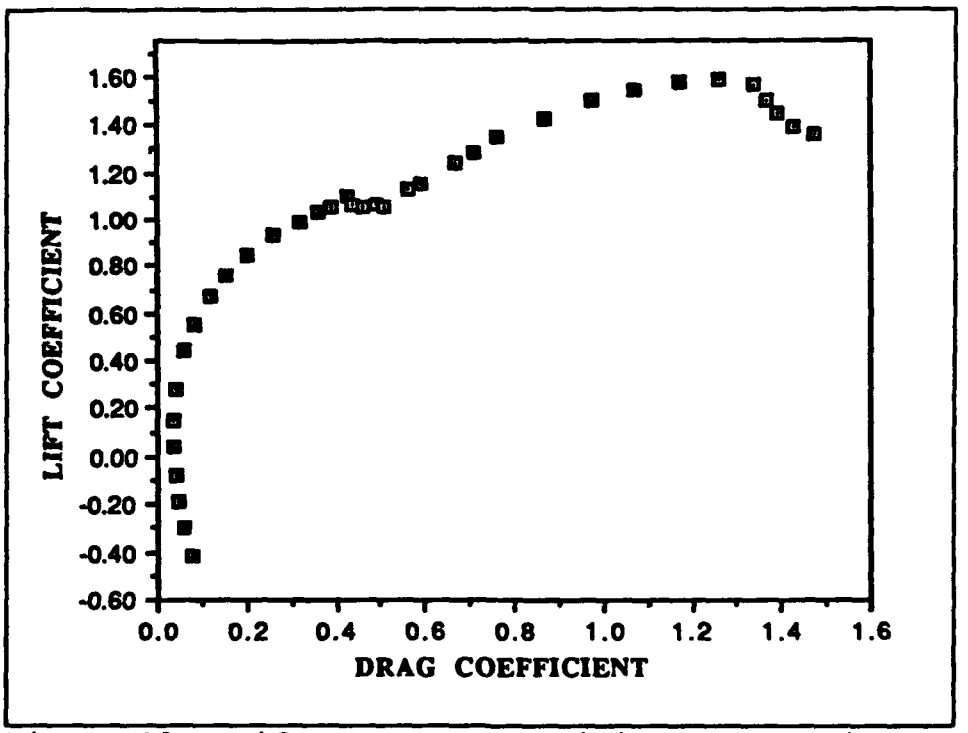

Figure 12. Lift vs Drag Coefficient; Baseline

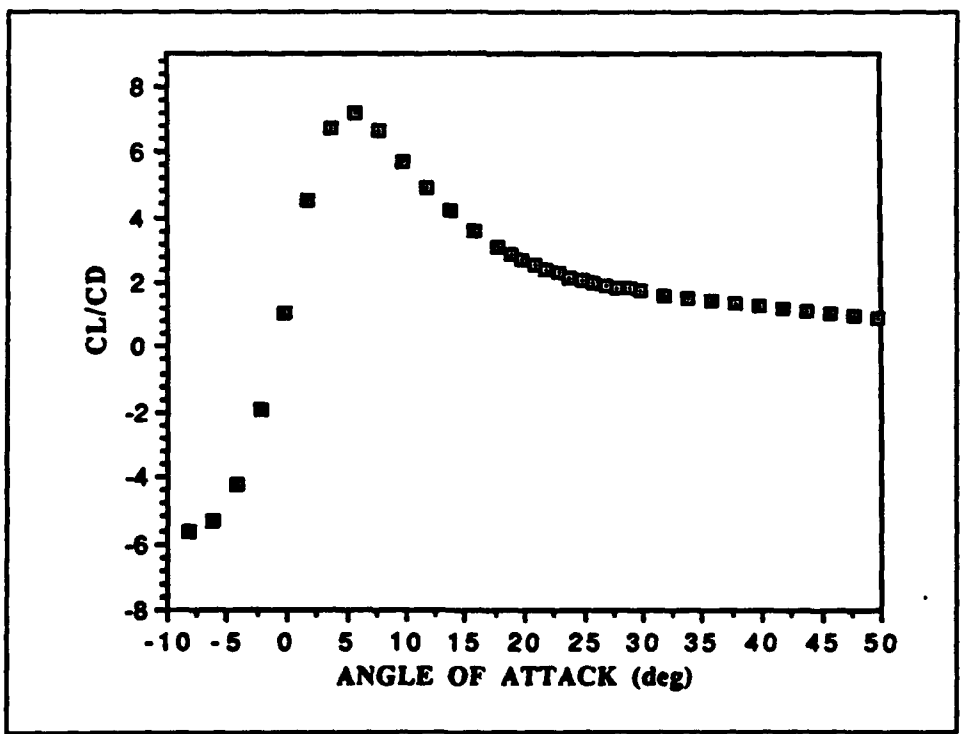

Figure 13. C_L/C_D vs. Angle of Attack; Baseline

B. CANARD/WING/BODY CONFIGURATION; AOA 10 DEGREES

Figure 14 shows the variation of C_L with canard deflection angle at a wing/body AOA of 10 degrees. The maximum C_L was 0.698 at 17 degrees. From -25 to 0 degrees the increase in C_L with canard deflection angle was fairly linear. Beyond 0 degrees the curve was non-linear with an increased data scatter. Lift began to decrease at deflection angles greater than 20 degrees.

When compared to the baseline wing/body configuration, lift was slightly enhanced for a canard deflection angles between 7 and about 20 degrees. Positioning the canard outside of this range actually caused a lift degradation. Lift was maximized at a canard angle of 17 degrees, where the maximum C_L was 3.41% greater than the baseline value of 0.675. At a canard deflection angle of 25 degrees C_L was 1.48% less than the baseline value. It can be seen that the lift enhancement with the addition of a canard is slight at the relatively low wing/body AOA of 10 degrees.

Figure 15 shows the variation of C_L with C_D for this case. The maximum C_L was 0.698 at a C_D of 0.188. C_D minimum was 0.094 at a C_L of 0.631. At a C_D of 0.120 and 0.143, C_L dropped slightly compared to the data trend. These two data points were repeatable and were not due to scatter. At a C_D of about 0.2 lift began to drop off markedly and drag increased greatly.

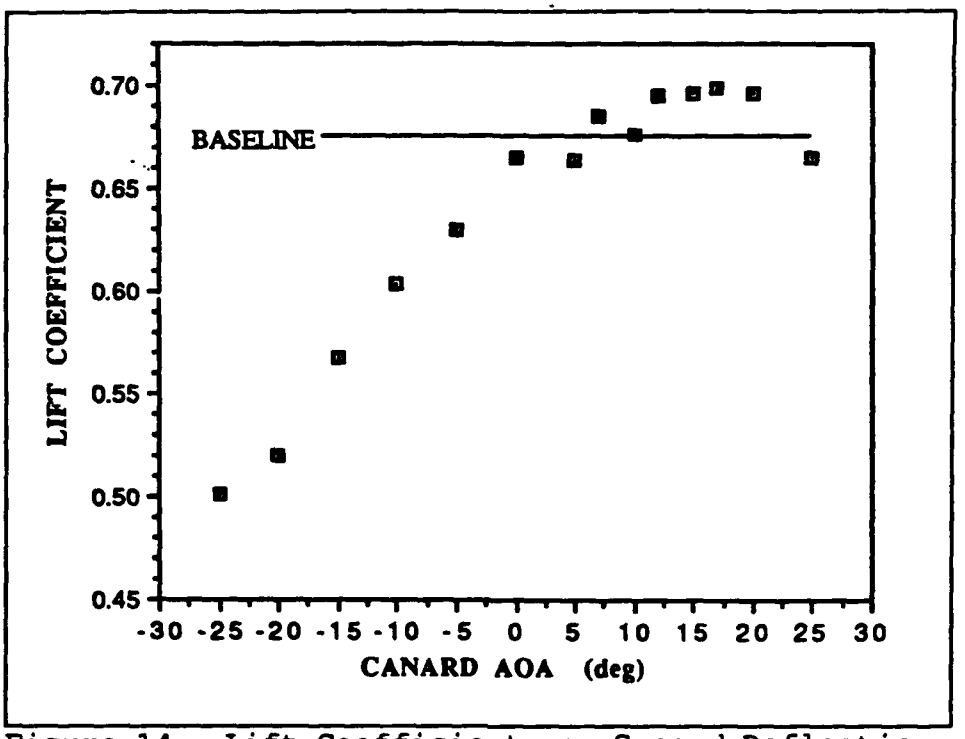

Figure 14. Lift Coefficient vs. Canard Deflection; AOA 10 Degrees

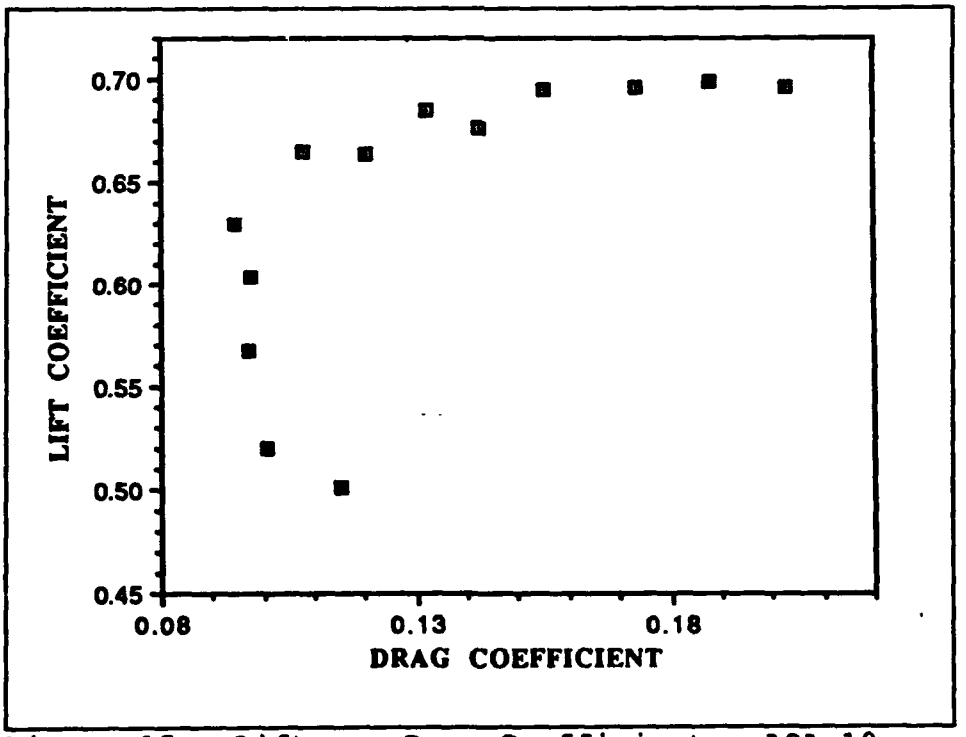

Figure 15. Lift vs. Drag Coefficient; AOA 10

C. CANARD/WING/BODY CONFIGURATION; AOA 22 DEGREES

Figure 16 shows the variation of C_L with canard deflection angle for a wing/body AOA of 22 degrees. The maximum C_L was 1.422 at a canard angle of 7 degrees. There was little data scatter and the curve was fairly smooth for all canard deflection angles tested. The lift varied in a strong non-linear fashion from a C_L of 0.97 to 1.36. A typical stall behavior was indicated, the lift coefficient leveling off to 1.30-1.35 after stall.

When compared to the baseline configuration, lift was greatly enhanced for a canard deflection angle between -15 and 25 degrees. Positioning the canard from -25 to about -15 degrees degraded the lift below the baseline value. As the canard angle was increased from -15 to 7 degrees, lift was enhanced significantly. Lift was maximized at a canard angle of 7 degrees, where the C_L was 34% greater than the baseline value of 1.061. From 7 to 25 degrees the values of C_L decreased with an increase in canard angle; but, the comparative lift enhancement was still significant. At a canard deflection angle of 25 degrees, C_L was still 24.5% greater than the baseline value. It should be noted that this enhancement is taking place at the wing/body angle of attack where the first stall occurred. Evidently the canard/wing interaction is preventing the wing separation from taking place, the canard vortex providing the energizing mechanism.

Figure 17 shows the variation of C_L with C_D. The maximum C_L was 1.422 at a C_D of 0.547. C_D minimum was 0.368 at a C_L of 1.007. The overall plot was relatively smooth with little data scatter. The slope was approximately linear from a C_D of 0.413 to 0.502. At a C_L greater than 1.422 stall occurred and lift dropped of markedly while drag increased.

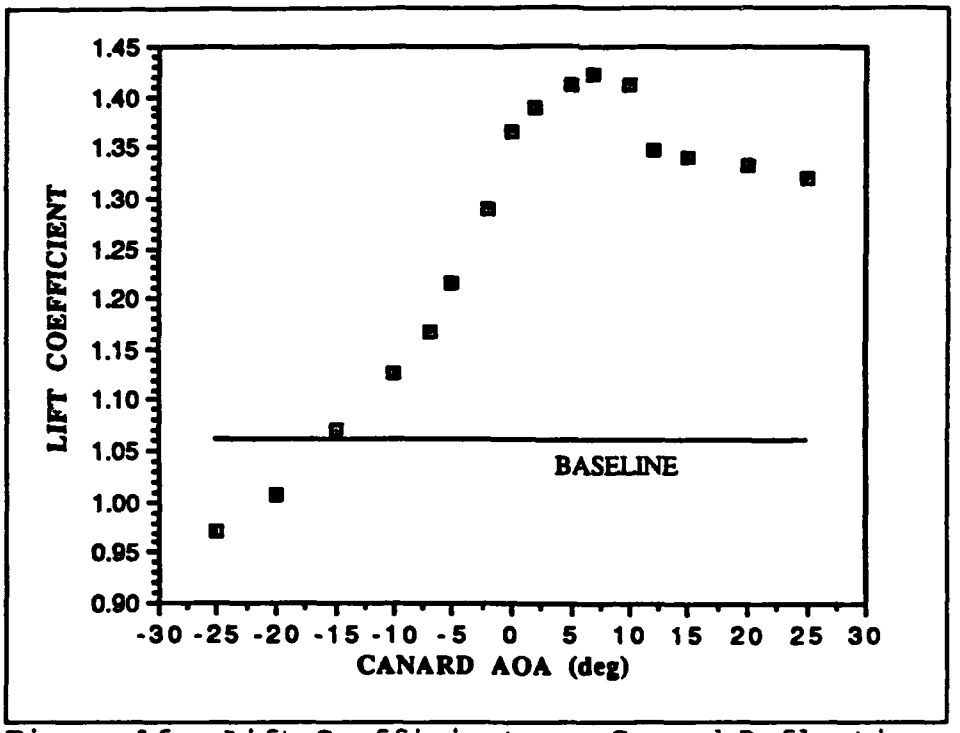

Figure 16. Lift Coefficient vs. Canard Deflection; AOA 22

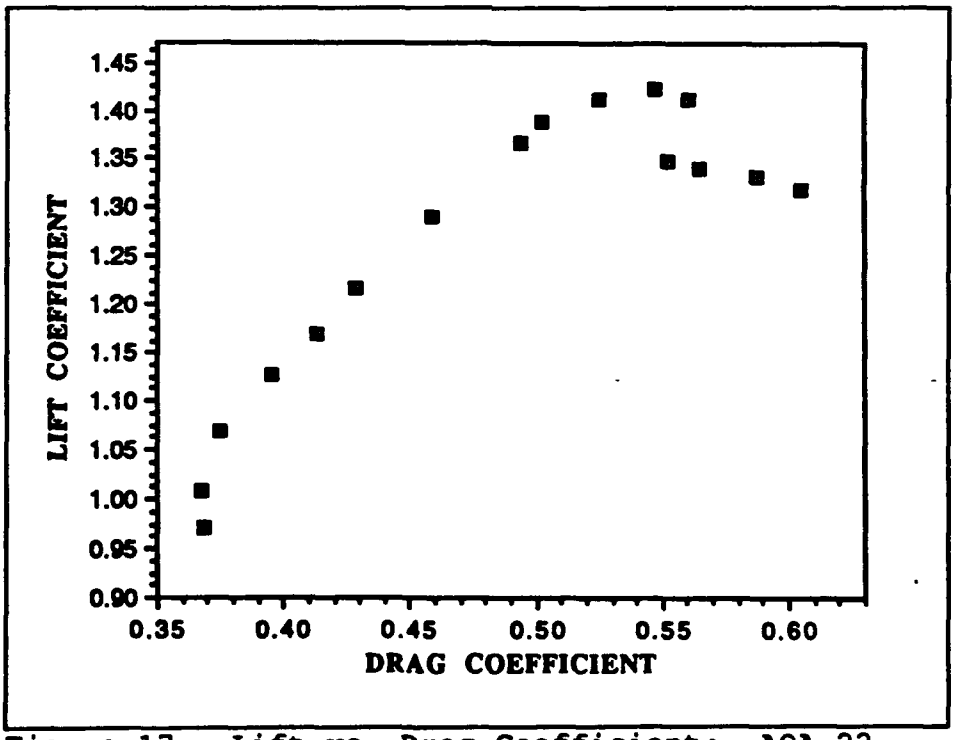

Figure 17. Lift vs. Drag Coefficient; AOA 22

D. CANARD/WING/BODY CONFIGURATION; AOA 34 DEGREES

Figure 18 shows the variation of C_L with canard deflection angle for a wing/body AOA of 34 degrees. This angle of attack is in the region midway along the second rise of the baseline configuration lift curve. The maximum C_L was 1.642 at a canard angle of -7 degrees. The C_L increased with canard angle from -25 to -7 degrees. At -7 degrees the primary C_L peak occurred; C_L then decreased with increasing canard angle until a canard deflection angle of 0 degrees. The C_L then increased with increasing canard deflection angle until an angle of 5 degrees was reached. At 5 degrees there was a secondary C_L peak of 1.625. At canard deflection angles greater than 5 degrees the canard/wing/body began to stall. Within a band of data scatter, the data were repeatable, in particular the twin-peaked behavior.

From -25 to -10 degrees lift was degraded using the canard. As the canard deflection angle was increased from -12 to -7 degrees, the lift was enhanced over the baseline case. Lift was maximized at a canard angle of -7 degrees, where C_L was 9.39% greater than the baseline value of 1.501. From -7 to 0 degrees C_L decreased with canard deflection; but the lift was still greater than the baseline configuration. Lift increased with increasing canard angle from 0 to 5 degrees. At a canard angle of 25 degrees C_L was 2.53% greater than the baseline value.

Figure 19 shows the variation of C_L with C_D. The maximum C_L was 1.642 at a C_D of 0.982. The plot was relatively smooth and linear for coefficients of drag less than 0.982. At a C_D of 0.982 the data became multi-valued, but all data points were shown to be repeatable. At a C_D greater than 1.058 stall occurred and lift decreased markedly while drag increased.

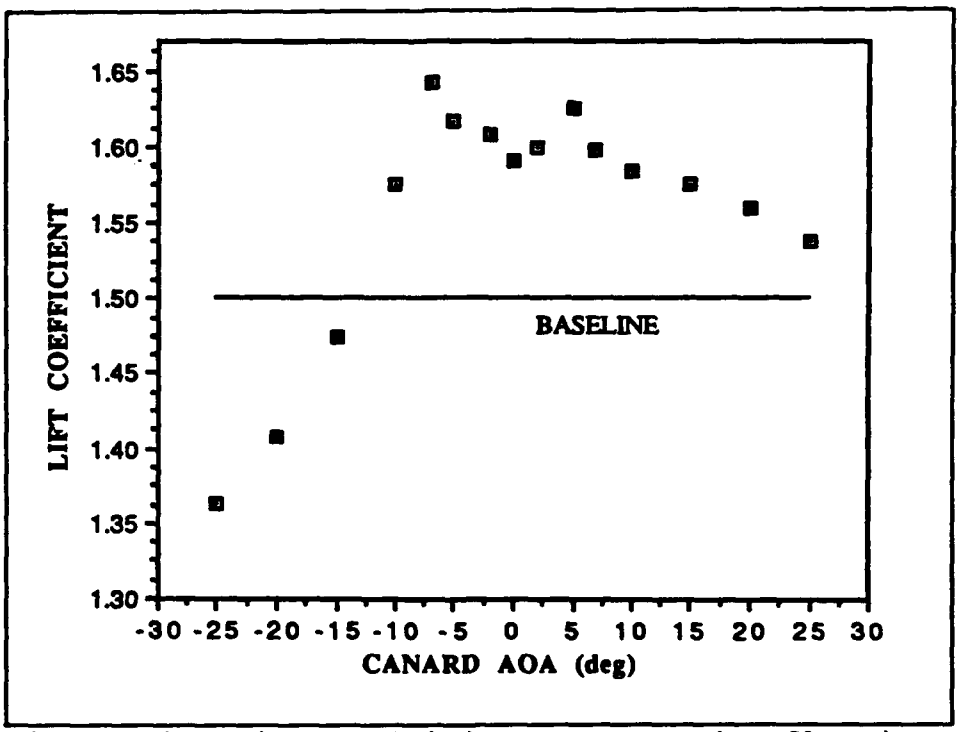

Figure 18. Lift Coefficient vs Canard Deflection; AOA 34

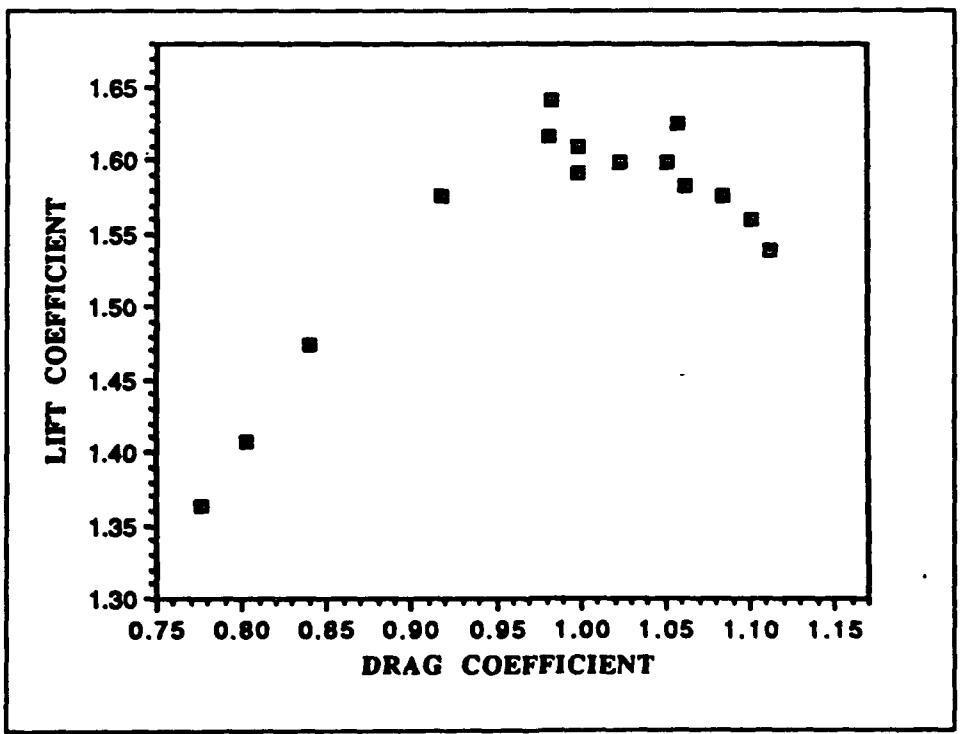

Figure 19. Lift vs. Drag Coefficient; AOA 34

E. CANARD/WING/BODY CONFIGURATION; AOA 40 DEGREES

Figure 20 shows the variation of C_L with canard deflection angle for a wing/body AOA of 40 degrees. This wing/body angle corresponds to the condition of the maximum C_L for the baseline configuration. The maximum C_L was 1.700 at a canard angle of -15 degrees. The C_L increased with canard deflection angle and the slope was fairly steep from -25 to -15 degrees. At canard deflection angles greater than -15 degrees the canard/wing/body began to stall.

Lift was enhanced compared to the baseline configuration for canard deflections between -25 and 15 degrees. Lift was degraded for canard angles greater than 15 degrees. A canard deflection between -20 and 5 degrees resulted in at least a 3.97% increase in lift over the baseline value of 1.586. Lift was maximized at a canard deflection of -15 degrees ,where the C_L was 7.19% greater than the baseline value. From -15 to 0 degrees C_L decreased slightly with canard deflection to 1.680; but overall the lift was still greater than the baseline. C_L was 15.45% less than the baseline value at a canard deflection of 25 degrees.

Figure 21 shows the variation of C_L with C_D. The maximum C_L was 1.700 at a C_D of 1.214. C_D minimum was 1.099 at a C_L of 1.586, though this minimum is due to the limited data points taken rather than to an infinite slope. The plot was relatively linear for coefficients of drag less than 1.214.

At a C_D of 1.240 the data became slightly scattered. At a C_D of 1.240 the canard/wing/body began to stall and at a C_D of 1.325, C_L lift dropped precipitously while there was little change in C_D.

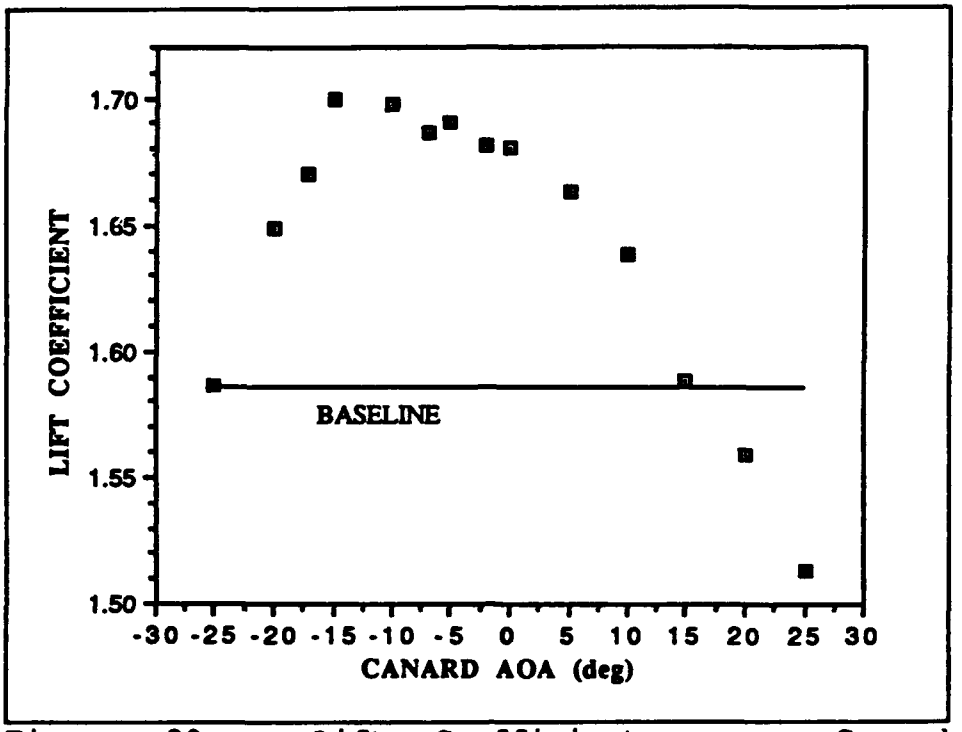

Figure 20. Lift Coefficient vs. Canard Deflection; AOA 40

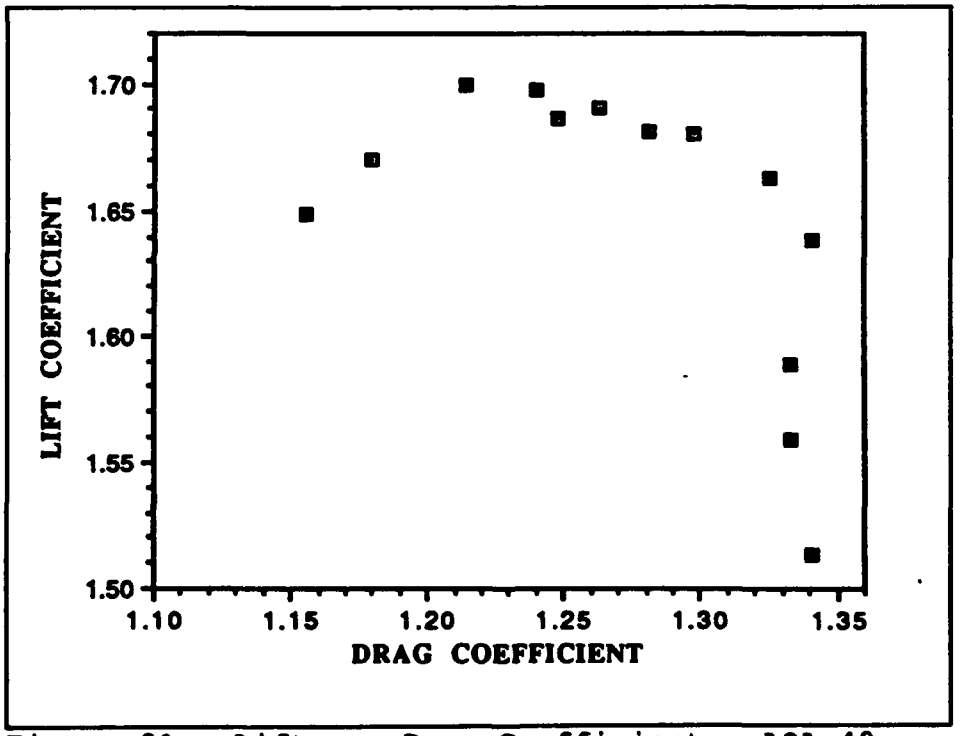

Figure 21. Lift vs. Drag Coefficient; AOA 40

F. CANARD/WING/BODY CONFIGURATION; AOA 48 DEGREES

Figure 22 shows the variation of C_L with canard deflection angle for a wing/body AOA of 48 degrees. This wing/body angle is deep in the second post-stall region for the baseline configuration. The maximum C_L was 1.649 at -17 degrees. The shape of the plot was similar to the plot shown in Figure 20 for the wing/body at an AOA of 40 degrees. C_L increased with canard deflection for angles less than -17 degrees. At canard deflection angles greater than -17 degrees, stall occurred and the C_L decreased rapidly with increased canard deflection.

Lift was enhanced compared to the baseline configuration for canard deflections between -25 and 20 degrees. Lift was degraded for canard deflection angles greater than 20 degrees. A canard deflection between -25 and 0 degrees resulted in at least a 13.92% increase in lift over the baseline value of 1.394. Lift was maximized at a canard deflection of -17 degrees, where the C_L was 18.29% greater than the baseline value. C_L was 1.15% less than the baseline value at a canard deflection of 25 degrees. In this post-stall regime, the canard/wing interaction remains effective over a much wider angle-of-attack range than for the previous cases.

Figure 23 shows the variation of C_L with C_D. The maximum C_L was 1.649 at a C_D of 1.534. For coefficients of drag less than 1.541, C_L varied by less than +/- 0.9% from 1.635. At a C_D of 1.623 the canard/wing/body began to stall and C_L

decreased greatly to a value of 1.378 while C_D actually decreased by 0.05 to 1.573. It is interesting to observe that at canard deflection angles greater than 0 degrees, the drag decreases with decreasing lift, an anomaly in a typical post-stall regime.

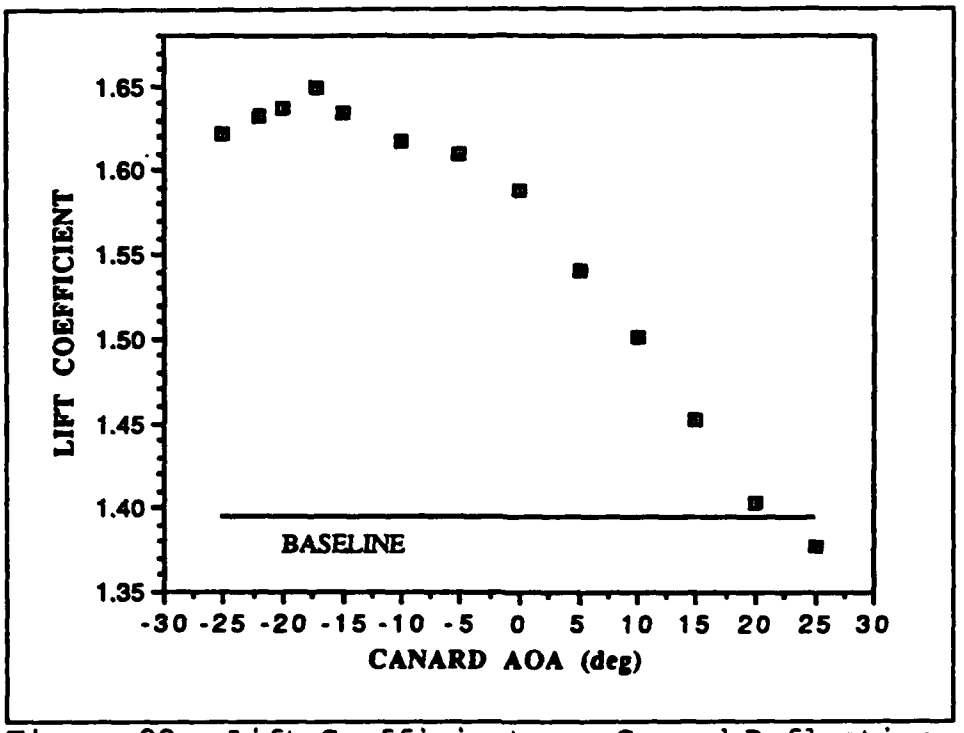

Figure 22. Lift Coefficient vs. Canard Deflection; AOA 48

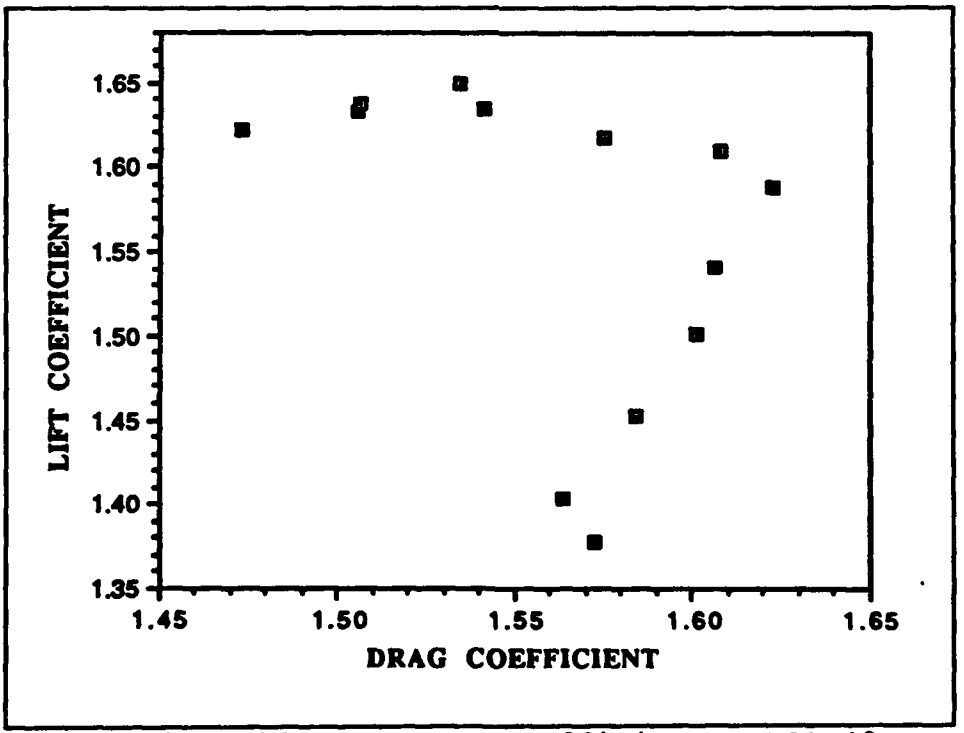

Figure 23. Lift vs. Drag Coefficient; AOA 48

G. COMPARISON BETWEEN WING/BODY AND CANARD/WING/BODY

Figure 24 shows the comparative lift of the wing/body and the canard/wing/body configuration. As predicted by Lacey, there was little lift enhancement using a close-coupled canard at wing/body angles of attack less than 18 degrees. The maximum C_L at 10 degrees AOA was only 3.4% greater than the baseline value. At 22 degrees AOA, where the first stall occurred, the lift was greater than the baseline value by 34%. This dramatic increase in lift is thought to be due to the downwash of the close-coupled canard impinging upon the flowfield of the wing, thereby delaying the onset of flow separation. At 34 degrees AOA, the lift was 9.4% greater than the baseline value. At 40 degrees AOA, where the lift was previously maximized for the wing/body configuration, the lift was 7.2% greater than the baseline value. In general, the lift enhancement was not as great where major separation did not previously exist for angles of attack tested in the baseline configuration. At 48 degrees AOA, where the second stall occurred, the lift was greater than the baseline value by 18.3% This great increase in lift is thought to be due to the vortex of the close-coupled canard constructively interfering with the vortex of the wing, thus delaying the onset of flow separation.

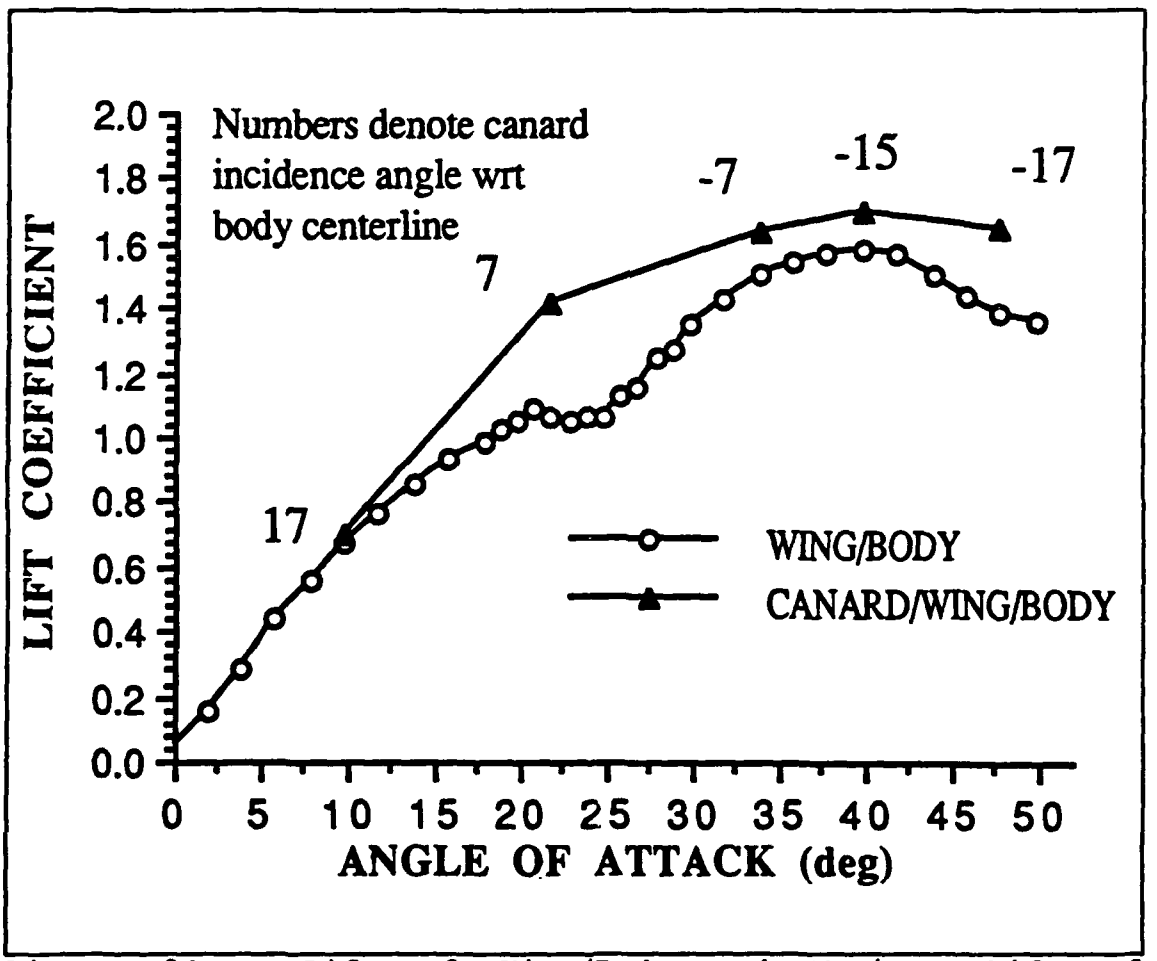

Figure 24. Lift of Wing/Body and Maximum Lift of Canard/Wing/Body vs. Angle of Attack

Figure 25 compares the lift of the wing/body to the minimum lift of the canard/wing/body and to the lift of the canard/wing/body with the canard at a canard fixed deflection angle of -5 degrees. To illustrate that the canard must be positioned properly for each wing/body AOA, the minimum lift obtained when the canard deflection angle was varied was also plotted. Not too surprisingly, if the canard was positioned to minimize the overall lift, the lift of the canard/wing/body was less than that of the wing/body configuration. But at an AOA of 48 degrees, with the canard positioned to minimize overall lift, the lift was only 1.15% less than the wing/body configuration. In fact, at an AOA of 48 degrees, if the canard was at any canard deflection angle other than 25 degrees the lift was improved over the baseline value.

Experimental results indicated that a canard deflection angle could be chosen that enhanced lift at a number of different wing/body angles of attack. In fact, if the canard was positioned at the approximate average canard deflection angle that maximized lift for all runs, a -5 degree incidence angle with respect to the centerline of the fuselage, the lift was enhanced for all tested wing/body angles of attack except at 10 degrees. At an AOA of 10 degrees, the lift was 6.5% less than the baseline value. The lift was 14.6% greater than the baseline value at an AOA of 22 degrees. At AOA's of 34 and 40 degrees, the lift was 7.7% and 6.6% greater than the corresponding baseline values. The lift was 15.5% greater

than the baseline value at an AOA of 48 degrees. Positioning the canard at -5 degrees did not maximize the lift for any wing/body AOA; but, if it is desired to minimize the weight and complexity of a moveable canard system while increasing the lift over a large AOA range, a fixed -5 degree canard incidence angle is a good potential choice for the configuration studied.

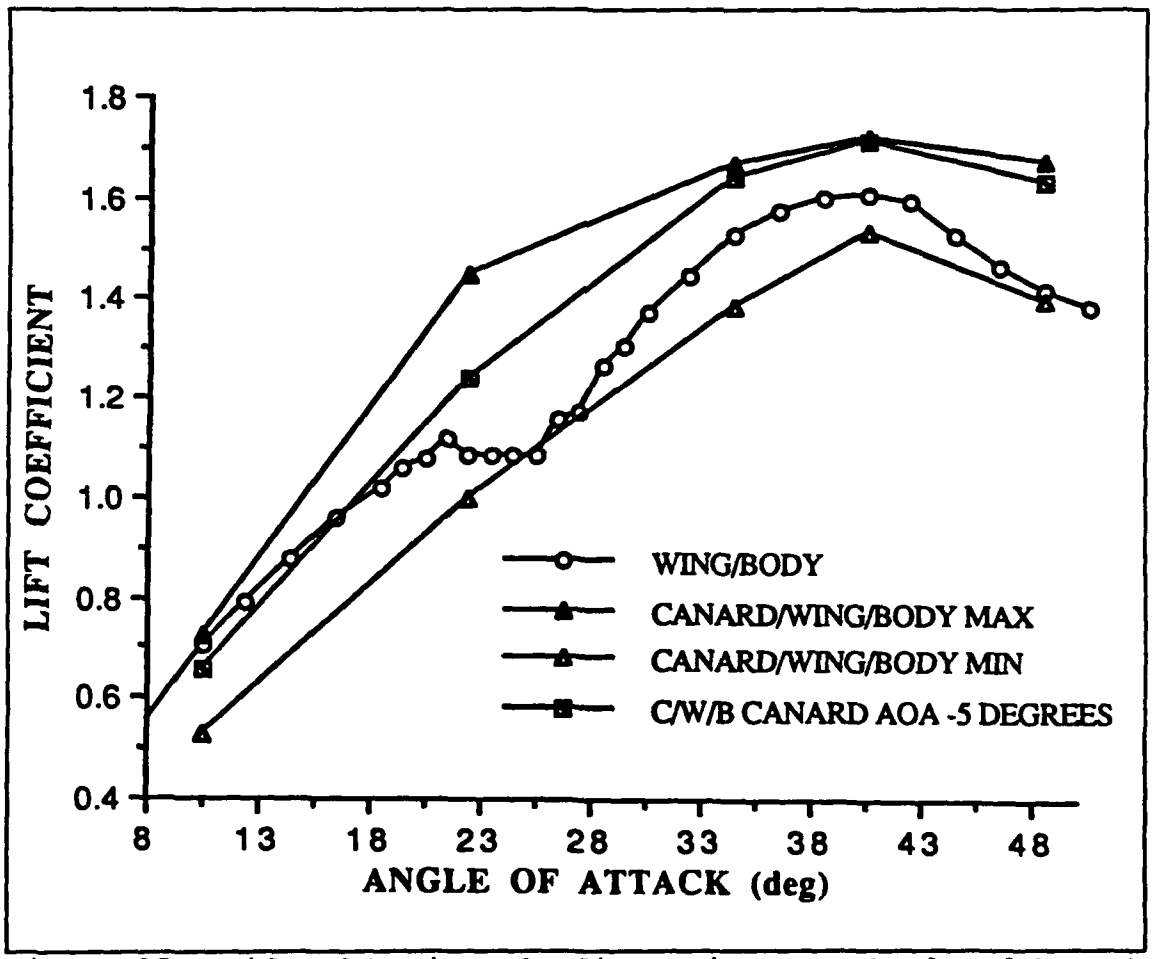

Figure 25. Lift of Various Configurations vs. Angle of Attack

Figure 26 compares the baseline drag polar for the wing/body configuration with the drag polar for the canard/wing/body configuration using a canard deflection that maximized the lift for each wing/body AOA. For all tested angles of attack except 10 degrees, the lift was greater for the canard/wing/body than for the wing/body configuration at the same drag coefficient.

Figure 27 compares the lift-to-drag ratio for the wing/body configuration with that for the canard/wing/body configuration. For the canard/wing/body, the C_L/C_D at each tested AOA was greater than the baseline value for all tested wing/body angles of attack except at 10 degrees. At an AOA of 10 degrees, the C_L/C_D ratio was 34.5% less than the baseline value. The C_L/C_D ratios were 7.4%, 8.9%, 11.4%, and 10.4% greater than the baseline values at angles of attack of 22, 34, 40, and 48 degrees. Essentially, using a properly located close-coupled canard exacted a penalty in C_L/C_D only at low angles of attack, below a lift coefficient of 0.35. At higher angles of attack, the increase in C_L/C_D over the baseline value was as great as 11.4%.

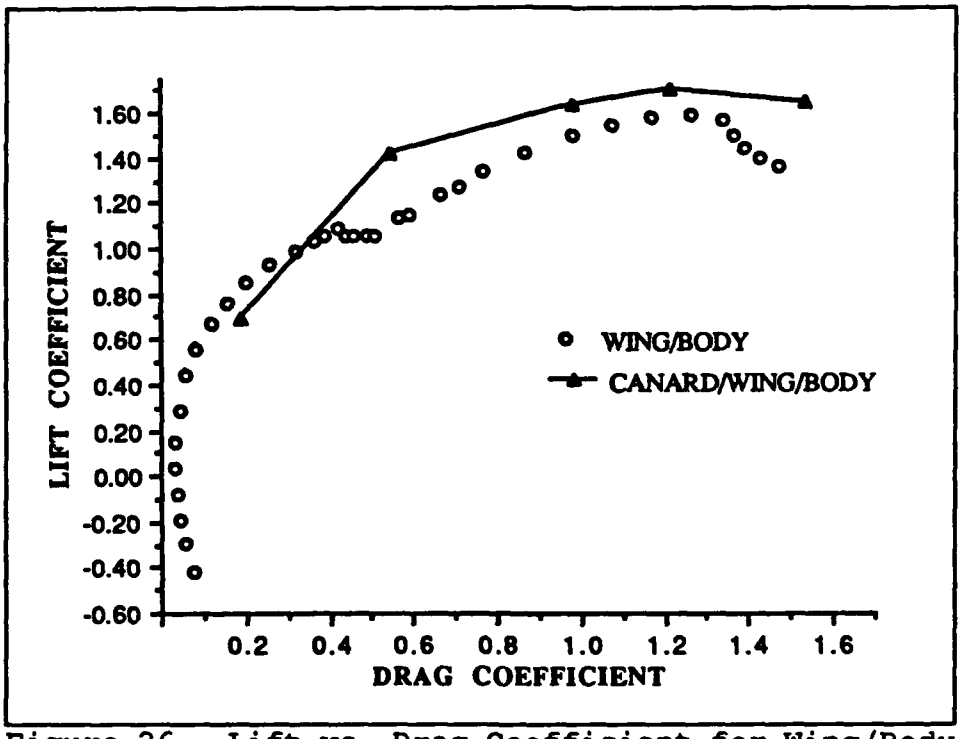

Figure 26. Lift vs. Drag Coefficient for Wing/Body and Canard/Wing/Body

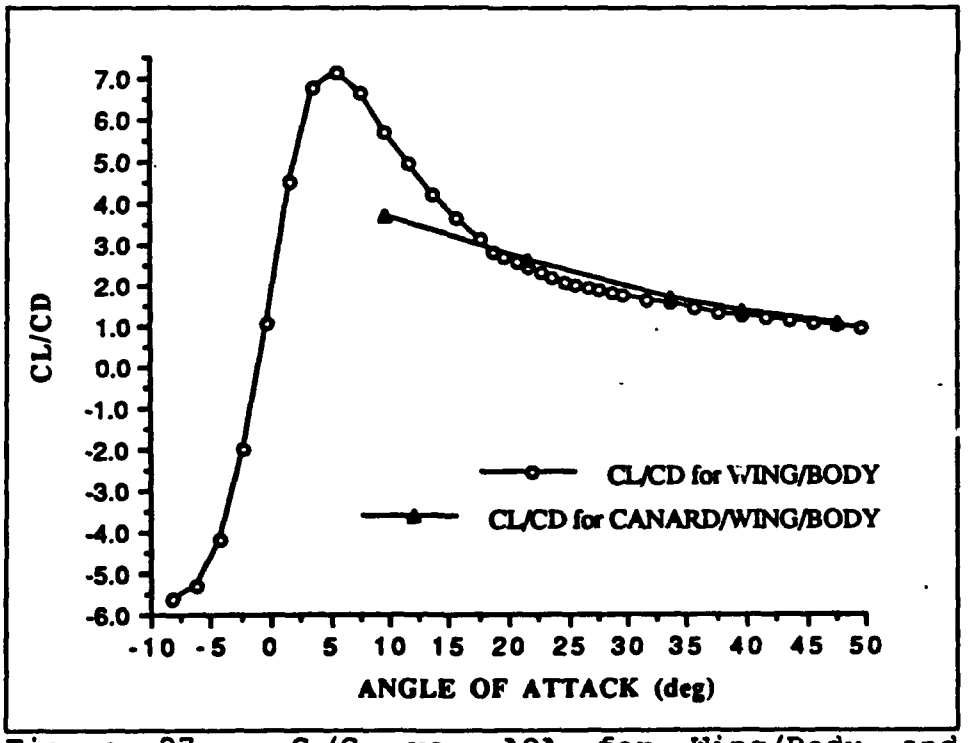

Figure 27. C_L/C_D vs. AOA for Wing/Body and Canard/Wing/Body

Figure 28 shows the variation of the canard absolute AOA for maximum lift of the canard/wing/body configuration with the wing/body AOA. The canard absolute AOA was measured with respect to the freestream velocity, as opposed to the fuselage reference line. The average canard absolute AOA for wing/body angles of attack of 10, 22, 34, and 40 degrees was 26.8

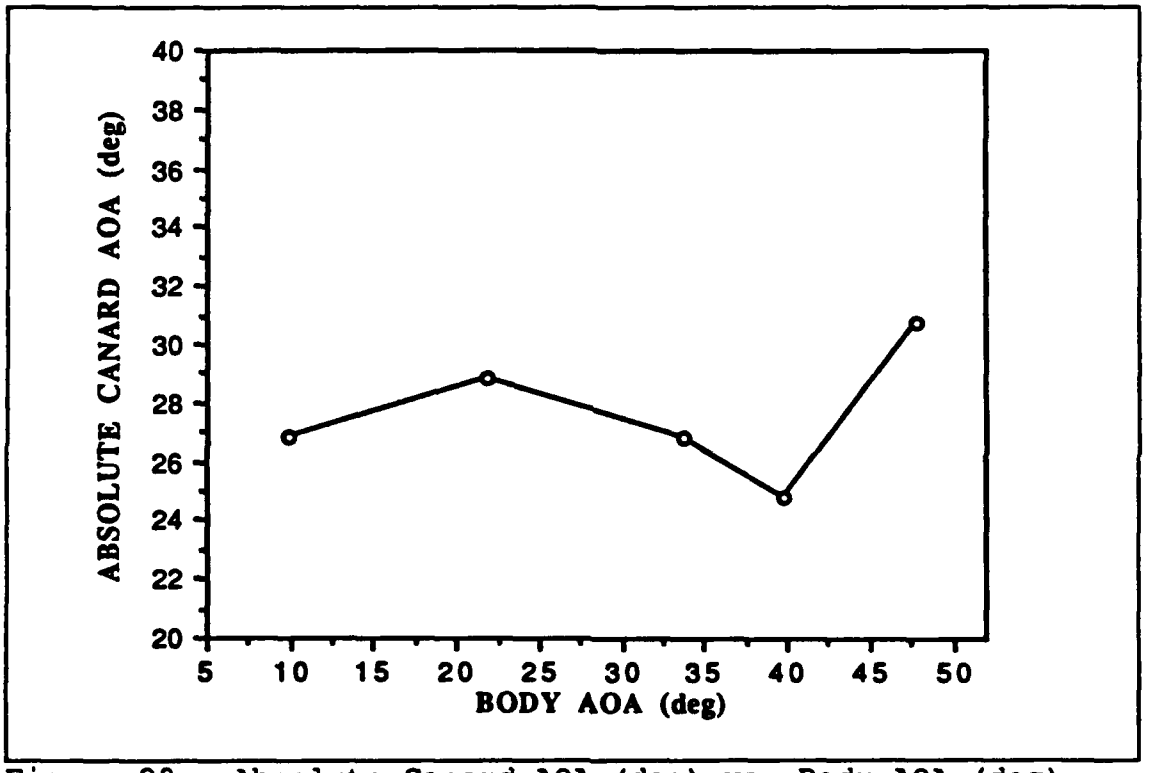

Figure 28. Absolute Canard AOA (deg) vs. Body AOA (deg)

degrees. The canard absolute AOA varied only by +/- 2 degrees across the wing/body angle-of-attack range. At a wing/body AOA of 48 degrees, the canard absolute AOA was 30.8 degrees, 4 degrees greater than the previous average. The C_L versus canard deflection angle plot for the 48-degree wing/body AOA, Figure 22, indicates that a canard deflection angle of -20

degrees could have been chosen, vice -25 degrees, as the canard deflection angle that nearly maximized lift. This choice would have resulted in an canard absolute AOA of 28 degrees which is much closer to the average canard absolute AOA, for the wing/body angles of attack of 10, 22, 34, and 40 degrees, of 26.8 degrees. It appears, then, that the absolute canard angle of attack to maximize lift enhancement is relatively constant and independent of the wing/body AOA.

IV. CONCLUSIONS AND RECOMMENDATIONS

A baseline study to find the lift and drag characteristics of a low-aspect-ratio wing/body configuration across an angle-of-attack range of -8 to 50 degrees was conducted. A further study to find the comparative lift enhancement using the same wing/body and a close-coupled canard for wing/body angles of attack of 10, 22, 34, 40, and 48 degrees and canard deflection angles from -25 to 25 degrees was carried out. The following conclusions were reached:

(1) With a canard properly located longitudinally and horizontally, lift was enhanced at all tested wing/body angles of attack when compared to the baseline configuration.

(2) The comparative lift increase using a canard deflection angle that maximized lift was the most dramatic at or near the stall conditions for the wing/body alone case. At a wing/body AOA of 22 degrees, where the first stall occurred, the lift was increased 34% over the baseline value. At a wing/body AOA of 48 degrees, where the second stall occurred, the lift was increased 18.3% over the baseline value. These increases in the lift are thought to be due to the vortex of the canard constructively interfering with the main-wing vortex, thereby delaying the onset of flow separation. Note that these enhancements already take into account the lift due to increased reference area.

(3) Using a canard, the lift was increased by only 3.4% for a wing/body AOA of 10 degrees. Lacey's earlier work anticipated this result. Lacey showed that for angles of attack less the 18 degrees unfavorable interference occurred between the canard and wing, and little if any lift enhancement could be expected [Ref. 6].

(4) Lift was not enhanced for all canard deflection angles, which varied between -25 and 25 degrees in this study. In general, to maximize the lift the canard absolute angle of attack, measured with respect to the freestream velocity, should be about 27 degrees for the tested configuration. The canard deflection-angle range over which lift was enhanced was very much wing/body AOA dependent. As the angle of attack increased, the band of canard deflection angles that lead to lift enhancement widened, but at an AOA of 10 degrees this band was quite narrow.

(5) If it is desired to avoid the potential weight and complexity of a moveable canard system, fixing the canard at a -5 degree deflection angle significantly improved lift at all but the lowest wing/body angles of attack. At an AOA of 48 degrees, the lift was only 3% less than the maximum lift using a moveable canard.

(6) Using a close-coupled canard improved the C_L/C_D ratio at all angles of attack except at 10 degrees. The canard did cause a significant penalty of 34.5% in the C_L/C_D ratio at an AOA of 10 degrees. It should be noted that at

this cruise flight condition, where the AOA of the wing is small, the AOA of the canard is required to be large. The drag penalty is due to the high induced drag of the canard. At these cruise conditions, a high-AOA lifting canard could not be trimmed, and use of the canard is a poor way to achieve an enhanced lift. At this high-speed condition, a more likely situation would be to set the canard at a neutral AOA and use only the main wing for lift. In this case, only the main wing would be used as the reference area, and a more reasonable lift coefficient could be achieved with little drag penalty. In other words, the canard is only used at high angles of attack, and the apparent penalty at cruise conditions is provided by an unrealistic situation.

Recommendations for future experimental research are:

(1) Conduct flow visualization tests of the wing/body and canard/wing/body configuration to qualify and compare flowfields about the model at angles of attack of 10, 22, 34, 40, and 48 degrees, and to study the surface flow separation and reattachment effects. Perform wake surveys with a five-hole probe at chosen angles of attack, with and without the canard at best deflection angle, to map the location and strength of the vortices.

(2) Conduct a further study using an oscillating canard and the same reflection plane tunnel balance, model and wing/body angles of attack for comparison to the static canard configuration.

This thesis has shown that a properly located close-coupled canard can greatly enhance lift at high angles of attack with no drag penalty when compared to a wing/body configuration. If it is desired to perhaps more elegantly enhance lift at higher angles of attack and avoid some of the pitfalls associated with thrust vectoring -- such as the expense, weight penalty, and excessive fuel consumption -- the use of a close-coupled canard may be an excellent choice.

APPENDIX A. MODEL DESIGN

The previous work of Lacey and others was used to set many of the design parameters of the canard/wing model. Lacey used a canard-area-to-wing-area ratio of 0.20, where the areas were referenced to the centerline of the fuselage. It was necessary that the body of the model used in this design be larger than that used by Lacey to allow for adequate instrumentation space for the canard-moving mechanism. Had a similar area ratio to Lacey's been used, an exposed canard area that was much smaller than Lacey's would have resulted. Accordingly, an exposed-canard-area-to-wing area (referenced to the centerline of the fuselage) ratio of 0.20 was chosen, which compared favorably to Lacey's ratio of 0.13. [Ref.6]

Aspect ratios of 2 for the canard and 3 for the wing were used, based upon the earlier work of Behrbohm. A leading edge sweep of 60 degrees for the canard and 50 degrees for the main wing were used to ensure strong leading edge vortices for lift enhancement. The canard and wing were straight-tapered and taper ratios of .1 and .15 respectively were chosen based upon existing aircraft designs. Equations (9), (10), and (11) were used to derive the dimensions of the planforms. [Ref. 19]

$$AR = 2\frac{b}{C_r(1 + \lambda)} \qquad (9)$$

$$AR = \frac{b^2}{S} \tag{10}$$

$$MAC = \frac{2}{3}\left(C_r + C_t - \frac{C_r C_t}{C_r + C_t}\right) \tag{11}$$

Where:

AR	Aspect Ratio
b	Span
C_r	Length of root chord
C_t	Length of tip chord
λ	Taper ratio C_t/C_r
S	Area of wing or canard
MAC	Wing mean aerodynamic chord

The airfoil section NACA 64A008 was chosen for the wing and canard based upon Lacey's previous work. Er-El and Seginer used flat plates for the canard and wing of their model which resulted in sharp leading edges for the wing and the canard [Ref. 9]. A rounded leading edge for the wing and canard was used in this design to more closely model what is found on a number of existing aircraft. No attempt was made to trip the boundary layer. The Reynolds number based on the wing mean aerodynamic chord was 9.5×10^5.

The location of the canard with respect to the wing was a critical dimension. If the canard was positioned too far away or too close, there would be no lift enhancement or even

possibly a lift degradation. The 40-percent exposed root chord of the canard and the quarter-chord of the wing with respect to the centerline of the fuselage were the reference points used for the longitudinal separation of the canard and wing. The ratio of the longitudinal separation of the canard and wing, x/c_{mac}, should be no greater than 1.5; yet, the canard and wing surfaces should not overlap. Correspondingly, an $x/c_{mac} = 1.2$ was chosen which resulted in a 2.33-inch separation between the exposed trailing edge of the canard and the exposed leading edge of the wing. Vertically the canard was positioned so that the non-dimensional distance of the canard above the wing, z/c_{mac}, equaled 0.2. A value of $z/c_{mac} = 0.2$ resulted in a 1.9-inch separation between the canard and wing. The pivot point of the canard was 40 percent of the exposed root chord. The pivot point of the balance was 17.18 inches from the tip of the model. [Ref. 6]

The model's length of 36 inches, width of 4.5 inches, height of 3 inches, and semi-span, measured from the reflection plane to the wingtip, of 12.1 inches ensured that the balance would be loaded by large forces while the tunnel was in operation. The size of the model also allowed for adequate space for the canard positioning motor. Initially it was thought that the canard would be driven by remote radio control. It was found that the servo mechanism was unable to hold the canard in position at a tunnel ΔP of 17 cm H_2O. A lead screw mechanism with electric motor was then designed and

built by lab personnel to positively control the canard at all tunnel ΔP's. The electric cabling for the model lead through a hole in the model base plate and balance assembly to a controller outside the tunnel. The canard was deflected using the controller and a variable power supply. Lines drawn on the canard section body allowed the canard to be accurately aligned. Figure 29 gives the geometric characteristics for the canard and wing. Figures 30 through 36 show the model and canard positioning motor.

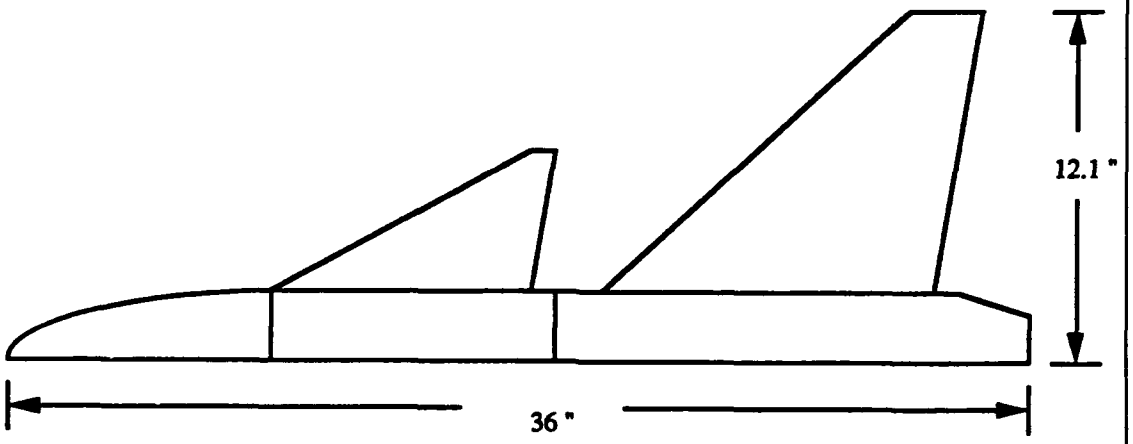

	WING	CANARD
Airfoil Section (NACA)	64A008	64A008
Area (semi-span), in^2		
Projected Area	97.9	50.7
Exposed Area	59.6	19.3
Exposed Semi-Span, inches	9.1	4.4
Semi-Span, inches (centerline)	12.1	7.4
Chord, inches		
Root (centerline)	14	13.3
Root (exposed)	11	8
Tip	2.1	0.8
Aspect Ratio	3	2
Taper Ratio	0.15	0.1
Sweepback Angle, degrees		
Leading Edge	50	60
Trailing Edge	10.6	5.5
Incidence Angle, degrees	0	-
Dihedral Angle, degrees	0	0
Twist Angle, degrees	0	-

Figure 29. Model Geometric Characteristics

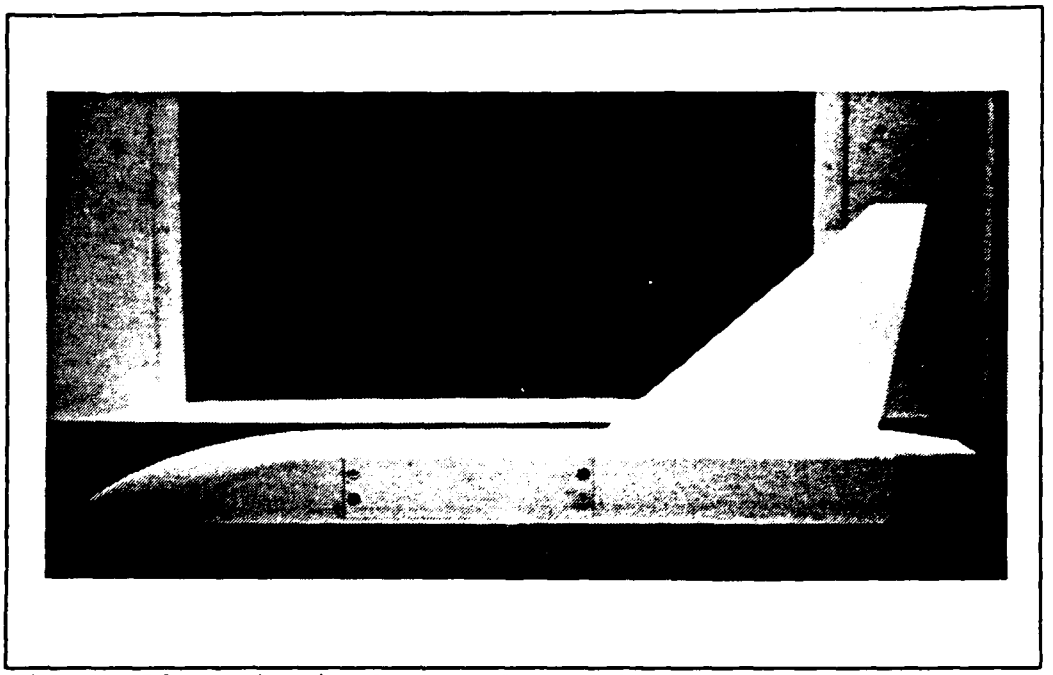

Figure 30. Wing/Body; Left-Hand Side View

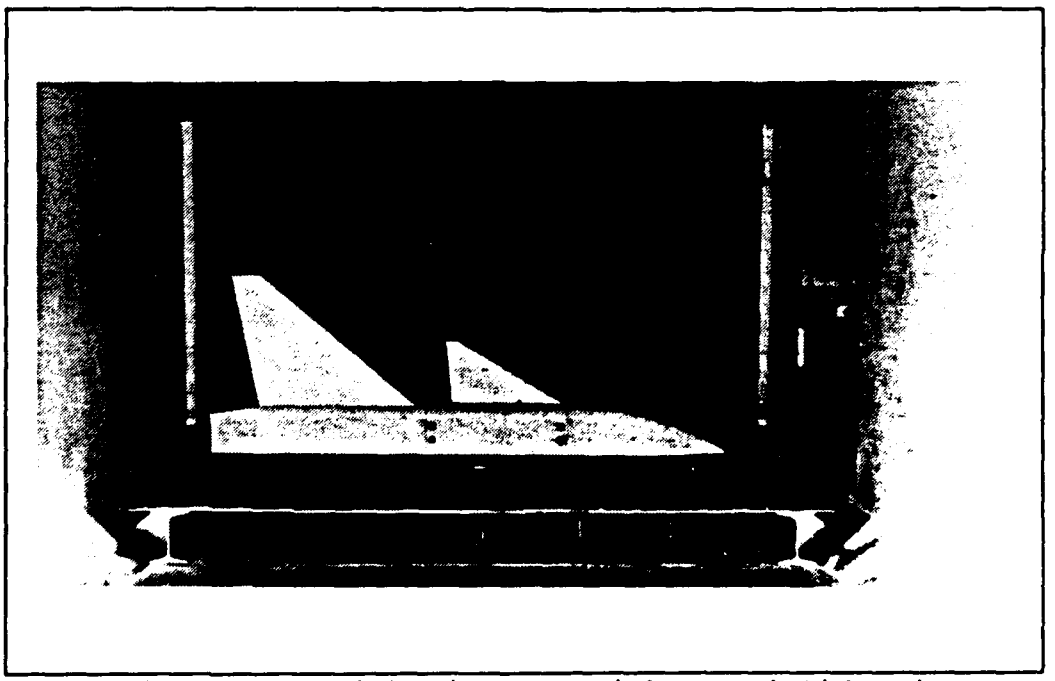

Figure 31. Canard/Wing/Body; Right-Hand Side View

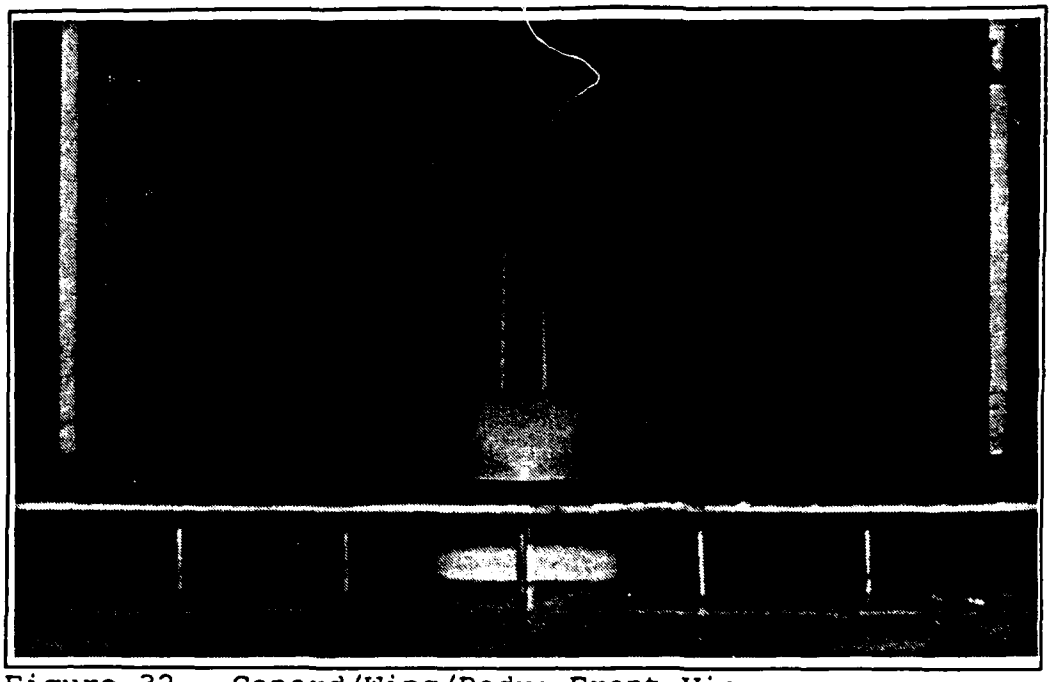

Figure 32. Canard/Wing/Body; Front View

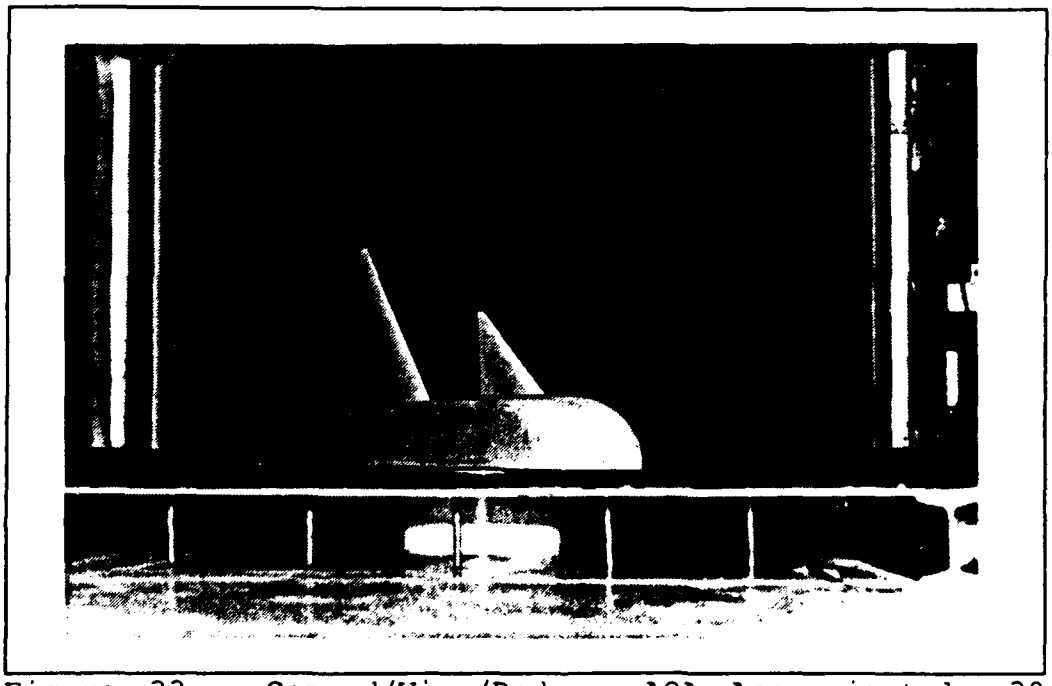

Figure 33. Canard/Wing/Body; AOA Approximately 30 Degrees

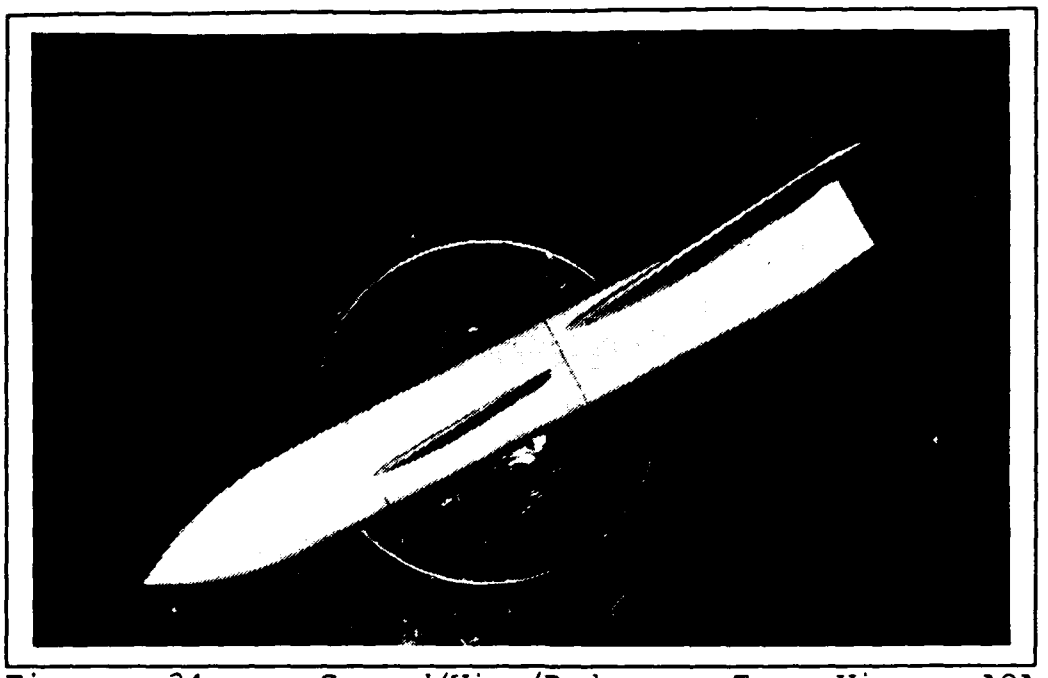

Figure 34. Canard/Wing/Body; Top View, AOA Approximately 30 Degrees

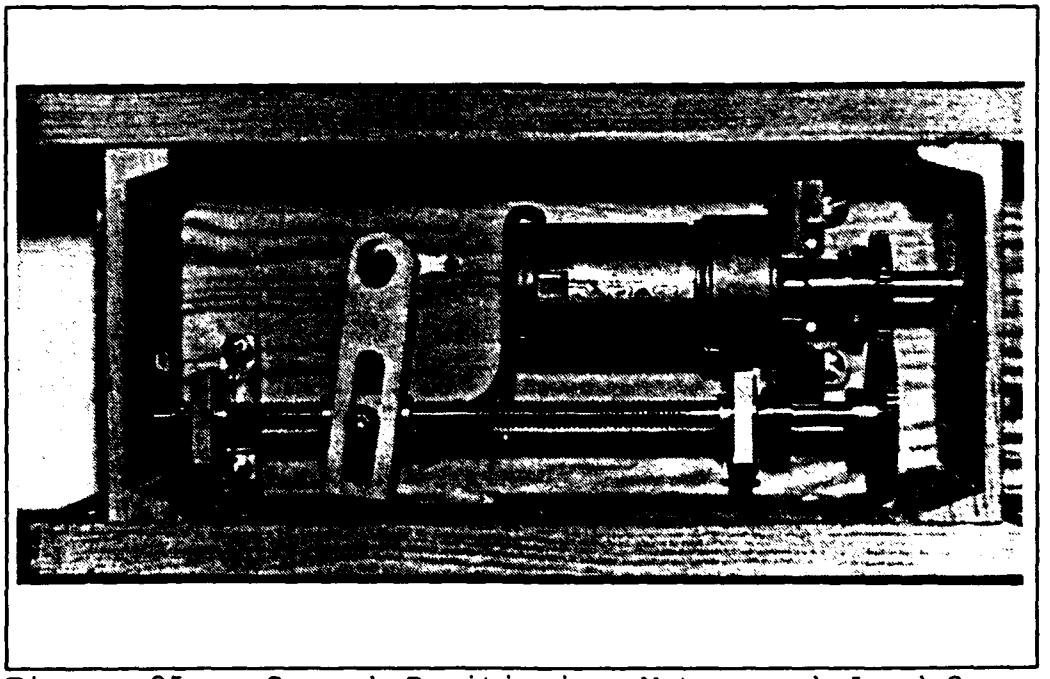

Figure 35. Canard Positioning Motor and Lead-Screw Mechanism

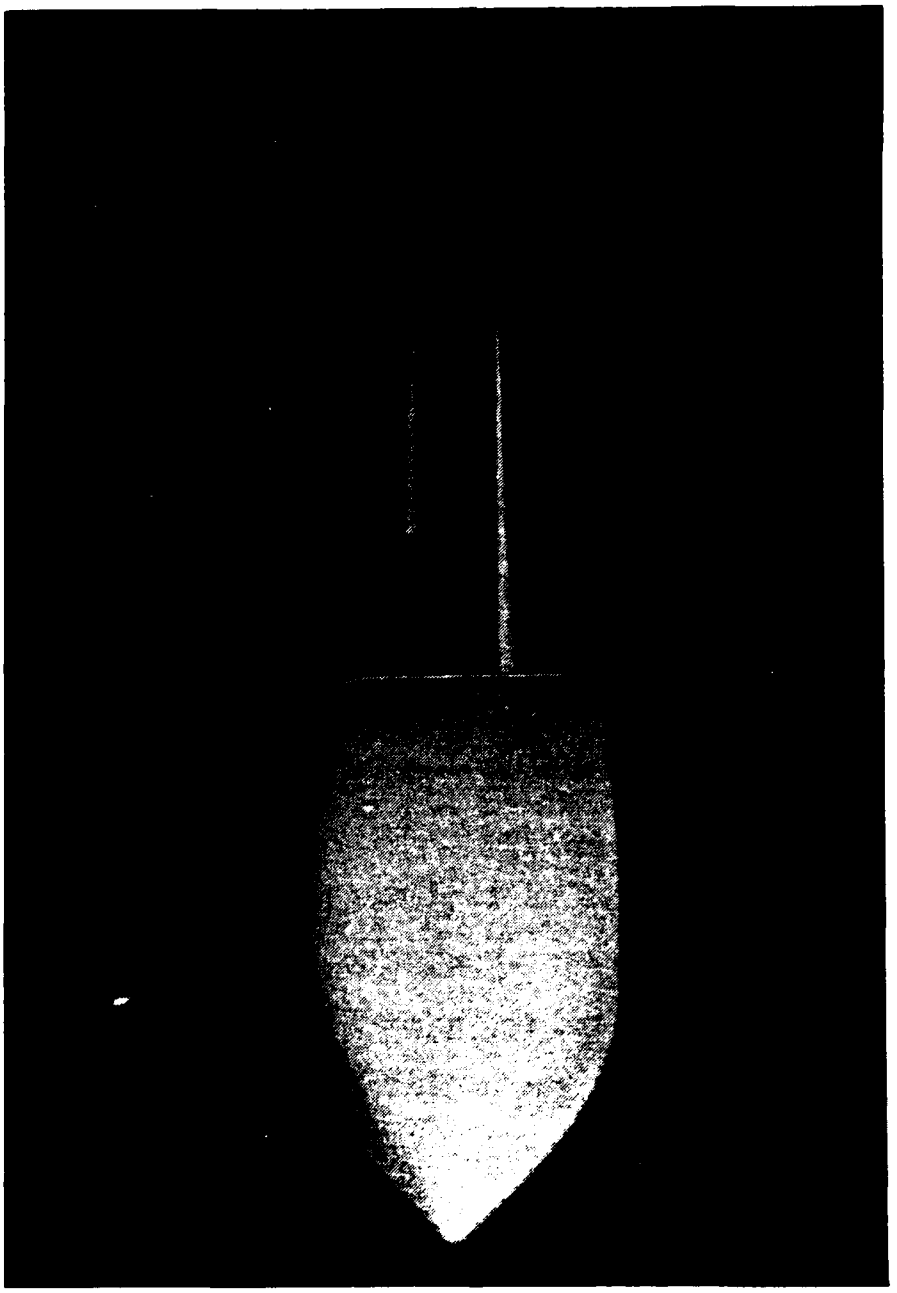

Figure 36. Canard/Wing/Body; Front View

APPENDIX B. BALANCE CALIBRATION

The external strain-gage balance used was built to facilitate the measurement of normal and axial forces and pitching moment in the NPS low speed wind tunnel. Each external strain-gage bridge had four active legs for automatic temperature compensation. The normal and axial moments were measured by two orthogonal strain-gage bridges cemented on the balance column at positions A and B separated by a vertical distance of 26.5 inches, as shown in Figure 37. With the wind tunnel in operation the force and moment on the model created a different moment on the upper, bridge B, and the lower, bridge A, strain-gage bridges. Once the balance was accurately calibrated, the voltage outputs from the lower and upper normal or axial bridges could be converted to moments and subtracted from one another, then divided by the vertical separation of the bridges to find the normal or axial force. Figure 38 shows a photograph of the balance and rotating mechanism used to calculate the normal and axial forces and to position the model at various angles of attack. Figures 39 to 41 show the wiring for the strain-gage bridges.

The sign conventions used for the normal and axial forces are shown in Figure 42. Balance nomenclature is as follows. E_{AN} was the voltage output from the lower normal force

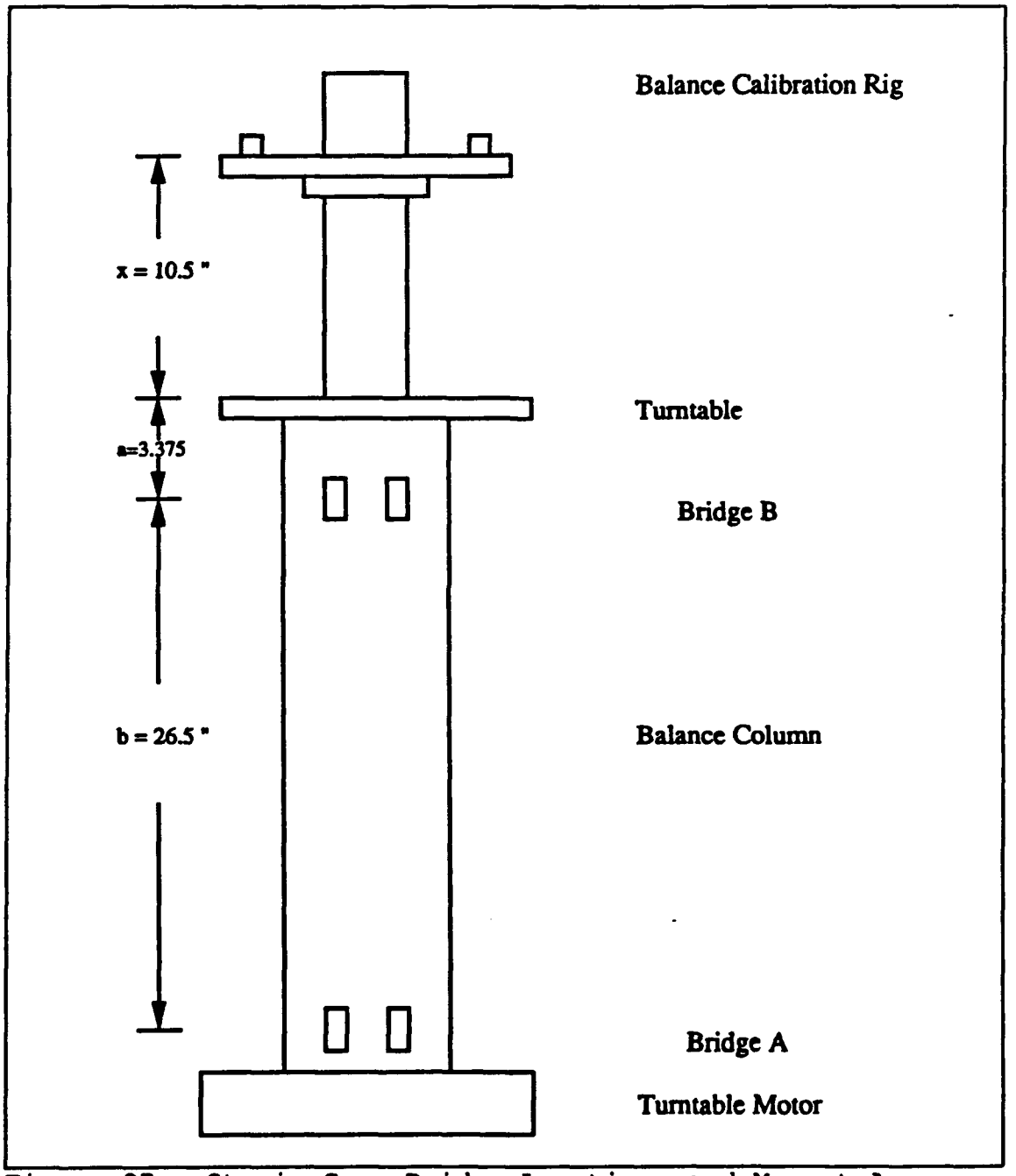

Figure 37. Strain-Gage Bridge Locations and Moment Arms

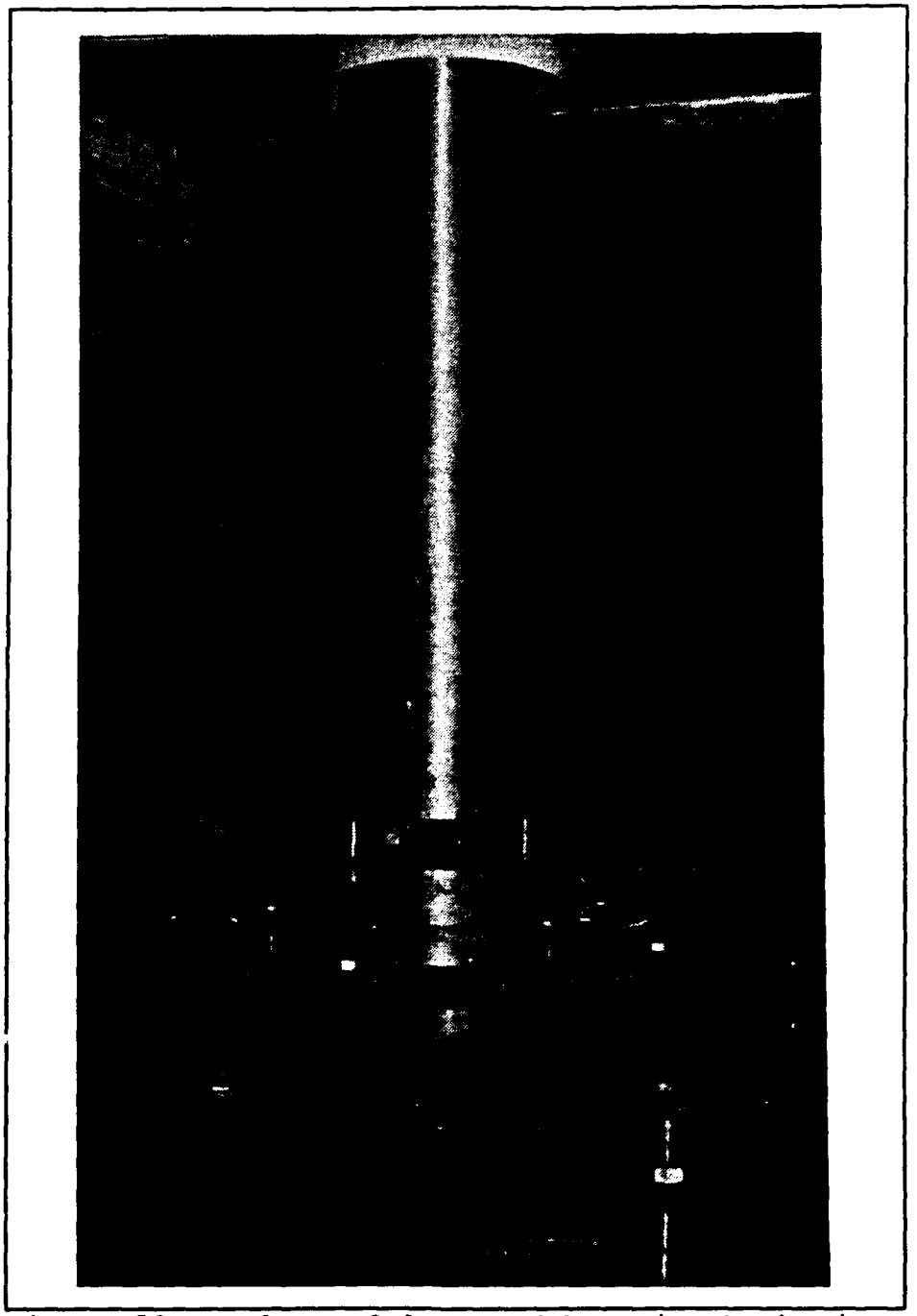

Figure 38. Balance Column and Rotating Mechanism

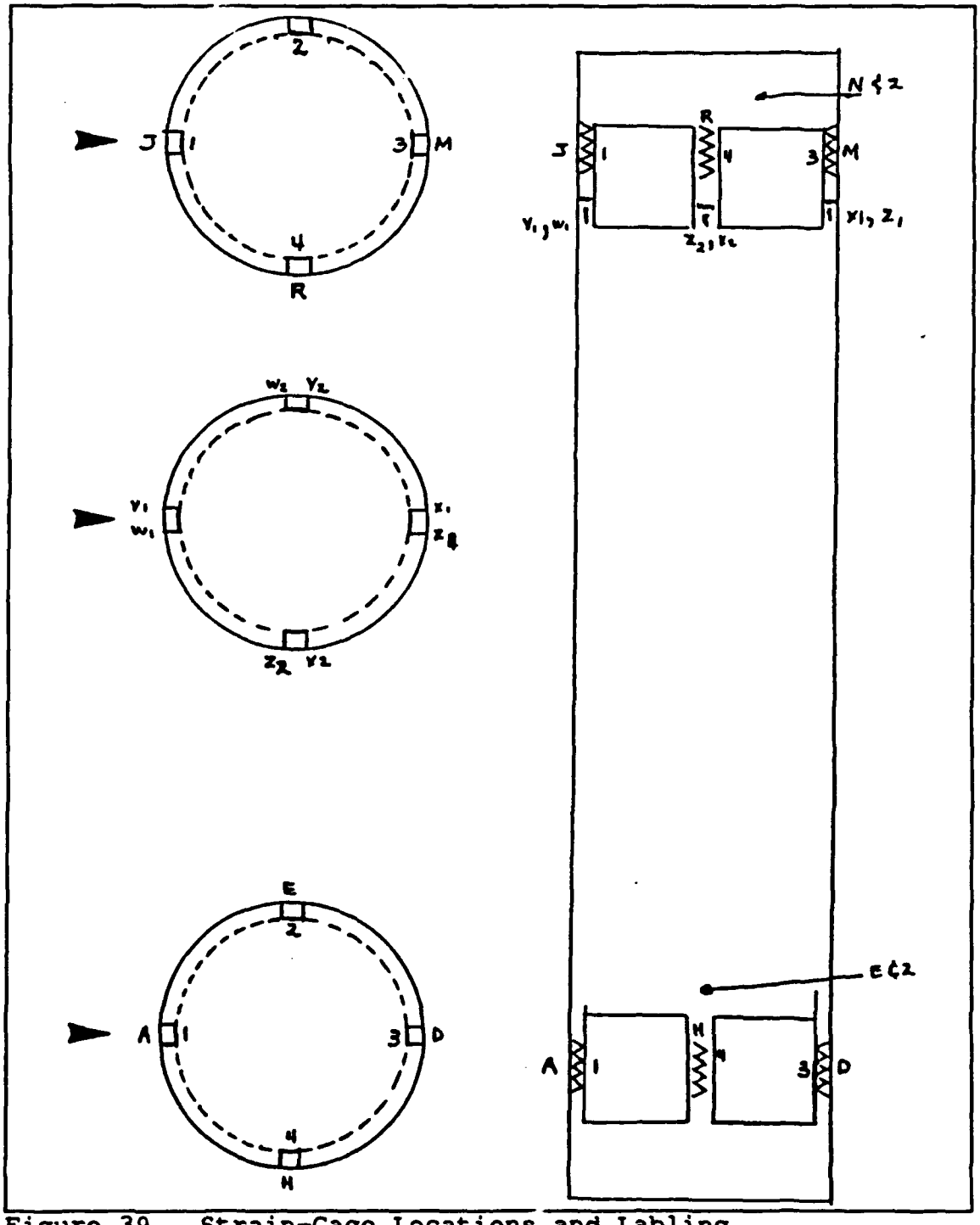

Figure 39. Strain-Gage Locations and Labling

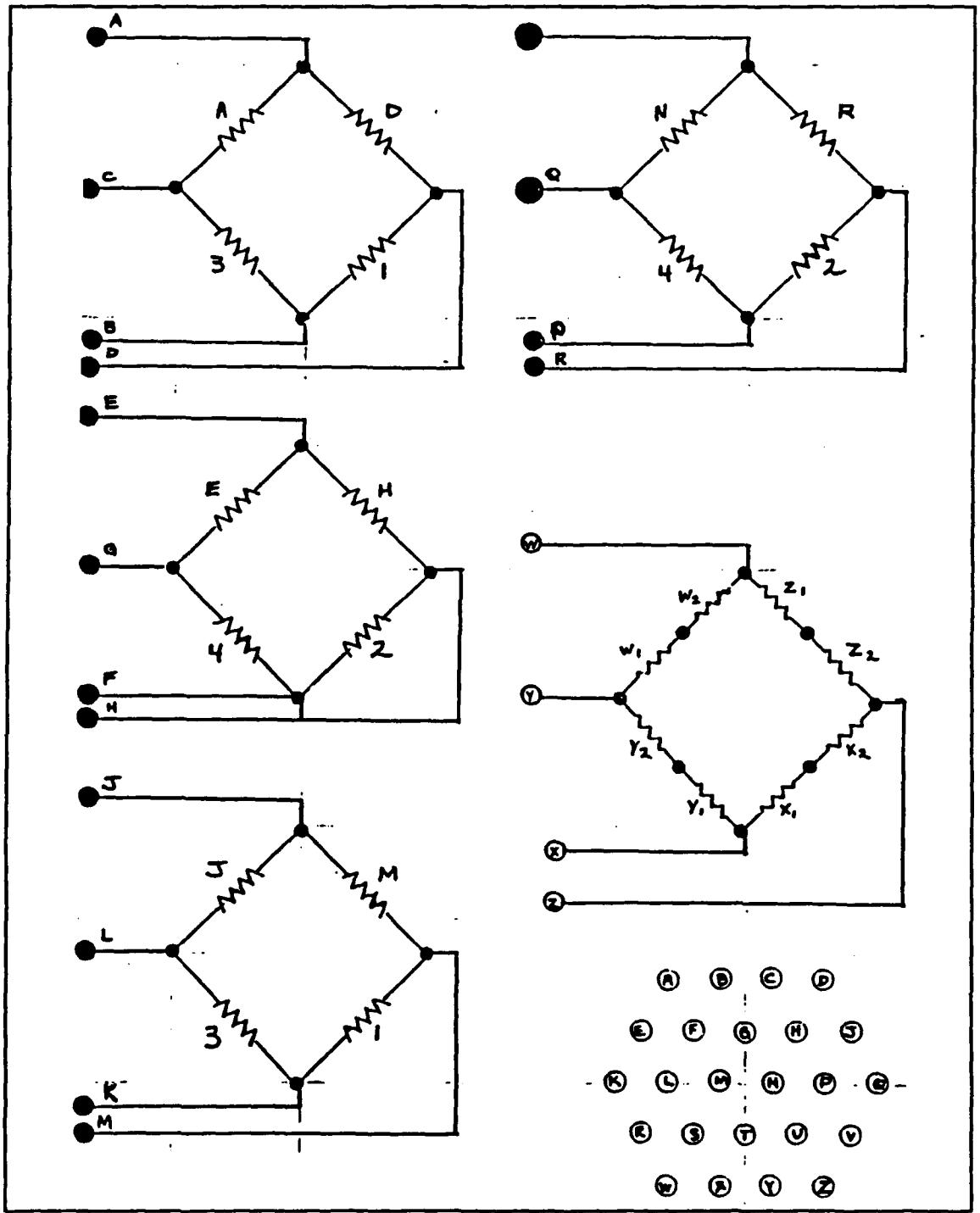

Figure 40. Strain-Gage Bridges and Canon Plug

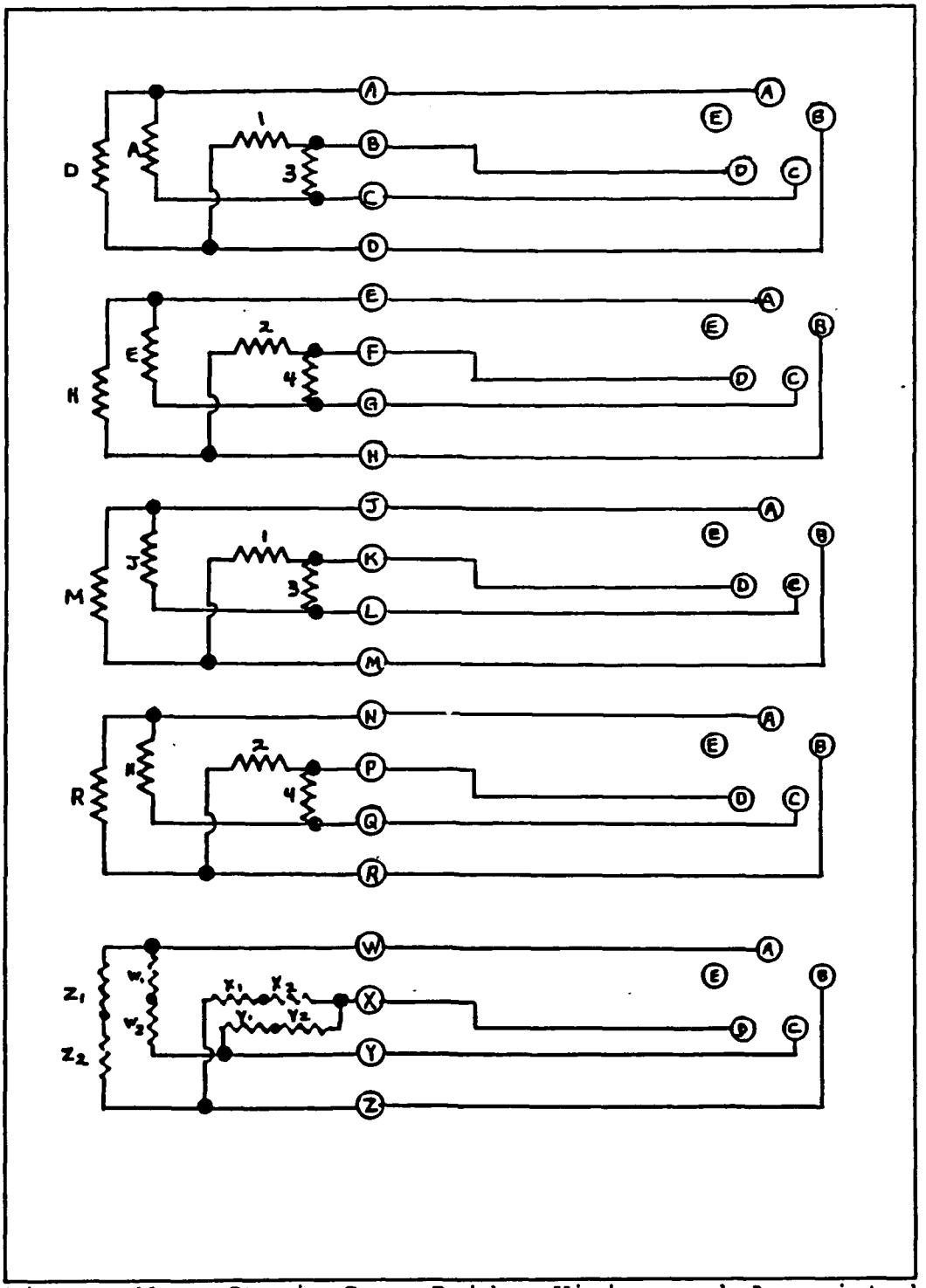

Figure 41. Strain-Gage Bridge Wiring and Associated Canon Plugs that Connect to the Signal Conditioners

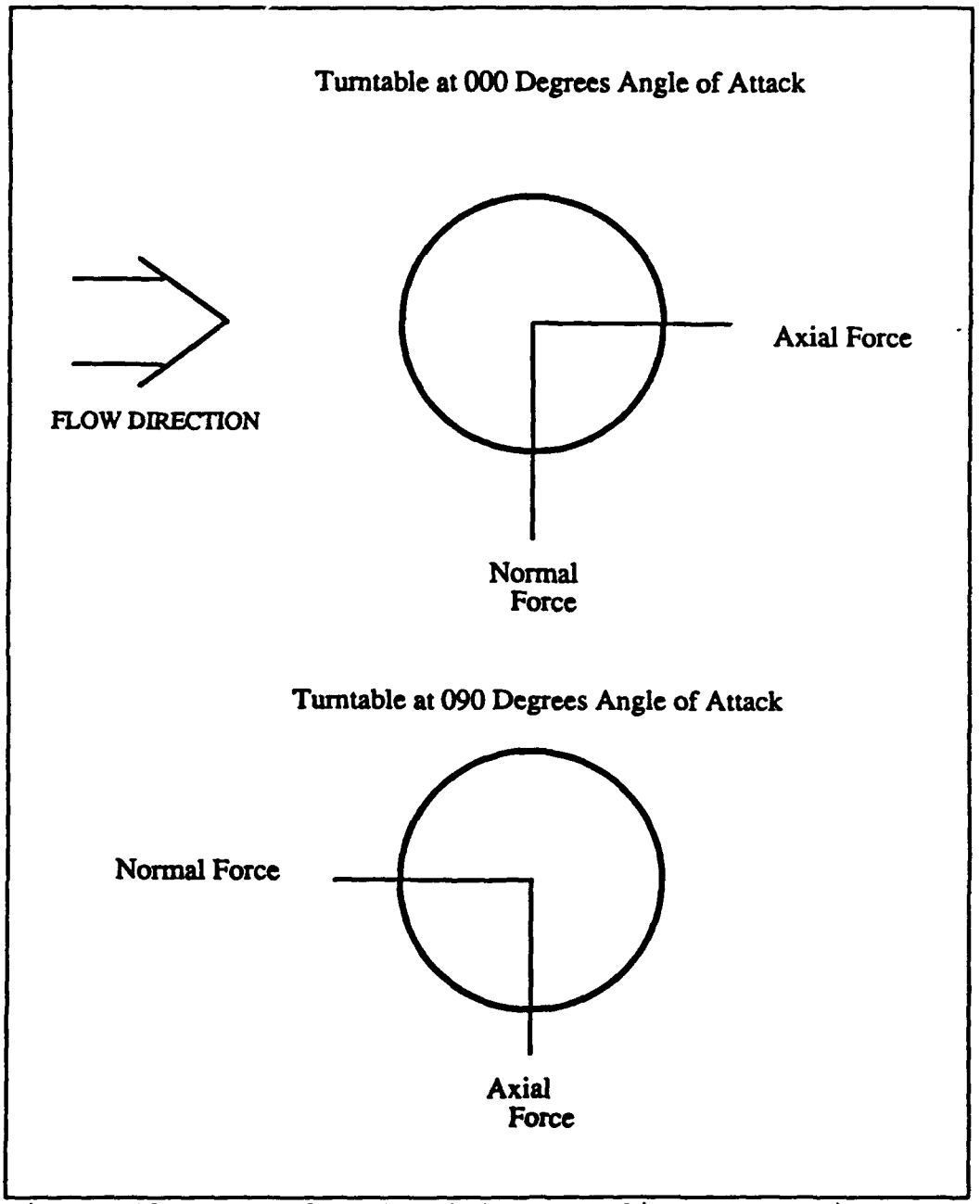

Figure 42. Normal and Axial Force Sign Conventions

strain-gage bridge and E_{AA} was the voltage output from the lower axial bridge. Additionally, E_{BN} was the voltage output from the upper normal bridge and E_{BA} was the voltage output from the upper axial bridge. The letter "a" is the vertical distance between the upper bridge and the base of the calibration rig of 3.375 inches. The letter "x" represents the vertical distance between the base of the calibration rig and the attachment point of the cable to the rig of 10.5 inches. The letter "b" is the vertical distance between the upper and lower strain-gage bridges of 26.5 inches.

Equations (12) and (13) are the basic equations used to find the normal and axial moments on the balance at the lower and upper bridge positions. For equation (12), the electri-

$$\begin{vmatrix} E_{AN} \\ E_{AA} \end{vmatrix} = \begin{vmatrix} A_{11} & A_{12} \\ A_{21} & A_{22} \end{vmatrix} \begin{vmatrix} M_{AN} \\ M_{AA} \end{vmatrix} \qquad (12)$$

$$\begin{vmatrix} E_{BN} \\ E_{BA} \end{vmatrix} = \begin{vmatrix} B_{11} & B_{12} \\ B_{21} & B_{22} \end{vmatrix} \begin{vmatrix} M_{BN} \\ M_{BA} \end{vmatrix} \qquad (13)$$

cal output in volts at the lower normal and axial strain-gage bridges, bridge location A, equalled a coefficient matrix, A, multiplied by a moment matrix in ft-lbs for the lower bridge that consisted of normal and axial components. For equation (13), the electrical output at the upper normal and axial strain-gage bridges, bridge location B, equalled a coefficient matrix, B, multiplied by a moment matrix for the upper bridge that consisted of a normal and axial component. The

coefficient matrices were found by calibrating the balance with known weights. In general, the diagonal components of the A and B coefficient matrices, A_{11}, A_{22}, B_{11}, and B_{22}, were larger than the off-diagonal components by at least one or two orders of magnitude. The off-diagonal components were due to the slight misalignment of the strain gages which caused interaction between them. Under ideal conditions, the off-diagonal components are close to zero. In general, balance interactions are due to misalignment of the balance or plastic deformation of the balance [Ref. 18]. Balance misalignment causes a linear or first degree error whereas balance plastic deformation would cause a second order or non-linear error [Ref. 18]. The calibration procedure used only corrected for misalignment of the strain gages, for the balance was never plastically deformed. Equations (14) through (17) were used during the calibration to calculate axial and normal moments at the upper and lower bridges, using the moment arms a, b, and x.

$$M_{AN} = Normal\ Force(b + a + x) \tag{14}$$

$$M_{AA} = Axial\ Force(b + a + x) \tag{15}$$

$$M_{BN} = Normal\ Force(a + x) \tag{16}$$

$$M_{BA} = Axial\ Force(a + x) \quad (17)$$

Before the balance could be calibrated a loading rig had to be designed. One of the main requirements was that it be very rigid to preclude any chance of elastic or plastic deformation of the rig. Secondly, it had to have arms that could rotate and move vertically for attaching the cabling and weights so that the balance could be calibrated in various directions with different moment arms. The calibration rig was pulled horizontally using known weights suspended on a cable, stand, and pulley assembly. The calibration rig is shown in Figures 43 to 45.

Prior to calibrating the balance the span voltages for the bridges were set. They were set by suspending a weight of about 10 lbs from the calibration rig and turning the span voltage adjustment knob for each signal conditioner so that the readout on a Hewlett-Packard digital multimeter was about 1 volt. Once the span voltages were set, they were not altered for the duration of the experiment.

The diagonal components A_{11} and B_{11} were found by rotating the balance to 000 degrees angle of attack for loading the balance in the pure normal direction, then loading successively larger weights in approximately 2-lb increments on the calibration rig and plotting the resultant voltage output versus the weight. Figures 46 and 47 and Table 4 show

plots of the magnitude of voltage output in volts versus weight in pounds and the data used for the plots. The gradients of the voltage versus weight plots, E_{AN}/N and E_{BN}/N, from Figures 46 and 47 respectively, were used in equations (18) and (19) to find the diagonal components A_{11} and B_{11} of the coefficient matrices.

$$A_{11} = \frac{E_{AN}/Normal\ Force}{(b+a+x)} \qquad (18)$$

$$B_{11} = \frac{E_{BN}/Normal\ Force}{(a+x)} \qquad (19)$$

The diagonal components A_{22} and B_{22} were found by rotating the balance to 90 degrees AOA for loading the balance in the pure axial direction, then following a similar procedure to that used to find A_{11} and B_{11}. The gradients used for voltage output versus weight, E_{AA}/A and E_{BA}/A, are found in Figures 48 and 49. Table 5 gives the data used in the plots. The gradients were used in equations (20) and (21) to find the diagonal components A_{22} and B_{22}.

$$A_{22} = \frac{E_{AA}/Axial\ Force}{(b+a+x)} \qquad (20)$$

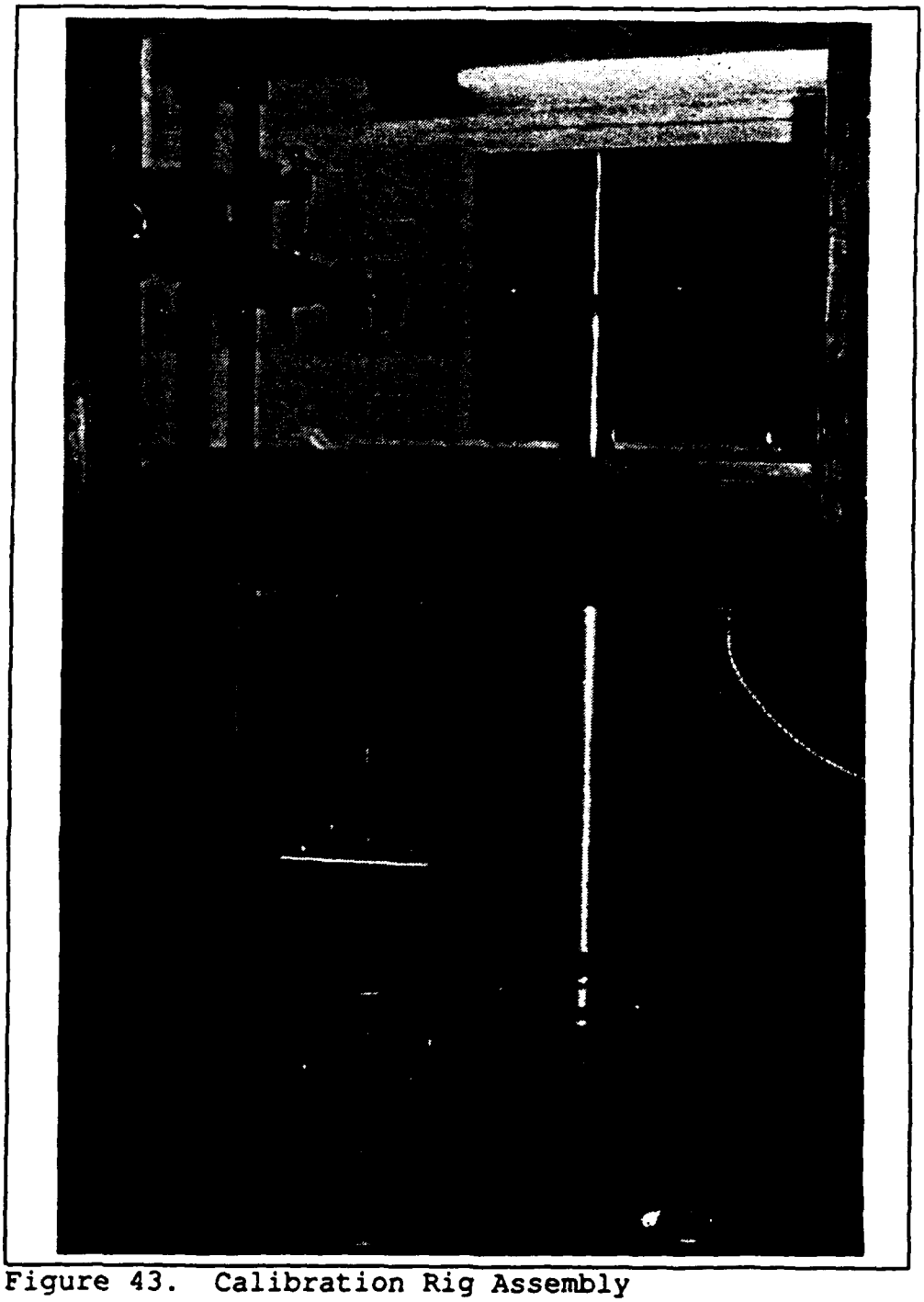

Figure 43. Calibration Rig Assembly

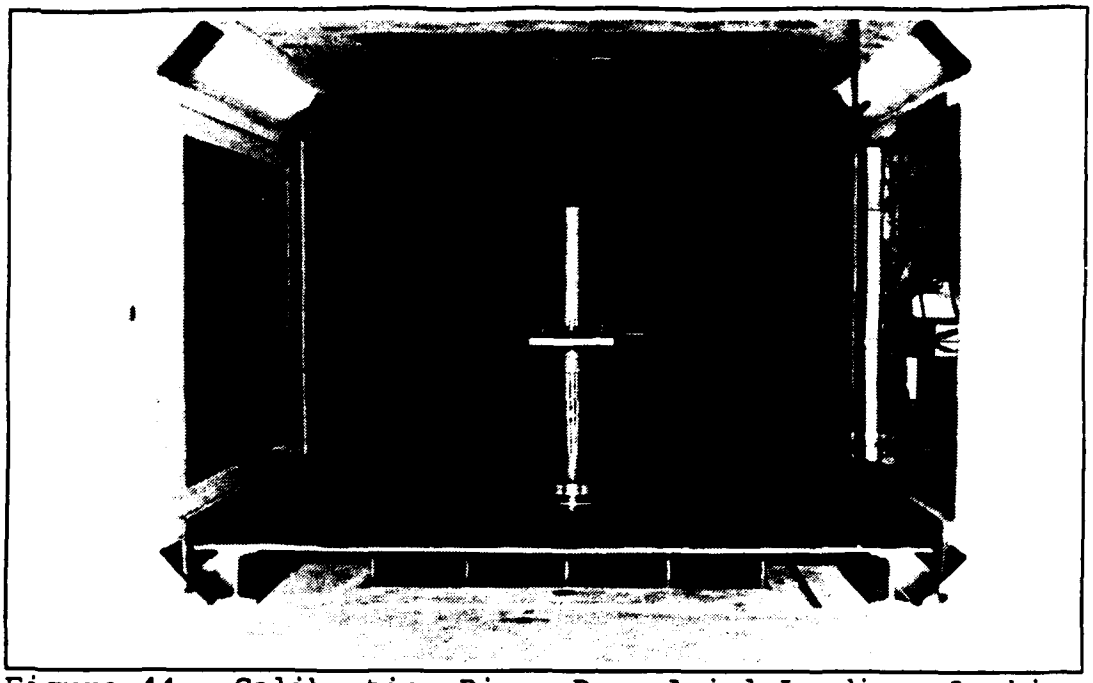

Figure 44. Calibration Rig; Pure Axial Loading, Looking Down Wind Tunnel

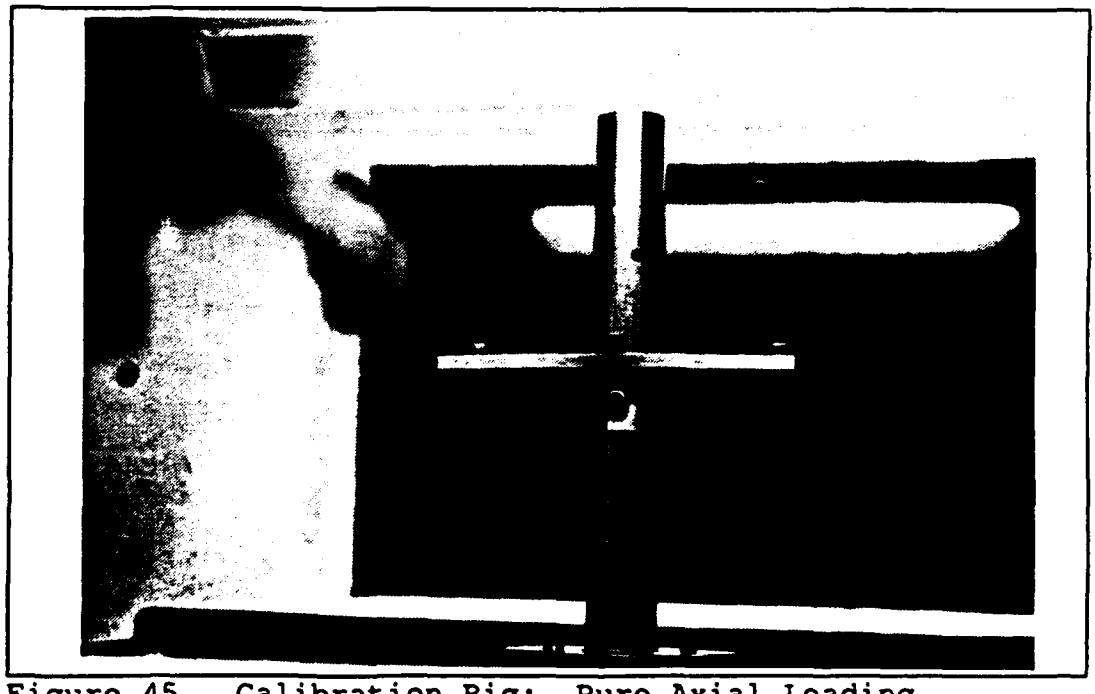

Figure 45. Calibration Rig; Pure Axial Loading

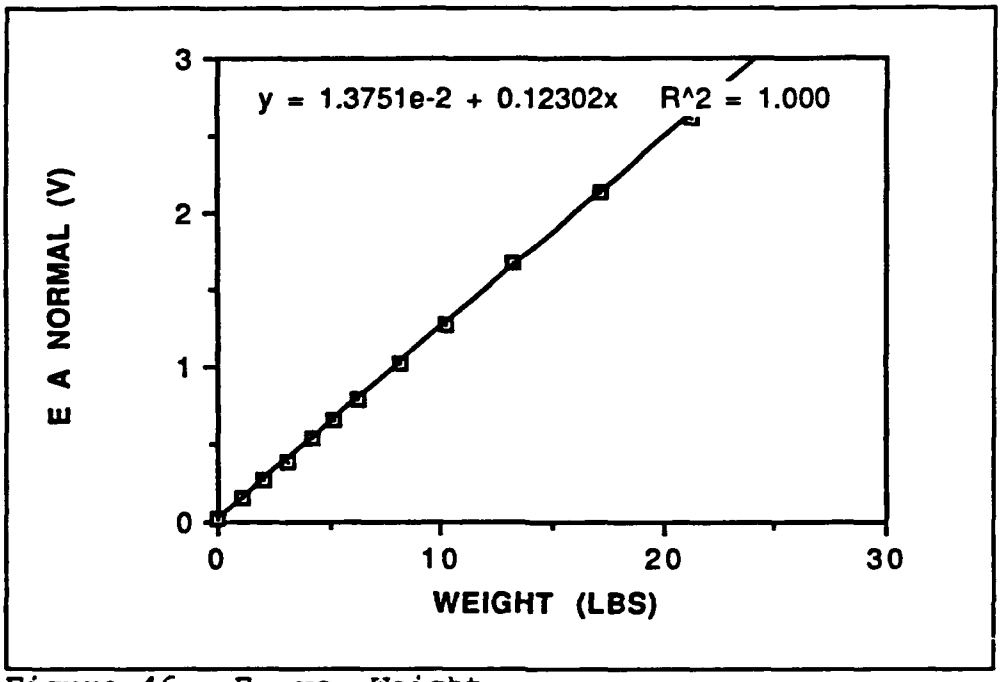

Figure 46. E_{AN} vs. Weight

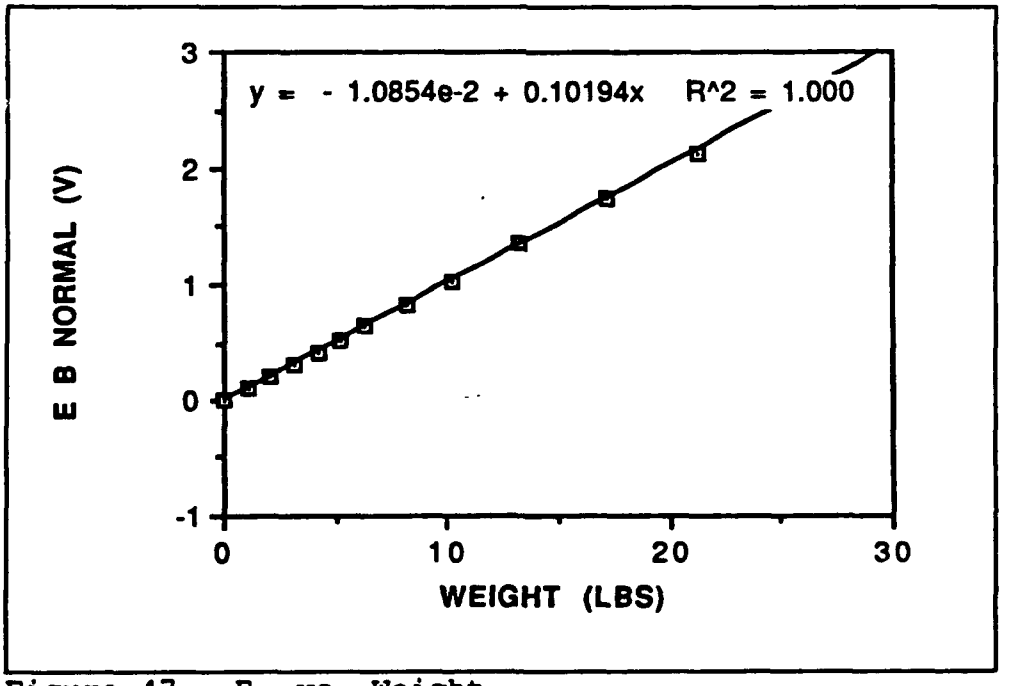

Figure 47. E_{BN} vs. Weight

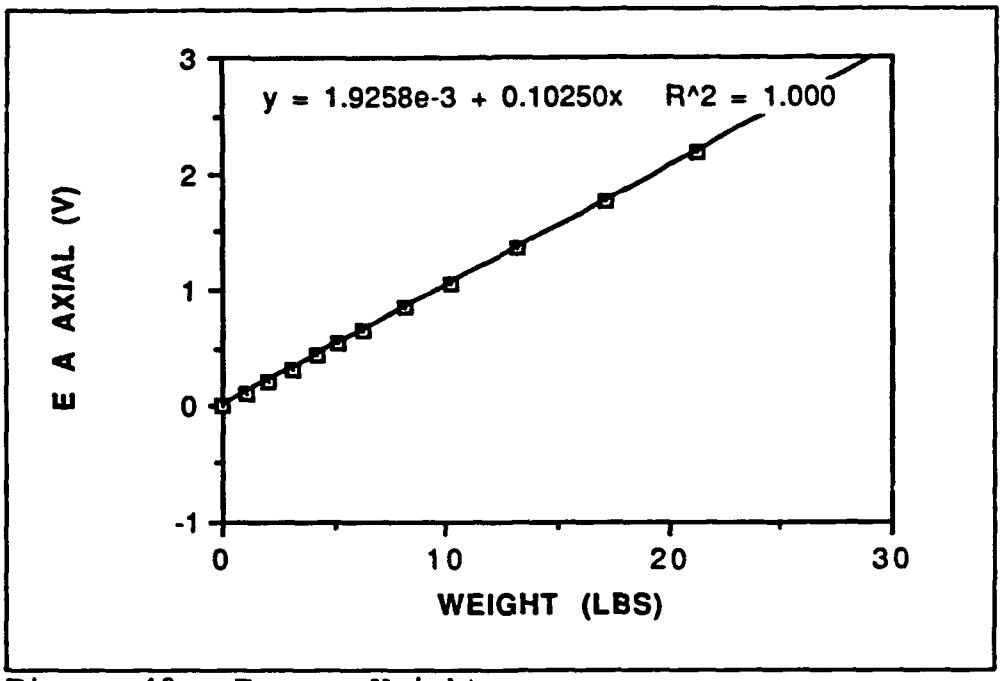

Figure 48. E_{AA} vs. Weight

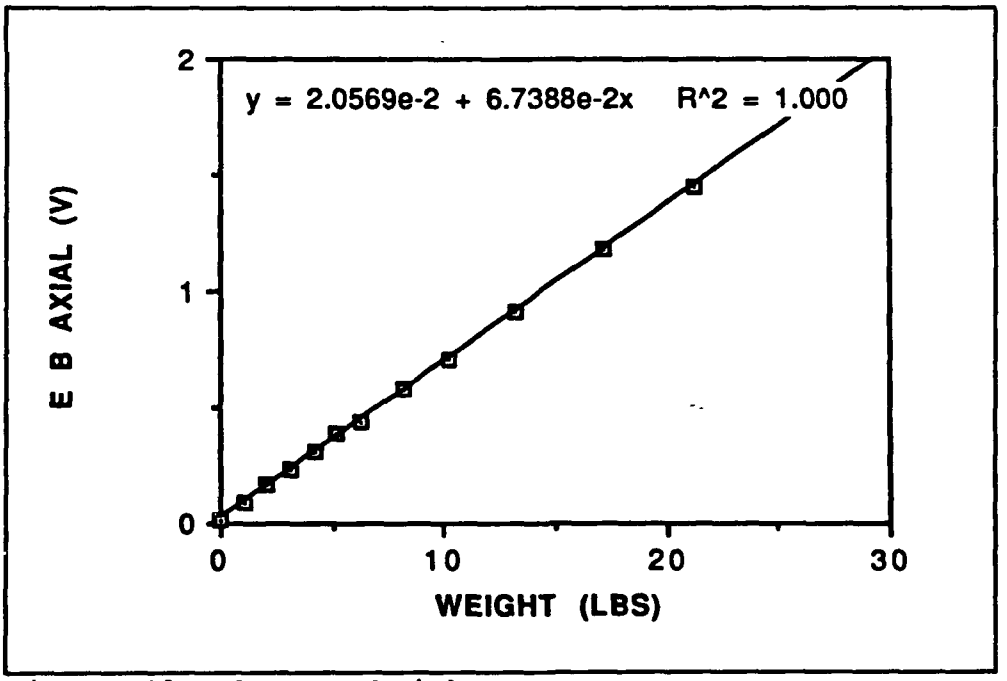

Figure 49. E_{BA} vs. Weight

Table 4. Strain-Gage Bridge Outputs for Pure Normal Forces

WEIGHT (LBS)	EA AXIAL (V)	EB AXIAL (V)	EA NORM (V)	EB NORM (V)
1.0754	-0.005	-0.026	0.146	0.097
2.0714	-0.006	-0.027	0.266	0.199
3.0780	-0.008	-0.029	0.387	0.299
4.2155	-0.010	-0.032	0.535	0.421
5.2144	-0.012	-0.034	0.660	0.520
6.2190	-0.013	-0.037	0.782	0.630
8.2180	-0.017	-0.044	1.013	0.817
10.2215	-0.019	-0.051	1.261	1.025
13.2216	-0.024	-0.063	1.675	1.362
17.2241	-0.032	-0.082	2.139	1.750
21.2328	-0.038	-0.099	2.607	2.139
0.0000	-0.002	-0.028	0.011	-0.012

Table 5. Strain-Gage Bridge Outputs for Pure Axial Forces

WEIGHT (LBS)	EA AXIAL (V)	EB AXIAL (V)	EA NORM (V)	EB NORM (V)
1.0754	0.109	0.092	0.002	-0.004
2.0714	0.215	0.161	0.004	-0.002
3.0780	0.317	0.229	0.005	-0.002
4.2155	0.441	0.309	0.005	-0.002
5.2144	0.549	0.380	0.007	-0.002
6.2190	0.635	0.435	0.008	-0.001
8.2180	0.845	0.577	0.009	-0.001
10.2215	1.039	0.703	0.013	0.000
13.2216	1.352	0.910	0.017	0.000
17.2241	1.770	1.181	0.022	0.001
21.2328	2.181	1.453	0.025	0.003
0.0000	-0.001	0.016	0.000	-0.004

$$B_{22} = \frac{(E_{BA}/Axial\ Force)}{a+x} \qquad (21)$$

The off-diagonal coefficients A_{12}, A_{21}, B_{12}, and B_{21} were found by choosing an angle of attack and a weight for a combined loading,i.e, a turntable angle of attack equal to 55 degrees and a weight of 17 pounds, then using the resultant electrical output and known diagonal coefficients to solve the equation for the off-diagonal coefficient. Equation (22) is an example of solving for an unknown off-diagonal coefficient.

$$A_{12} = \frac{E_{AN} - A_{11}(Normal\ Force)(a+b+x)}{(Axial\ Force)(a+b+x)} \qquad (22)$$

Once all the calibration coefficients were found for the matrices, the A or B matrix was then inverted and an unknown moment out of the normal or axial bridges could be solved for. Equations (23) and (24) are the final calibration matrix equations for the upper and lower strain-gage bridges. To find the normal force, the moment from the upper normal bridge at position B was subtracted from the moment from the lower normal bridge at position A. The result was then divided by b, the distance between the strain-gage bridges. This method subtracted out any residual moment on the model for the determination of moments due solely to normal and axial forces. The axial force was found in a similar fashion. See

equations (25) and (26). The lift and drag were computed using equations (3) and (4) found in the Apparatus section.

$$\begin{vmatrix} M_{AN} \\ M_{AA} \end{vmatrix} = \begin{vmatrix} 27.26281 & -.48797 \\ -.04932 & 32.53814 \end{vmatrix} \begin{vmatrix} E_{AN} \\ E_{AA} \end{vmatrix} \quad (23)$$

$$\begin{vmatrix} M_{BN} \\ M_{BA} \end{vmatrix} = \begin{vmatrix} 11.30306 & -.70957 \\ -.1350659 & 17.25848 \end{vmatrix} \begin{vmatrix} E_{BN} \\ E_{BA} \end{vmatrix} \quad (24)$$

$$Normal\ Force = \frac{M_{AN} - M_{BN}}{b} \quad (25)$$

$$Axial\ Force = \frac{M_{AA} - M_{BA}}{b} \quad (26)$$

APPENDIX C. DATA ACQUISITION PROGRAM

```
0100 'THIS DATA ACQUISTION PROGRAM HAS BEEN MODIFIED BY LT.
YUAN AND LT KERSH
0110 'FOR THE EXTERNAL STRAIN GAGE BALANCE.  THE USER IS
ENCOURAGED TO MODIFY
0120 'THE ORIGINAL PROGRAM, READ.BAS FOR THEIR OWN PURPOSE.
1000 DEF SEG: CLEAR, &HFE00: GOTO 1030          'Begin PCIB
Program Shell
1010 GOTO 2900                  'User program
1020 GOTO 2670                  'Error handling
1030 I=&HFE00                    'Copyright Hewlett-Packard
1984,1985
1040 PCIB.DIR$=ENVIRON$("PCIB")
1050 I$=PCIB.DIR$+"\PCIBILC.BLD"
1060 BLOAD I$,I
1070 CALL I(PCIB.DIR$,I%,J%): PCIB.SEG=I%
1080 IF J%=0 THEN GOTO 1120
1090 PRINT "Unable to load.";
1100 PRINT "   (Error #";J%;")"
1110 END
1120 '
1130 DEF SEG=PCIB.SEG: O.S=5: C.S=10: I.V=15
1140 I.C=20: L.P=25: LD.FILE=30
1150 GET.MEM=35: L.S=40: PANELS=45: DEF.ERR=50
1160 PCIB.ERR$=STRING$(64,32): PCIB.NAME$=STRING$(16,32)
1170 CALL DEF.ERR(PCIB.ERR,PCIB.ERR$,PCIB.NAME$,PCIB.GLBERR):
PCIB.BASERR=255
1180 ON ERROR GOTO 1020
1190 J=-1
1200 I$=PCIB.DIR$+"\PCIB.SYN"
1210 CALL O.S(I$)
1220 IF PCIB.ERR<>0 THEN ERROR PCIB.BASERR
1230 I=0
1     2     4     0                 C     A     L     L
I.V(I,READ.REGISTER,READ.SELFID,DEFINE,INITIALIZE.SYSTEM)
1250 IF PCIB.ERR<>0 THEN ERROR PCIB.BASERR
1     2     6     0                 C     A     L     L
I.V(I,ENABLE.SYSTEM,DISABLE.SYSTEM,INITIALIZE,POWER.ON)
1270 IF PCIB.ERR<>0 THEN ERROR PCIB.BASERR
1280 CALL I.V(I,MEASURE,OUTPUT,START,HALT)
1290 IF PCIB.ERR<>0 THEN ERROR PCIB.BASERR
1     3     0     0                 C     A     L     L
I.V(I,ENABLE.INT.TRIGGER,DISABLE.INT.TRIGGER,ENABLE.OUTPUT,D
ISABLE.OUTPUT)
1310 IF PCIB.ERR<>0 THEN ERROR PCIB.BASERR
1320 CALL I.V(I,CHECK.DONE,GET.STATUS,SET.FUNCTION,SET.RANGE)
```

```
1330 IF PCIB.ERR<>0 THEN ERROR PCIB.BASERR
1340 CALL I.V(I,SET.MODE,WRITE.CAL,READ.CAL,STORE.CAL)
1350 IF PCIB.ERR<>0 THEN ERROR PCIB.BASERR
1360 CALL I.V(I,DELAY,SAVE.SYSTEM,J,J)
1370 IF PCIB.ERR<>0 THEN ERROR PCIB.BASERR
1380 I=1
1390 CALL I.V(I,SET.GATETIME,SET.SAMPLES,SET.SLOPE,SET.SOURCE)
1400 IF PCIB.ERR<>0 THEN ERROR PCIB.BASERR
1410 CALL I.C(I,FREQUENCY,AUTO.FREQ,PERIOD,AUTO.PER)
1420 IF PCIB.ERR<>0 THEN ERROR PCIB.BASERR
1430 CALL I.C(I,INTERVAL,RATIO,TOTALIZE,R100MILLI)
1440 IF PCIB.ERR<>0 THEN ERROR PCIB.BASERR
1450 CALL I.C(I,R1,R10,R100,R1KILO)
1460 IF PCIB.ERR<>0 THEN ERROR PCIB.BASERR
1470 CALL I.C(I,R10MEGA,R100MEGA,CHAN.A,CHAN.B)
1480 IF PCIB.ERR<>0 THEN ERROR PCIB.BASERR
1490 CALL I.C(I,POSITIVE,NEGATIVE,COMN,SEPARATE)
1500 IF PCIB.ERR<>0 THEN ERROR PCIB.BASERR
1510 I=2
1520 I=3
1530 CALL I.V(I,ZERO.OHMS,SET.SPEED,J,J)
1540 IF PCIB.ERR<>0 THEN ERROR PCIB.BASERR
1550 CALL I.C(I,DCVOLTS,ACVOLTS,OHMS,R200MILLI)
1560 IF PCIB.ERR<>0 THEN ERROR PCIB.BASERR
1570 CALL I.C(I,R2,R20,R200,R2KILO)
1580 IF PCIB.ERR<>0 THEN ERROR PCIB.BASERR
1590 CALL I.C(I,R20KILO,R200KILO,R2MEGA,R20MEGA)
1600 IF PCIB.ERR<>0 THEN ERROR PCIB.BASERR
1610 CALL I.C(I,AUTOM,R2.5,R12.5,J)
1620 IF PCIB.ERR<>0 THEN ERROR PCIB.BASERR
1630 I=4
1      6      4      0                    C      A      L      L
I.V(I,SET.COMPLEMENT,SET.DRIVER,OUTPUT.NO.WAIT,ENABLE.HANDSH
AKE)
1650 IF PCIB.ERR<>0 THEN ERROR PCIB.BASERR
1      6      6      0                    C      A      L      L
I.V(I,DISABLE.HANDSHAKE,SET.THRESHOLD,SET.START.BIT,SET.NUM.
BITS)
1670 IF PCIB.ERR<>0 THEN ERROR PCIB.BASERR
1680 CALL I.V(I,SET.LOGIC.SENSE,J,J,J)
1690 IF PCIB.ERR<>0 THEN ERROR PCIB.BASERR
1700 CALL I.C(I,POSITIVE,NEGATIVE,TWOS,UNSIGNED)
1710 IF PCIB.ERR<>0 THEN ERROR PCIB.BASERR
1720 CALL I.C(I,OC,TTL,R0,R1)
1730 IF PCIB.ERR<>0 THEN ERROR PCIB.BASERR
1740 CALL I.C(I,R2,R3,R4,R5)
1750 IF PCIB.ERR<>0 THEN ERROR PCIB.BASERR
1760 CALL I.C(I,R6,R7,R8,R9)
1770 IF PCIB.ERR<>0 THEN ERROR PCIB.BASERR
1780 CALL I.C(I,R10,R11,R12,R13)
1790 IF PCIB.ERR<>0 THEN ERROR PCIB.BASERR
```

```
1800 CALL I.C(I,R14,R15,R16,J)
1810 IF PCIB.ERR<>0 THEN ERROR PCIB.BASERR
1820 I=6
1      8      3      0                    C      A      L      L
I.V(I,SET.FREQUENCY,SET.AMPLITUDE,SET.OFFSET,SET.SYMMETRY)
1840 IF PCIB.ERR<>0 THEN ERROR PCIB.BASERR
1850 CALL I.V(I,SET.BURST.COUNT,J,J,J)
1860 IF PCIB.ERR<>0 THEN ERROR PCIB.BASERR
1870 CALL I.C(I,SINE,SQUARE,TRIANGLE,CONTINUOUS)
1880 IF PCIB.ERR<>0 THEN ERROR PCIB.BASERR
1890 CALL I.C(I,GATED,BURST,J,J)
1900 IF PCIB.ERR<>0 THEN ERROR PCIB.BASERR
1910 I=7
1      9      2      0                    C      A      L      L
I.V(I,AUTOSCALE,CALIBRATE,SET.SENSITIVITY,SET.VERT.OFFSET)
1930 IF PCIB.ERR<>0 THEN ERROR PCIB.BASERR
1      9      4      0                    C      A      L      L
I.V(I,SET.COUPLING,SET.POLARITY,SET.SWEEPSPEED,SET.DELAY)
1950 IF PCIB.ERR<>0 THEN ERROR PCIB.BASERR
1      9      6      0                    C      A      L      L
I.V(I,SET.TRIG.SOURCE,SET.TRIG.SLOPE,SET.TRIG.LEVEL,SET.TRIG
.MODE)
1970 IF PCIB.ERR<>0 THEN ERROR PCIB.BASERR
1      9      8      0                    C      A      L      L
I.V(I,GET.SINGLE.WF,GET.TWO.WF,GET.VERT.INFO,GET.TIMEBASE.IN
FO)
1990 IF PCIB.ERR<>0 THEN ERROR PCIB.BASERR
2      0      0      0                    C      A      L      L
I.V(I,GET.TRIG.INFO,CALC.WFVOLT,CALC.WFTIME,CALC.WF.STATS)
2010 IF PCIB.ERR<>0 THEN ERROR PCIB.BASERR
2      0      2      0                    C      A      L      L
I.V(I,CALC.RISETIME,CALC.FALLTIME,CALC.PERIOD,CALC.FREQUENCY
)
2030 IF PCIB.ERR<>0 THEN ERROR PCIB.BASERR
2      0      4      0                    C      A      L      L
I.V(I,CALC.PLUSWIDTH,CALC.MINUSWIDTH,CALC.OVERSHOOT,CALC.PRE
SHOOT)
2050 IF PCIB.ERR<>0 THEN ERROR PCIB.BASERR
2      0      6      0                    C      A      L      L
I.V(I,CALC.PK.TO.PK,SET.TIMEOUT,SCOPE.START,MEASURE.SINGLE.W
F)
2070 IF PCIB.ERR<>0 THEN ERROR PCIB.BASERR
2080 CALL I.V(I,MEASURE.TWO.WF,J,J,J)
2090 IF PCIB.ERR<>0 THEN ERROR PCIB.BASERR
2100 CALL I.C(I,R10NANO,R100NANO,R1MICRO,R10MICRO)
2110 IF PCIB.ERR<>0 THEN ERROR PCIB.BASERR
2120 CALL I.C(I,R100MICRO,R1MILLI,R10MILLI,R100MILLI)
2130 IF PCIB.ERR<>0 THEN ERROR PCIB.BASERR
2140 CALL I.C(I,R1,R10,R20NANO,R200NANO)
2150 IF PCIB.ERR<>0 THEN ERROR PCIB.BASERR
2160 CALL I.C(I,R2MICRO,R20MICRO,R200MICRO,R2MILLI)
```

```
2170 IF PCIB.ERR<>0 THEN ERROR PCIB.BASERR
2180 CALL I.C(I,R20MILLI,R200MILLI,R2,R20)
2190 IF PCIB.ERR<>0 THEN ERROR PCIB.BASERR
2200 CALL I.C(I,R50NANO,R500NANO,R5MICRO,R50MICRO)
2210 IF PCIB.ERR<>0 THEN ERROR PCIB.BASERR
2220 CALL I.C(I,R500MICRO,R5MILLI,R50MILLI,R500MILLI)
2230 IF PCIB.ERR<>0 THEN ERROR PCIB.BASERR
2240 CALL I.C(I,R5,R50,CHAN.A,CHAN.B)
2250 IF PCIB.ERR<>0 THEN ERROR PCIB.BASERR
2260 CALL I.C(I,EXTERNAL,POSITIVE,NEGATIVE,AC)
2270 IF PCIB.ERR<>0 THEN ERROR PCIB.BASERR
2280 CALL I.C(I,DC,TRIGGERED,AUTO.TRIG,AUTO.LEVEL)
2290 IF PCIB.ERR<>0 THEN ERROR PCIB.BASERR
2300 CALL I.C(I,X1,X10,STANDARD,AVERAGE)
2310 IF PCIB.ERR<>0 THEN ERROR PCIB.BASERR
2320 I=8
2330 CALL I.V(I,OPEN.CHANNEL,CLOSE.CHANNEL,J,J)
2340 IF PCIB.ERR<>0 THEN ERROR PCIB.BASERR
2350 CALL C.S
2360 IF PCIB.ERR<>0 THEN ERROR PCIB.BASERR
2370 I$=PCIB.DIR$+"\PCIB.PLD"
2380 CALL L.P(I$)
2390 IF PCIB.ERR<>0 THEN ERROR PCIB.BASERR
2400 I$="DMM.01": I=3: J=0: K=0: L=1
2410 CALL DEFINE(DMM.01,I$,I,J,K,L)
2420 IF PCIB.ERR<>0 THEN ERROR PCIB.BASERR
2430 I$="Func.Gen.01": I=6: J=0: K=1: L=1
2440 CALL DEFINE(FUNC.GEN.01,I$,I,J,K,L)
2450 IF PCIB.ERR<>0 THEN ERROR PCIB.BASERR
2460 I$="Scope.01": I=7: J=0: K=2: L=1
2470 CALL DEFINE(SCOPE.01,I$,I,J,K,L)
2480 IF PCIB.ERR<>0 THEN ERROR PCIB.BASERR
2490 I$="Counter.01": I=1: J=0: K=3: L=1
2500 CALL DEFINE(COUNTER.01,I$,I,J,K,L)
2510 IF PCIB.ERR<>0 THEN ERROR PCIB.BASERR
2520 I$="Dig.In.01": I=4: J=0: K=4: L=1
2530 CALL DEFINE(DIG.IN.01,I$,I,J,K,L)
2540 IF PCIB.ERR<>0 THEN ERROR PCIB.BASERR
2550 I$="Dig.Out.01": I=4: J=1: K=4: L=1
2560 CALL DEFINE(DIG.OUT.01,I$,I,J,K,L)
2570 IF PCIB.ERR<>0 THEN ERROR PCIB.BASERR
2580 I$="Relay.Act.01": I=8: J=0: K=5: L=1
2590 CALL DEFINE(RELAY.ACT.01,I$,I,J,K,L)
2600 IF PCIB.ERR<>0 THEN ERROR PCIB.BASERR
2610 I$="Relay.Mux.01": I=2: J=0: K=6: L=1
2620 CALL DEFINE(RELAY.MUX.01,I$,I,J,K,L)
2630 IF PCIB.ERR<>0 THEN ERROR PCIB.BASERR
2640 I$=ENVIRON$("PANELS")+"\PANELS.EXE"
2650 CALL L.S(I$)
2660 GOTO 1010
2670 IF ERR=PCIB.BASERR THEN GOTO 2700
```

```
2680 PRINT "BASIC error #";ERR;" occurred in line ";ERL
2690 STOP
2700 TMPERR=PCIB.ERR: IF TMPERR=0 THEN TMPERR=PCIB.GLBERR
2710 PRINT "PC Instrument error #";TMPERR;" detected at line
";ERL
2720 PRINT "Error: ";PCIB.ERR$
2730 IF LEFT$(PCIB.NAME$,1)<>CHR$(32) THEN PRINT "Instrument:
";PCIB.NAME$
2740 STOP
2750 COMMON PCIB.DIR$,PCIB.SEG
2760 COMMON LD.FILE,GET.MEM,PANELS,DEF.ERR
2    7    7    0              C    O    M    M    O    N
PCIB.BASERR,PCIB.ERR,PCIB.ERR$,PCIB.NAME$,PCIB.GLBERR
2    7    8    0              C    O    M    M    O    N
READ.REGISTER,READ.SELFID,DEFINE,INITIALIZE.SYSTEM,ENABLE.SY
STEM,DISABLE.SYSTEM,INITIALIZE,POWER.ON,MEASURE,OUTPUT,START
,HALT,ENABLE.INT.TRIGGER,DISABLE.INT.TRIGGER,ENABLE.OUTPUT,D
ISABLE.OUTPUT,CHECK.DONE,GET.STATUS
2    7    9    0              C    O    M    M    O    N
SET.FUNCTION,SET.RANGE,SET.MODE,WRITE.CAL,READ.CAL,STORE.CAL
,DELAY,SAVE.SYSTEM,SET.GATETIME,SET.SAMPLES,SET.SLOPE,SET.SO
URCE,ZERO.OHMS,SET.SPEED,SET.COMPLEMENT,SET.DRIVER,OUTPUT.NO
.WAIT,ENABLE.HANDSHAKE,DISABLE.HANDSHAKE
2    8    0    0              C    O    M    M    O    N
SET.THRESHOLD,SET.START.BIT,SET.NUM.BITS,SET.LOGIC.SENSE,SET
.FREQUENCY,SET.AMPLITUDE,SET.OFFSET,SET.SYMMETRY,SET.BURST.C
OUNT,AUTOSCALE,CALIBRATE,SET.SENSITIVITY,SET.VERT.OFFSET,SET
.COUPLING,SET.POLARITY,SET.SWEEPSPEED
2    8    1    0              C    O    M    M    O    N
SET.DELAY,SET.TRIG.SOURCE,SET.TRIG.SLOPE,SET.TRIG.LEVEL,SET.
TRIG.MODE,GET.SINGLE.WF,GET.TWO.WF,GET.VERT.INFO,GET.TIMEBA
E.INFO,GET.TRIG.INFO,CALC.WFVOLT,CALC.WFTIME,CALC.WF.STATS,C
ALC.RISETIME,CALC.FALLTIME,CALC.PERIOD
2    8    2    0              C    O    M    M    O    N
CALC.FREQUENCY,CALC.PLUSWIDTH,CALC.MINUSWIDTH,CALC.OVERSHOOT
,CALC.PRESHOOT,CALC.PK.TO.PK,SET.TIMEOUT,SCOPE.START,MEASURE
.SINGLE.WF,MEASURE.TWO.WF,OPEN.CHANNEL,CLOSE.CHANNEL
2    8    3    0              C    O    M    M    O    N
FREQUENCY,AUTO.FREQ,PERIOD,AUTO.PER,INTERVAL,RATIO,TOTALIZE,
R100MILLI,R1,R10,R100,R1KILO,R10MEGA,R100MEGA,CHAN.A,CHAN.B,
POSITIVE,NEGATIVE,COMN,SEPARATE,DCVOLTS,ACVOLTS,OHMS,R200MIL
LI,R2,R20,R200,R2KILO,R20KILO,R200KILO
2    8    4    0              C    O    M    M    O    N
R2MEGA,R20MEGA,AUTOM,R2.5,R12.5,POSITIVE,NEGATIVE,TWOS,UNSIG
NED,OC,TTL,R0,R1,R2,R3,R4,R5,R6,R7,R8,R9,R10,R11,R12,R13,R14
,R15,R16,SINE,SQUARE,TRIANGLE,CONTINUOUS,GATED,BURST,R10NANO
,R100NANO,R1MICRO,R10MICRO,R100MICRO
2    8    5    0              C    O    M    M    O    N
R1MILLI,R10MILLI,R100MILLI,R1,R10,R20NANO,R200NANO,R2MICRO,R
20MICRO,R200MICRO,R2MILLI,R20MILLI,R200MILLI,R2,R20,R50NANO,
R500NANO,R5MICRO,R50MICRO,R500MICRO,R5MILLI,R50MILLI,R500MIL
```

```
LI,R5,R50,CHAN.A,CHAN.B,EXTERNAL,POSITIVE
2     8     6     0                C     O     M     M     O     N
NEGATIVE,AC,DC,TRIGGERED,AUTO.TRIG,AUTO.LEVEL,X1,X10,STANDAR
D,AVERAGE
2     8     7     0                C     O     M     M     O     N
DMM.01,FUNC.GEN.01,SCOPE.01,COUNTER.01,DIG.IN.01,DIG.OUT.01,
RELAY.ACT.01,RELAY.MUX.01
2880 'End PCIB Program Shell
2890 '
2900 'Program to scan with the DMM and RELAY.MUX.01
2910 'This program was writen by T.SESTAK and modified by
2920 'P. ROANE , P. RABANG, J.SOMMERS, and J. Kersh for use
2925 'with the balance designed by Prof. Schmidt et al.
2926 '
2930 '
2940 'The next section after the SHELL program directs reading
2950 'the voltages from the balance, computes forces measured
2960 'by the strain gages, then stores the values in two
arrays,
2970 'one for the TARE one for FORCE.  This data file can then
2980 'be used for graphs or other displays.  Each test run
2990 'will create a file on the A and C drives that consist
3000 'raw data that has been manipulated into normal, axial,
3010 'lift, and drag forces.  The raw data is stored on the
3020 'C drive in a BALANFILE.
3030 'Arrays are dimensioned here
3       0       4       0                        D       I       M
READING[7],FORCE[140,9],TARE[8],TREAD[7,10],LAB[7],DROP[7]
3050 COLOR 14,1,1
3060 CLS
3070 KEY OFF
3080 AOA=0                      'Last modified on 27Sep90
3085 TEMP=0
3090 VALUE=5
3092 CLS:LOCATE 11,10:PRINT "IN THIS PROGRAM,"
3094 LOCATE 12,10:PRINT "YOU HAVE TO ANSWER ALL THE QUESTION
BY CAPITAL LETTERS."
3096 LOCATE 13,10:PRINT "SO, PLEASE TURN ON THE 'CAPS LOCK',
THANKS!"
3098 LOCATE 15,10:INPUT "ENTER <CR> TO CONTINUE";INPT$
3100 CNDAOA=0
3110 CLS:LOCATE 11,28:PRINT"SETTING UP DATA FILES"
3115 LOCATE 13,20:INPUT "ENTER THE OUTPUT DATA FILE NAME";D$
3120 D$=D$+".DAT"
3130 'The program writes the data to several files.
3140 STATEFILE$ = "C:\PCIB\WIND.HPC"          'stored in PCIB
subdirectory
3150 DATAFILE$ = "C:\KERSH\"+D$               'stored on drive
C
3160 DISKFILE$ = "A:"+D$                      'stored on drive
A
```

```
3170 BALANFILE$ = "C:\KERSH\B"+D$            'stored on drive
C
3180 '
3190 RELAY.SETTLING.TIME = .90          'Can be changed, but
don't!
3200 LOCATE 16,35:PRINT"D O N E"
3210 CALL DELAY(VALUE)
3220 '
3230 CLS:LOCATE 12,28:PRINT"INITIALIZING INSTRUMENTS"
3240 CALL INITIALIZE.SYSTEM(STATEFILE$)
3250 IF PCIB.ERR <> 0 THEN ERROR PCIB.BASERR
3260 CALL ENABLE.SYSTEM
3270 IF PCIB.ERR <> 0 THEN ERROR PCIB.BASERR
3280 LOCATE 16,35:PRINT"D O N E"
3290 CALL DELAY(VALUE)
3300 '
3310 'This part of the program is to preserve the data if
3320 'if the program is aborted in mid-run.  Parity errors
3330 'in the Hewlett Packard PC Instruments setup caused by
3340 'electrical noise and undervoltage at NPS requires
3350 'this.  A voltage regulated, uninteruptible power supply
3360 'would ameliorate this problem. Just in case- this little
3370 'sequence allows reentry into the program and the data
3380 'arrays with minimal inconvenience.
3390 '
3400 CLS:LOCATE 12,20:INPUT"WERE YOU INTERRUPTED (Y OR N)";A$
3410 IF A$="Y" THEN GOTO 3500
3420 '
3430 'The next two variables are counters in the arrays
3440 'FORCE and TARE
3450 '
3460 TRIAL = 0
3470 TRY = 0
3480 GOTO 3690
3490 '
3500  LOCATE  14,15:INPUT  "WHAT'S  THE  INTERRUPTED  FILE
NAME";ITDF$
3510 ITDF$="C:\LAWRENCE\"+ITDF$+".DAT"
3520 OPEN ITDF$ FOR INPUT AS #1
3    5    3    0    I    N    P    U    T    #    1    ,
TARE(1),TARE(2),TARE(3),TARE(4),TARE(5),TARE(6),TARE(7),TARE
(8)
3540 FOR X = 1 TO 140
3  5  5  0                          I  N  P  U  T      #  1  ,
FORCE(X,1),FORCE(X,2),FORCE(X,3),FORCE(X,4),FORCE(X,5),FORCE
(X,6),FORCE(X,7),FORCE(X,8),FORCE(X,9)
3560    IF FORCE(X,1)=0 THEN ABCD=X:GOTO 3590
3570    AOA=FORCE(X,2)
3575    TEMP=FORCE(X,9)
3580 NEXT X
3590 TRY=ABCD-1
```

```
3600 TRIAL=ABCD-1
3610 CLOSE #1
3620 GOTO 3700
3640 '
3650 'A$ is used as a marker for interrupted run sequences
3660 'in the program, it is set to "N" so the
3670  'uninterrupted sequences are used unless otherwise
directed
3680 '
3690 A$="N"
3700 '
3710 '
3720 'Prompt to begin each scan or quit program if desired
3730 '
3740 CLS:LOCATE 12,10
3750  INPUT "TO START SCAN ENTER ANY KEY EXCEPT Q, Q TO
QUIT";ANSWER$
3760 IF ANSWER$ = "Q" THEN GOTO 6655
3770 '
3780 'This section enters AOA, Canard AOA, and Temperature for
each
3790 'trial and displays them in the printout.
3800 CLS:LOCATE 12,10
3810 PRINT "THE LAST ANGLE OF ATTACK WAS ";AOA
3820 LOCATE 13,10:PRINT "THE LAST CANARD AOA WAS ";CNDAOA
3830 LOCATE 14,10:PRINT "THE LAST TEMPERATURE WAS ";TEMP
3840 LOCATE 16,10:INPUT "ENTER THE ANGLE OF ATTACK (AOA) FOR
THIS TRIAL";AOA
3850  LOCATE 17,10:INPUT "ENTER THE CANARD AOA FOR THIS
TRIAL";CNDAOA
3860  LOCATE 18,10:INPUT "ENTER THE TEMPERATURE FOR THIS
TRIAL";TEMP
3870 READING(1)=AOA
3880 AOA= 90 - AOA       'Model mounted at a turntable AOA of
090 deg
3890 'OAA=              'Voltage offset values can be entered
here
3900 'OBA=              'if the offset values are not time or
3910 'OAN=               'temperature dependent.
3920 'OBN=
3930 CYCLE = 0
3940 CLS:LOCATE 13,10:INPUT "THE Eo FOR EAA IS";OAA
3950 CLS:LOCATE 14,10:INPUT "THE Eo FOR EBA IS";OBA
3960 LOCATE 15,10:INPUT "THE Eo FOR EAN IS";OAN
3970 LOCATE 16,10:INPUT "THE Eo FOR EBN IS";OBN
3980 'The user may reject the current readings and input a new
set.
3990 '
4000 CLS
4010  PRINT"********************  DIRECT  BALANCE  READINGS
************************
```

```
4020 PRINT"                          CHECK OF SYSTEM OPERATION
4030 PRINT
4031 PRINT"IN VOLTS       EAA         EBA         EAN         EBN"
4032 '
4040 PRINT"********       ***         ***         ***         ***"
4041 '
4060 'This file is for storing the direct voltage readings and
averages.
4070 'The data file is continually appended for each tunnel
run.
4080 'The data is for further analysis of the direct voltage
readings.
4090 OPEN BALANFILE$ FOR APPEND AS #3
4100 '
4110 FOR CNT = 1 TO 10
4120 FOR CHANNEL = 2 TO 5
4130    CALL OUTPUT(RELAY.MUX.01, CHANNEL)
4140            IF PCIB.ERR <> 0 THEN ERROR PCIB.BASERR
4150    CALL DELAY(RELAY.SETTLING.TIME)
4160            IF PCIB.ERR <> 0 THEN ERROR PCIB.BASERR
4170    CALL MEASURE(DMM.01, READING[CHANNEL])
4180            IF PCIB.ERR <> 0 THEN ERROR PCIB.BASERR
4185 READING(CHANNEL)=READING(CHANNEL)
4190 TREAD(CHANNEL,CNT) = READING(CHANNEL)
4200 NEXT CHANNEL
4210 PRINT USING
                  "                +.######   +.######   +.######
+   .   #   #   #   #   #   #              +   .   #   #   #   #   #   #
+.######";READING(2),READING(3),READING(4),READING(5)
4220 PRINT #3, USING
                       "   +###.#  +.######  +.######  +.######
+   .   #   #   #   #   #   #              +   .   #   #   #   #   #   #
+.######";READING(1),READING(2),READING(3),READING(4),READIN
G(5)
4230 NEXT CNT
4240 '
4250 '  CALL SUBROUTINE TO AVERAGE READINGS
4260 GOSUB 6690
4270 '
4280 PRINT"- - - - - - - - - - - - - - - - - - - - - - - - - -
- - - - - - - - - -"
4290 PRINT USING
                  "MEAN VALUE +.######   +.######   +.######
+   .   #   #   #   #   #   #              +   .   #   #   #   #   #   #
+.######";READING(2),READING(3),READING(4),READING(5),READIN
G(6),READING(7)
4300 PRINT #3, USING
                       "   +###.#  +.######  +.######  +.######
+   .   #   #   #   #   #   #              +   .   #   #   #   #   #   #
+.######";READING(1),READING(2),READING(3),READING(4),READIN
G(5),READING(6),READING(7)
```

```
4310 CLOSE #3
4320 PRINT" ":BEEP
4330 PRINT"<CR> TO CONTINUE, "1" TO GET NEW READINGS"
4340 INPUT XYZ
4350 IF XYZ=1 GOTO 3940
4360 '
4370 'The voltage readings from the balance are corrected with
the zero offset
4380 'so that their slope passes through the coordinate
origin.
4390 'The corrected values are then applied to the balance
interaction
4400 'equations.
4410 '************** CONVERT SIGNAL TO FORCES **************
4420 '*****************************************************
4430 'The calibration matrices were multiplied by a factor of
1000.
4440 'Ensure that a gain of 1000 is set on the Pacific
Amplifier.
4450 '
4460 '
4470 'The next section was added to compensate for the
dependence
4480 'of Channel 3, strain bridge EBA, on temperature.
Channel
4490 '3 was found to be linearly dependent upon temperature
for
4500 'temperatures greater than about 73.5 degrees.
4510 '
4520 '
4530 TF= TEMP-73.5
4540 IF TF>0 THEN READING(3)= READING(3)+.0565*TF
4550 'TF is used as a variable name for temperature difference
4560 '
4570 '
4580 '
4590 EAA=READING(2)-OAA     'The offsets are applied to the
channels
4600 EBA=READING(3)-OBA
4610 EAN=READING(4)-OAN
4620 EBN=READING(5)-OBN
4630 '
4640 '
5130 '
5140 '
5150 '
5160 '
5170 FOR I = 1 TO 10
5180 '
5190 '
5500 '
```

```
5510 '
5520 '
5530   '*****************  Balance   Interaction   Equations
*****************
5540 '
5550 'These balance interaction equations were developed by
5560 'John Kersh.  You must ensure that they still apply via
a
5570  'calibration  procedure.    The  calibration  procedure
involves
5580 'hanging known weights off the calibration rig at known
turn
5590 'table angles of attack.  The actual normal and axial
forces
5600 'are then found using Normal= Weight*cos(AOA) and Axial=
5610 'Weight*sin(AOA).
5620 '
5630 '
5640 '
5650 '
5660 MAN=27.26281*EAN - .487970*EAA    'Watch sign convention
here
5670 MAA=-.0493204*EAN + 32.538138*EAA
5680 MBN=11.303456*EBN - .7095687*EBA
5690 MBA=-.1350659*EBN + 17.258483*EBA
5700 BB=2.2083  'Separation of upper and lower strain bridges,
5710 '           'B and A, in feet.
5720 'Large parts of this program were untouched!
5730 'A marker for the iterations
5740 CYCLE = CYCLE + 1
5750 NEXT I
5760 '
5770 '***************  FORCE EQUATIONS ********************
5780 '
5790 '
5800 'Normal, Axial, Lift, and, Drag forces are calculated
here.
5810 '
5820 '
5830 NORMAL = (MAN-MBN)/BB
5840 '
5850 AXIAL = (MAA-MBA)/BB
5860    DRAG=    AXIAL*SIN(.01745329*AOA)    -
NORMAL*COS(.01745329*AOA)
5870    LIFT=    AXIAL*COS(.01745329*AOA)    +
NORMAL*SIN(.01745329*AOA)
5880 '
5890 '
5900 TRIAL = TRIAL + 1
5910 INPUT "THIS IS NOT A TARE READING.  HIT <CR>";AN$
5920 IF AN$ <> "Y" GOTO 6190
```

```
5930 COLOR 0,10,10:CLS
5935 IF A$="Y" THEN TRIAL=TRIAL-1:GOTO 5950
5940 TRIAL = 0
5950 TRY = TRY + 1
6000 TARE(1) = TRY
6010 TARE(2) = AOA
6020 TARE(3) = NORMAL
6030 TARE(4) = AXIAL
6040 TARE(5) = LIFT
6050 TARE(6) = 0
6060 TARE(7) = DRAG
6070 TARE(8) = 0
6080 '
6090 '  PRINT THE TARING DATA
6100 PRINT"
      "
6110 PRINT"* * * * * * * * * * * * TARE CALCULATIONS * * * *
* * * * * * * * *
6120 PRINT
                  "  TRIAL    A0A    NORMAL    SIDE     AXIAL
  PITCH    ROLL     YAW"
6130 PRINT
                  "    #      DEG    POUNDS    POUNDS    POUNDS
 FT-LBS    FT-LBS    FT-LBS"
6140 PRINT
                  "  *****    *****    ******    ******    ******
 ******    ******    ******"
6150 '
6160 PRINT USING"     ##    +##.##    ###.##    ###.##    ###.##
#    #    #    .    #    #              #    #    #    .    #    #
###.##";TARE(1),TARE(2),TARE(3),TARE(4),TARE(5),TARE(6),TARE
(7),TARE(8)
6170 BEEP:INPUT "ENTER <CR> TO CONTINUE";INPT$:IF A$="Y" THEN
GOTO 6350
6180 GOTO 6460
6190 '
6240 FORCE(TRIAL,1) = TRIAL
6250 FORCE(TRIAL,2) = AOA
6260 FORCE(TRIAL,3) = CNDAOA
6270 FORCE(TRIAL,4) = NORMAL
6280 FORCE(TRIAL,5) = AXIAL
6290 FORCE(TRIAL,6) = LIFT
6300 FORCE(TRIAL,7) = DRAG
6310 FORCE(TRIAL,8) = TEMP
6320 FORCE(TRIAL,9) = TEMP
6330 'print the values and store in file
6340 '
6350 PRINT"
      "
6360 PRINT"* * * * * * * * * * * * FORCE CALCULATIONS * * * *
* * * * * * * * *
```

```
6370 PRINT "  TRIAL   AOA    CANARD   NORMAL     AXIAL    LIFT
  DRAG   TEMP"
6371 'YAW"
6380 PRINT
6381 PRINT "    #     DEG      DEG      LBS       LBS      LBS
   LBS     F"
6390 'PRINT
6391 '   *****   *****    ******    ******    ******    ******
******   *******"
6400 'a loop to list all values so far
6410 '
6420 FOR J = 1 TO TRIAL
6430 PRINT USING"    ##    +###.#   +###.##   +###.##   +###.##
+   #   #   #   .   #   #                  +   #   #   #   .   #   #
+###.##";FORCE(J,1),FORCE(J,2),FORCE(J,3),FORCE(J,4),FORCE(J
,5),FORCE(J,6),FORCE(J,7),FORCE(J,8)
6440 NEXT J
6450 BEEP:INPUT "ENTER <CR> TO CONTINUE";INPT$
6460 '
6470 'Writes the data to the output data files
6480 COLOR 14,1,1:CLS
6490 OPEN DATAFILE$ FOR OUTPUT AS #1
6500 OPEN DISKFILE$ FOR OUTPUT AS #2
6    5    1    0        W    R    I    T    E    #    1    ,
TARE(1),TARE(2),TARE(3),TARE(4),TARE(5),TARE(6),TARE(7),TARE
(8)
6    5    2    0        W    R    I    T    E    #    2    ,
TARE(1),TARE(2),TARE(3),TARE(4),TARE(5),TARE(6),TARE(7),TARE
(8)
6530 FOR X = 1 TO 140
6  5  5  0                          W  R  I  T  E      #  1  ,
FORCE(X,1),FORCE(X,2),FORCE(X,3),FORCE(X,4),FORCE(X,5),FORCE
(X,6),FORCE(X,7),FORCE(X,8),FORCE(X,9)
6  5  6  0                          W  R  I  T  E      #  2  ,
FORCE(X,1),FORCE(X,2),FORCE(X,3),FORCE(X,4),FORCE(X,5),FORCE
(X,6),FORCE(X,7),FORCE(X,8),FORCE(X,9)
6570 NEXT X
6580 CLOSE #1
6590 CLOSE #2          'To view the corrected voltage output
6600 LOCATE 9,10:PRINT "THE CORRECTED CHN(2) READING WAS";EAA
6610 LOCATE 10,10:PRINT "THE CORRECTED CHN(3) READING WAS";EBA
6620 LOCATE 11,10:PRINT "THE CORRECTED CHN(4) READING WAS";EAN
6630 LOCATE 12,10:PRINT "THE CORRECTED CHN(3) READING WAS";EBN
6640  LOCATE 14,10:INPUT "DO YOU WANT ANOTHER SCAN (Y OR
N)";ANSW$
6645 A$="N"
6650 IF ANSW$ <>"N" THEN GOTO 3700
6655 CLS:LOCATE 12,15:INPUT "DO YOU REALLY WANT TO QUIT";AW$
6660 IF AW$<>"Y" THEN GOTO 3700
6665 GOSUB 7060
6670 END
```

```
6680 '
6690 'This subroutine averages the balance voltage readings
6700 'by computing the mean and standard deviation.
6710 'Any readings less or greater than one standard deviation
6720 'are thrown out and a new mean is computed
6730 '
6740 FOR CHANNEL = 2 TO 5
6750 N=10:FLAG=0
6760 SSDEV=0
6770    'Mean of balance voltage readings
6780 SREAD = 0
6790 FOR CNT = 1 TO 10
6800 SREAD = SREAD + TREAD(CHANNEL,CNT)
6810 NEXT CNT
6820 MEAN = SREAD/N
6830 READING(CHANNEL) = MEAN
6840 IF (FLAG=1) THEN GOTO 7010
6850    'Standard deviation routine
6860 FOR CNT = 1 TO 10
6870 DIF = TREAD(CHANNEL,CNT) - MEAN
6880 SDEV = DIF * DIF
6890 SSDEV = SSDEV + SDEV
6900 NEXT CNT
6910 DEV = SQR(SSDEV/N)
6920 HI = MEAN + DEV
6930 LO = MEAN - DEV
6940 FOR CNT = 1 TO 10
6950 ARG = TREAD(CHANNEL,CNT)
6960 IF (ARG < HI) AND (ARG > LO) THEN GOTO 6990
6970 TREAD(CHANNEL,CNT) = 0
6980 N = N - 1:FLAG=1
6990 NEXT CNT
7000 DROP(CHANNEL)=10-N:GOTO 6780
7010 NEXT CHANNEL
7020 PRINT "READINGS DROP      ";DROP(2);"      ";DROP(3);"
   ";DROP(4);"         ";DROP(5);"         ";DROP(6);"
";DROP(7)
7030 RETURN
7040 END
7050 '
7060 'THIS SUBROUTINE ENTER THE EXPERIMENT CONDITIONS.
7070 COLOR 14,5,5:CLS
7080    LOCATE   12,10:INPUT   "ENTER   EXPERIMENT   DATE
(YYMMDD)";YMD:LAB(1)=YMD
7090   LOCATE   13,10:INPUT   "ENTER   THE   EXPERIMENT   GRID
NO.";G:LAB(2)=G
7100  LOCATE  14,10:INPUT  "WAS  THE  CANARD  IN  PLACE?  1=NO,
2=YES";B:LAB(3)=B
7110   LOCATE   15,10:INPUT   "ENTER   THE   NEXT   STARTING
AOA";S:LAB(4)=S
7115 TEMPSUM=0
```

```
7120 FOR X=1 TO TRIAL
7125    TEMPSUM=TEMPSUM+FORCE(X,9)
7130 NEXT X
7135 TAV=TEMPSUM/TRIAL:LAB(5)=TAV
7140  LOCATE  17,10:INPUT  "ENTER  EXPR  TUNNEL  DYN  PRESSURE
(cmH2O)";DP:LAB(6)=DP
7150   LOCATE   18,10:INPUT   "ENTER   EXPR   PRESSURE   (in.
Hg)";PRE:LAB(7)=PRE*70.739
7160 '
7170 OPEN DATAFILE$ FOR OUTPUT AS #1
7180 OPEN DISKFILE$ FOR OUTPUT AS #2
7    1    9    0         W    R    I    T    E    #    1    ,
TARE(1),TARE(2),TARE(3),TARE(4),TARE(5),TARE(6),TARE(7),TARE
(8)
7    2    0    0         W    R    I    T    E    #    2    ,
TARE(1),TARE(2),TARE(3),TARE(4),TARE(5),TARE(6),TARE(7),TARE
(8)
7210 FOR X = 1 TO 140
7    2    2    0                   W    R    I    T    E
#1,FORCE(X,1),FORCE(X,2),FORCE(X,3),FORCE(X,4),FORCE(X,5),FO
RCE(X,6),FORCE(X,7),FORCE(X,8),FORCE(X,9)
7  2  3  0                         W  R  I  T  E      #  2  ,
FORCE(X,1),FORCE(X,2),FORCE(X,3),FORCE(X,4),FORCE(X,5),FORCE
(X,6),FORCE(X,7),FORCE(X,8),FORCE(X,9)
7240 NEXT X
7    2    5    0         W    R    I    T    E    #    1    ,
LAB(1),LAB(2),LAB(3),LAB(4),LAB(5),LAB(6),LAB(7)
7    2    6    0         W    R    I    T    E    #    2    ,
LAB(1),LAB(2),LAB(3),LAB(4),LAB(5),LAB(6),LAB(7)
7270 CLOSE #1
7280 CLOSE #2
7290 '
7300 '
7310 CLS:LOCATE 12,10
7320 PRINT "GAME OVER! MAN!":BEEP:BEEP
7330 RETURN
7340 END
```

APPENDIX D. DATA MANIPULATION/CORRECTION PROGRAM

```
1000 '  PROGRAM BY M.P. RABANG AND LT YUAN, C.C TO READ FORCE
AND
1005 '   MOMENT VALUES FROM A DATA AQUISITION PGM TITLED
READ.BAS
1010 '  THIS PROGRAM WAS MODIFIED LT J.M. KERSH TO MANIPULATE
THE
1015 '   THE PGM ENTITLED JMK.BAS.   JMK.BAS IS THE DATA
AQUISITION
1020 '  PROGRAM FOR THE CLOSE-COUPLED CANARD/WING MODEL.
1030 DIM TARE[8], FORCE[140,9], COEF[140,9], LAB[11]
1040 COLOR 14,1,1
1050 CLS
1060 KEY OFF
1070   '***************Last   Modified   on   18   OCT   90
**********************
1080 LOCATE 11,7
1090 INPUT"ENTER THE NAME OF THE INPUT FILE";D$
1100 F$=D$+".DAT"
1110 INFILE$="C:\KERSH\"+F$
1120 CF$="CF"+F$
1130 OUTFILE$="C:\KERSH\"+CF$
1140 DISKFILE$="A:"+CF$
1150 ' Force values are read from the input data file
1160 OPEN INFILE$ FOR INPUT AS #1
1    1    7    0    I    N    P    U    T    #    1    ,
TARE(1),TARE(2),TARE(3),TARE(4),TARE(5),TARE(6),TARE(7),TARE
(8)
1180 FOR X = 1 TO 140
1    1    9    0    I    N    P    U    T    #    1    ,
FORCE(X,1),FORCE(X,2),FORCE(X,3),FORCE(X,4),FORCE(X,5),FORCE
(X,6),FORCE(X,7),FORCE(X,8),FORCE(X,9)
1200 NEXT X
1    2    1    0    I    N    P    U    T    #    1    ,
LAB(1),LAB(2),LAB(3),LAB(4),LAB(5),LAB(6),LAB(7)
1220 CLOSE #1
1225 '
1230 YMD=LAB(1)          'YEAR MONTH DATE
1240 SCR=LAB(2)          'EXPERIMENT GRID NUMBER
1250 BODY=LAB(3)         'WAS THE CANARD IN PLACE
1260 STR=LAB(4)          'ANGLE OF ATTACK
1270 TAV=LAB(5)          'AVERAGE TEMPERATURE
1280 DP=LAB(6)           'DYNAMIC PRESSURE
1290 PRE=LAB(7)          'ATMOSPHERIC PRESSURE
1300 '
1330 '  OPEN THE DATA FILE SO EACH SCAN IS RECORDED
```

```
1340 TRANSFILE$="C:\KERSH\TRANS.DAT"
1370 '
1400 CLS:LOCATE 12,5
1410  INPUT"INPUT  FILE  HAS  BEEN  LOADED,  ENTER  <CR>  TO
CONTINUE";INPT$
1420 '
1430  '***************    BEGIN  COEFFICIENTS  CALCULATION
************
1440 IF BODY=1 THEN A=.681  ' Area of wing to centerline of
fuselage
1450 MU=3.719E-07        '
1460 RHO=PRE/(1545*(459.7+TAV))
1470 Q=-.026749+1.1149*DP
1480 IF BODY=2 THEN A=.815  'Area of wing and exposed area of
canard
1490 Q=Q*2.047
1500 VEL=SQR(2*Q/RHO)
1510 RED=(RHO*VEL*(9.52/12))/MU   'Ref Area is MAC of Wing to
centerline
1520 FLAG=0
1530 FOR X = 1 TO 140
1540 IF FORCE(X,1)=0 THEN GOTO 1730
1550 FLAG=FLAG+1
1560 COEF(X,1)=FORCE(X,1)
1570   COEF(X,2)=FORCE(X,2)-2.2   'Corrects   for   balance
misalignment
1580 COEF(X,3)=FORCE(X,3)
1590  COEF(X,4)=.955*FORCE(X,4)  'Corrects for calerror in
normal force
1600  COEF(X,5)=1.037*FORCE(X,5)  'Corrects for calerror in
axial force
1                    6                         1                         0
COEF(X,6)=COEF(X,5)*COS(.017453*COEF(X,2))+COEF(X,4)*SIN(.01
7453*COEF(X,2))
1                    6                         2                         0
COEF(X,7)=COEF(X,5)*SIN(.017453*COEF(X,2))-COEF(X,4)*COS(.01
7453*COEF(X,2))
1630  '************          Blockage  Correction  Routine
**********************
1640 IF COEF(X,2) = 0 THEN EPS=.00269    'Area of 4.5x3 inch
block
1650 EPBW=.0298*SIN(.017453*COEF(X,2))
1660 EPCND=.00383*SIN ((COEF(X,2)+COEF(X,3))*.017453)
1670 IF BODY=1 THEN EPS=ABS(EPBW)
1680 IF BODY=2 THEN EPS=EPBW+EPCND
1700 COEF(X,9)=COEF(X,7)/(A*Q*(1+(2*EPS)))
1710 COEF(X,8)=COEF(X,6)/(A*Q*(1+(2*EPS)))
1720 'Original pgm CORR>BAS greatly changed to account for
turntable
1730 'misalignment. Turntable was +2.2 degrees off.
1740 NEXT X
```

```
1750 LAB(8)=RHO
1760 LAB(9)=Q
1770 LAB(10)=VEL
1780 LAB(11)=RED
1790 OPEN OUTFILE$ FOR OUTPUT AS #1
1800 OPEN DISKFILE$ FOR OUTPUT AS #2
1810 OPEN TRANSFILE$ FOR APPEND AS #3
1  8  2  0                          W  R  I  T  E      #  1  ,
LAB(1),LAB(2),LAB(3),LAB(4),LAB(5),LAB(6),LAB(7),LAB(8),LAB(
9),LAB(10),LAB(11)
1  8  3  0                          W  R  I  T  E      #  2  ,
LAB(1),LAB(2),LAB(3),LAB(4),LAB(5),LAB(6),LAB(7),LAB(8),LAB(
9),LAB(10),LAB(11)
1  8  4  0                          W  R  I  T  E      #  3  ,
LAB(1),LAB(2),LAB(3),LAB(4),LAB(5),LAB(6),LAB(7),LAB(8),LAB(
9),LAB(10),LAB(11)
1850 FOR X=1 TO FLAG
1    8    6    0        W    R    I    T    E    #    1    ,
COEF(X,1),COEF(X,2),COEF(X,3),COEF(X,4),COEF(X,9),COEF(X,5),
COEF(X,6),COEF(X,7),COEF(X,8)
1    8    7    0        W    R    I    T    E    #    2    ,
COEF(X,1),COEF(X,2),COEF(X,3),COEF(X,4),COEF(X,9),COEF(X,5),
COEF(X,6),COEF(X,7),COEF(X,8)
1    8    8    0        W    R    I    T    E    #    3    ,
COEF(X,1),COEF(X,2),COEF(X,3),COEF(X,4),COEF(X,9),COEF(X,5),
COEF(X,6),COEF(X,7),COEF(X,8)
1890 NEXT X
1900 CLOSE #1
2000 CLOSE #2
2010 CLOSE #3
2020 '
2060 '  DISPLAY ROUTINE
2070  CLS:BEEP:LOCATE 10,5:INPUT "DO YOU WANT TO VIEW THE
OUTPUT";PANS$
2080 IF PANS$<>"Y" THEN GOTO 2290
2090 COLOR 0,10,10
2100 CLS
2110 PRINT"FILE NAME: ";CF$:PRINT" "
2120 PRINT"DATE (YYMMDD)                              ";YMD
2125 PRINT"SCREEN NO.                                 ";SCR
2130 PRINT"WAS THE CANARD IN PLACE? 1=NO, 2=YES ";BODY
2135 PRINT"THE LAST AOA FOR THE RUN WAS               ";STR
2140 PRINT"STATIC PRESSURE (LB/FT^2)                  ";PRE
2145 PRINT"AVERAGE TEMPERATURE (F)                    ";TAV
2150 PRINT"WIND TUNNNEL VELOCITY (FT/SEC)             ";VEL
2155 PRINT"WIND TUNNNEL DYNAMIC PRESSURE (cmH2O)";DP
2160 PRINT"AIR DENSITY (LBm/FT^3)                     ";RHO
2170 PRINT"REYNOLDS NUMBER                            ";RED
2180 PRINT"ACTUAL DYNAMIC PRESSURE (LB/FT^2)          ";Q
2185 BEEP:INPUT "ENTER <CR> TO CONTINUE";INPT$
2190 PRINT" "
```

```
2200 PRINT"* * * * * * * * * * * * * FORCE COEFFICIENTS  *
* * * * * * * * * * * * *
2210 PRINT" "
2220 PRINT "TRIAL   AOA    CNDAOA   NORMAL    AXIAL   LIFT
 DRAG     TEMP "
2221 '
2225 '
2230 PRINT "*****   ***    ******   ******    *****   ****
 ****     ****"
2240 FOR X=1 TO FLAG
2250 PRINT USING " ###    +###.#   +##.#    +##.###   +##.###
+  #  #  .  #  #  #            +  #  #  .  #  #  #
##.##";COEF(X,1),COEF(X,2),COEF(X,3),COEF(X,4),COEF(X,5),COE
F(X,6),COEF(X,7),COEF(X,8)
2255 IF X=20 OR X=40 OR X=60 OR X=80 THEN INPUT "ENTER <CR> TO
CONTINUE";INPT$
2257 '
2258 '
2260 '
2270 NEXT X
2280 BEEP:INPUT "ENTER <CR> TO CONTINUE";INPT$
2290 CLS:LOCATE 10,5:BEEP:INPUT "DO YOU WANT A HARDCOPY";ANS$
2300 IF ANS$<>"Y" THEN GOTO 2640
2310 LPRINT CHR$(27);"&l6E"        'Output changed to thesis
format
2312 LPRINT CHR$(27);"&l49F"      'These are toggles
2314 LPRINT CHR$(27);"&a10L"
2320 LPRINT"FORCE DATA FILENAME:";F$
2345 LPRINT"COEFFICIENT DATA FILENAME:";CF$:LPRINT" "
2350 LPRINT"DATE  (YYMMDD)                          ";YMD
2355 LPRINT"WAS THE CANARD IN PLACE? 1=NO,2=YES ";BODY
2360 LPRINT"ATMOSPHERIC PRESSURE (Inches Hg)     ";PRE/70.739
2370 LPRINT"AVERAGE TEMPERATURE (F)              ";TAV
2380 LPRINT"WIND TUNNEL VELOCITY (FT/SEC)        ";VEL
2390 LPRINT"WIND TUNNEL DYNAMIC PRESSURE (cmH2O)";DP
2400 LPRINT"AIR DENSITY (LBM/FT^3)               ";RHO
2410 LPRINT"REYNOLDS NUMBER                      ";RED
2420 LPRINT"ACTUAL DYNAMIC PRESSURE (LB/FT^2)    ";Q
2430 LPRINT" "
2440 LPRINT" "
2450 LPRINT"* * * * * * * * * *  FORCE READINGS   * * * * *
* * * * * *
2460 LPRINT" "
2470 LPRINT"TRIAL   AOA   CNDAOA   NORMAL    AXIAL     LIFT
DRAG    TEMP"
2480 LPRINT"   #   DEG   DEG    LBS      LBS      LBS      LBS
   DEG F"
2490 LPRINT"*****  ***    ***     ****      ****      ****
****    ******"
2500 FOR J = 1 TO FLAG
2520 LPRINT USING" ### +###.# +##.# +##.###  +##.###  +##.###
```

```
+      #      #      .      #      #      #
##.##";FORCE(J,1),FORCE(J,2),FORCE(J,3),FORCE(J,4),FORCE(J,5
),FORCE(J,6),FORCE(J,7),FORCE(J,8)
2530 NEXT J
2540 LPRINT" "
2550 LPRINT" "
2560 LPRINT"* * * * *  CORRECTED AOA, CL, CD, LIFT, AND DRAG
* * * * *
2570 LPRINT" "
2580 LPRINT"TRIAL  AOA  CNDAOA    C LIFT     C DRAG    LIFT
   DRAG "
2590 LPRINT"*****  ***    ***     ****       ****      ****
   ****    "
2600 FOR X = 1 TO FLAG
2610  LPRINT USING" ### +###.# +##.#    +##.####    +##.####
+   #   #   .   #   #   #   #              +   #   #   .   #   #   #   #
";COEF(X,1),COEF(X,2),COEF(X,3),COEF(X,8),COEF(X,9),COEF(X,6
),COEF(X,7)
2630 NEXT X
2640 COLOR 14,1,1:CLS:LOCATE 12,7:BEEP
2650 INPUT"DO YOU WANT ANOTHER RUN";AANS$
2660 IF AANS$<>"N" THEN GOTO 1050
2670 CLS:LOCATE 12,10:PRINT "GAME OVER! MAN!":BEEP:BEEP
2680 END
```

APPENDIX E. DATA SETS

Table 6. Baseline Configuration and Comparison to Canard/Wing/Body; Part A

A0A (DEG)	LIFT (LBS)	DRAG (LBS)	CL	CD	DATA RUN
-8.2	-11.1700	2.0010	-0.4198	0.0752	23AUGA.DAT
-6.2	-7.9040	1.5016	-0.2977	0.0566	A
-4.2	-4.9937	1.2017	-0.1885	0.0454	A
-2.2	-2.0504	1.2058	-0.0775	0.0388	A
-0.2	0.9644	0.9030	0.0365	0.0342	A
1.8	4.0655	0.8945	0.1538	0.0338	23AUGA.DAT.
3.8	7.4842	1.1027	0.2826	0.0416	A
5.8	11.7310	1.5756	0.4420	0.0594	A
7.8	14.7753	2.2435	0.5555	0.0844	A
9.8	17.9998	3.1626	0.6754	0.1187	A
11.8	20.3441	4.1417	0.7618	0.1551	23AUGB.DAT
13.8	22.7860	5.4213	0.8515	0.2026	B
15.8	25.0035	6.9427	0.9326	0.2589	B
17.8	26.6030	8.5957	0.9903	0.3200	20SEPA.DAT
18.8	27.7366	9.7539	1.0315	0.3627	A
19.8	28.3918	10.4862	1.0548	0.3896	A
20.8	29.4518	11.4483	1.0932	0.4249	A
21.8	28.6064	11.8033	1.0608	0.4377	A
22.8	28.5706	12.4834	1.0584	0.4625	A
23.8	28.6415	13.2223	1.0601	0.4894	A
24.8	28.6372	13.8457	1.0589	0.5120	A
25.8	30.6738	15.2944	1.1332	0.5650	A
26.8	31.1688	16.1211	1.1504	0.5950	A
27.8	33.6451	18.1506	1.2407	0.6693	A
28.8	34.6974	19.2472	1.2784	0.7091	A
29.8	36.5592	20.8344	1.3458	0.7670	23AUGC.DAT
31.8	38.7898	23.6592	1.4254	0.8694	C
33.8	40.9079	26.6938	1.5007	0.9793	C
35.8	42.2746	29.3636	1.5483	1.0754	C
37.8	43.0890	32.1095	1.5756	1.1741	23AUGD.DAT
39.8	43.4319	34.5808	1.5857	1.2625	D
41.8	43.0571	36.7935	1.5696	1.3413	D
43.8	41.2888	37.5997	1.5029	1.3687	D
45.8	39.7179	38.3503	1.4437	1.3940	D
47.8	38.4130	39.4170	1.3944	1.4308	D
49.8	37.5366	40.6866	1.3608	1.4750	D

Table 7. Baseline Configuration and Comparison to Canard/Wing/Body; Part B

AOA (DEG)	CL MAX WITH CANARD	CANARD AOA AT CL MAX	CL/CD FOR WING/BODY	MAX CL/CD WITH CANARD
-8.2			-5.600	
-6.2			-5.288	
-4.2			-4.200	
-2.2			-1.974	
-0.2			1.059	
1.8			4.529	
3.8			6.738	
5.8			7.153	
7.8			6.619	
9.8	0.698	17	5.672	3.7128
11.8			4.916	
13.8			4.192	
15.8			3.602	
17.8			3.094	
18.8			2.84	
19.8			2.705	
20.8			2.572	
21.8	1.422	7	2.422	2.5996
22.8			2.285	
23.8			2.168	
24.8			2.068	
25.8			2.005	
26.8			1.933	
27.8			1.855	
28.8			1.803	
29.8			1.755	
31.8			1.64	
33.8	1.642	-7	1.533	1.6704
35.8			1.44	
37.8			1.342	
39.8	1.7	-15	1.257	1.4003
41.8			1.171	
43.8			1.098	
45.8			1.036	
47.8	1.649	-17	0.974	1.075
49.8			0.923	

Table 8. Baseline Configuration and Comparison to Canard/Wing/Body; Part C

AOA (DEG)	ABSOLUTE CANARD AOA (DEG)	CD WITH CANARD AT CL MAXIMUM	MINIMUM CL USING CANARD	CANARD AOA AT CL MINIMUM	CL AT CANARD AOA OF -5 DEGREES
-8.2					
-6.2					
-4.2					
-2.2					
-0.2					
1.8					
3.8					
5.8					
7.8					
9.8	26.8	0.188	0.501	-25	0.631
11.8					
13.8					
15.8					
17.8					
18.8					
19.8					
20.8					
21.8	28.8	0.547	0.971	-25	1.216
22.8					
23.8					
24.8					
25.8					
26.8					
27.8					
28.8					
29.8					
31.8					
33.8	26.8	0.983	1.363	-25	1.617
35.8					
37.8					
39.8	24.8	1.214	1.513	25	1.691
41.8					
43.8					
45.8					
47.8	30.8	1.534	1.378	25	1.610
49.8					

Table 9. Wing/Body at a 10 Degree AOA

CANARD AOA	LIFT (LBS)	DRAG (LBS)	CL	CD	DATA RUN
-25	15.9395	3.6655	0.5007	0.1152	20SEPC.DAT
-20	16.5619	3.2091	0.5200	0.1007	C
-15	18.0877	3.0992	0.5675	0.0972	C
-10	19.2692	3.1160	0.6041	0.0977	C
-5	20.1266	3.1740	0.6306	0.0944	C
0	21.2552	3.4418	0.6655	0.1078	23SEPG.DAT
5	21.1985	3.8438	0.6633	0.1203	G
7	21.8989	4.2309	0.6851	0.1324	G
10	21.6258	4.5604	0.6763	0.1426	G
12	22.2098	4.9784	0.6944	0.1556	G
15	22.2755	5.5574	0.6962	0.1737	G
17	22.3500	6.0144	0.6983	0.1879	G
20	22.2796	6.5067	0.6959	0.2032	G
25	21.2853	7.1329	0.6645	0.2227	G

Table 10. Wing/Body at a 22 Degree AOA

CANARD AOA	LIFT (LBS)	DRAG (LBS)	CL	CD	DATA RUN
-25	31.3361	11.8939	0.9713	0.3687	22SEPA.DAT
-20	32.5169	11.8803	1.0073	0.3680	A
-15	34.5715	12.1208	1.0702	0.3752	A
-10	36.4250	12.7764	1.1269	0.3953	A
-7	37.7855	13.3625	1.1685	0.4132	A
-5	39.3184	13.8677	1.2156	0.4288	23SEPA.DAT
-2	41.7156	14.8393	1.2893	0.4586	A
0	44.2310	15.9831	1.3667	0.4939	A
2	44.9294	16.2654	1.3879	0.5025	A
5	45.7376	16.9976	1.4124	0.5249	A
7	46.0463	17.7145	1.4216	0.5469	A
10	45.7161	18.1777	1.4109	0.5610	A
12	43.6964	17.8816	1.3483	0.5518	A
15	43.4425	18.3095	1.3400	0.5648	A
20	43.2672	19.0409	1.3340	0.5870	A
25	42.8524	19.6500	1.3206	0.6055	A

Table 11. Wing/Body at a 34 Degree AOA

CANARD AOA	LIFT (LBS)	DRAG (LBS)	CL	CD	DATA RUN
-25	44.5152	25.3760	1.3630	0.7770	17SEPC.DAT
-20	45.9988	26.2313	1.4076	0.8027	C
-15	48.1965	27.4527	1.4739	0.8395	C
-10	51.5752	30.0208	1.5763	0.9175	24SEPA.DAT
-7	53.7445	32.1670	1.6420	0.9828	A
-5	52.9515	32.1368	1.6174	0.9816	A
-2	52.6874	32.7322	1.6088	0.9995	A
0	52.1269	32.7426	1.5913	0.9996	A
2	52.4038	33.5410	1.5995	1.0237	A
5	53.2707	34.6841	1.6254	1.0583	A
7	52.4110	34.4708	1.5989	1.0516	25SEPB.DAT
10	51.9213	34.8199	1.5835	1.0619	B
15	51.7202	35.5922	1.5766	1.0850	B
20	51.2194	36.1678	1.5607	1.1021	B
25	50.5124	36.5055	1.5387	1.1120	B

Table 12. Wing/Body at a 40 Degree AOA

CANARD AOA	LIFT (LBS)	DRAG (LBS)	CL	CD	DATA RUN
-25	52.1035	36.0908	1.5865	1.0989	18SEPD.DAT
-20	54.1898	37.9837	1.6490	1.1559	18SEPB.DAT
-17	54.9179	38.7684	1.6706	1.1793	24SEPB.DAT
-15	55.8909	39.9075	1.6998	1.2137	B
-10	55.8655	40.0806	1.6980	1.2402	B
-7	55.4968	41.0806	1.6863	1.2482	B
-5	55.6604	41.5648	1.6909	1.2627	B
-2	55.3475	42.2035	1.6809	1.2817	B
0	55.3350	42.7420	1.6801	1.2978	B
5	54.7972	43.6663	1.6630	1.3252	18SEPA.DAT
10	54.0037	44.1921	1.6382	1.3406	A
15	52.3813	43.9583	1.5884	1.3330	18SEPD.DAT
20	51.4276	44.2213	1.5589	1.3330	D
25	49.9234	43.9899	1.5129	1.3405	D

Table 13. Wing/Body at a 48 Degree AOA

CANARD AOA	LIFT (LBS)	DRAG (LBS)	CL	CD	DATA RUN
-25	53.6236	48.7047	1.6219	1.4731	25SEPA.DAT
-22	54.0085	49.7988	1.6329	1.5057	A
-20	54.1415	49.8229	1.6366	1.5060	A
-17	54.5741	50.7786	1.6491	1.5344	A
-15	54.1012	51.0222	1.6345	1.5414	A
-10	53.5873	52.1664	1.6181	1.5752	A
-5	53.3432	53.2749	1.6099	1.6079	19SEPA.DAT
0	52.6276	53.7827	1.5876	1.6225	19SEPB.DAT
5	51.1209	53.2744	1.5416	1.6065	B
10	49.7827	53.1249	1.5007	1.6014	B
15	48.1900	52.5577	1.4522	1.5838	B
20	46.5715	51.8891	1.4030	1.5632	B
25	45.7369	52.2085	1.3776	1.5725	B

LIST OF REFERENCES

1. McAtee, Thomas P., *Agility in Demand,* Aerospace America, Volume 26, Number 5, pp. 36-38, May 1988.

2. Herbst, W.B., *Future Fighter Technologies,* Journal of Aircraft, Volume 17, Number 8, pp. 561-566, August 1980.

3. Schefter, Jim, *X-31 How They're Inventing a Radical Way to Fly,* Popular Science, pp. 58-64, February 1989.

4. Carr, Lawrence W., *Progress in Analysis and Prediction of Dynamic Stall,* AIAA Journal, Volume 25, Number 1, pp. 6-17, January 1988.

5. Hummel, Dietrich, and Oelker, Hans-Christoph, *Investigations on the Vorticity Sheets of a Close-Coupled Delta-Canard Configuration,* Journal of Aircraft, Volume 26, Number 7, pp. 657-666, July 1989.

6. Lacey, David W., *Aerodynamic Characteristics of the Close-Coupled Canard as Applied to Low-to-Moderate Swept Wings Volume 1: General Trends,* DTNSRDC-79/001, January 1979.

7. Gunston, Bill, and Spick, Mike, *Modern Air Combat,* pp. 22-25, Salamander Book Co., 1983.

8. Stoll, F., and Koenig, D.G., *Large-Scale Wind-Tunnel Investigation of a Close-Coupled Canard-Delta-Wing Fighter Model Through High Angles of Attack,* AIAA-83-48373, pp. 1-15, October 1983.

9. Er-El, J., and Seginer, A., *Vortex Trajectories and Breakdown on Wing-Canard Configurations,* Journal of Aircraft, Volume 22, Number 8, pp. 641-648, August 1985.

10. Calarese, W., *Vortex Interaction Effects on the Lift/Drag Ratio of Close-Coupled Canard Configurations,* AIAA-87-1344, pp. 1-13, June 1987.

11. O'Leary, C.O., and Weir, B., *The Effects of Foreplanes on the Static and Dynamic Characteristics*

of a Combat Aircraft Model, AGARD Conference Proceedings No. 465, pp. 8-1-8-13, October 1989.

12. Huyer, Stephen A., and Luttges, Marvin W., *Unsteady Flow Interactions Between the Wake of an Oscillating Airfoil and a Stationary Trailing Airfoil,* AIAA-88-2581, pp. 473-482, 1988.

13. Ashworth, J., Mouch, T., and Luttges, M., *Visualization and Anemometry Analyses of Forced Unsteady Flows about and X-29 Model,* AIAA Paper 88-2570, 1988.

14. Mouch, T., McLaughlin, T., and Ashworth, J., *Unsteady Flows Produced by Small Amplitude Oscillations of the Canard of an X-29 Model,* AIAA Paper 89-2229, 1989.

15. Rabang, M.P., *Turbulence Effects on the High Angle of Attack Aerodynamics of a Vertically-Launched Missile,* Master's Thesis, Naval Postgraduate School, Monterey, CA, June 1988.

16. Pinaire, J.A., *Effects of Flowfield Turbulence on Asymmetric Vortices Over a Slender Body,* Master's Thesis, Naval Postgraduate School, Monterey, CA, December 1989.

17. Yuan, Chi-Chung, *The Effects of Forebody Strakes on Asymmetric Vortices on a Vertically Launched Missile,* Master's Thesis, Naval Postgraduate School, Monterey, CA, September 1990.

18. Rae, William H., and Pope, Alan, *Low-Speed Wind Tunnel Testing,* John Wiley and Sons, Inc., 1984.

19. Raymer, Daniel P., *Aircraft Design: a Conceptual Approach,* AIAA, Inc., 1989.

INITIAL DISTRIBUTION LIST

		No. Copies
1.	Defense Technical Information Center Cameron Station Alexandria, VA 22304-6145	2
2.	Library, Code 52 Naval Postgraduate School Monterey, CA 93943-5002	2
3.	Chairman Department of Aeronautics and Astronautics, Code AA Naval Postgraduate School Monterey, CA 93943-5000	1
4.	Commander Naval Air Systems Command Washington, D.C. 20360	1
5.	NASA Langley Research Center MS/1285 Technical Library Hampton, VA 23655	1
6.	NASA Ames Research Center Technical Library Moffet Field, CA 94035	1
7.	Prof. R.M. Howard Department of Aeronautics and Astronautics, Code AA/Ho Naval Postgraduate School Monterey, CA 93043-5000	2
8.	Mr. Benjy Neumann Naval Air Systems Command Aircraft Division--Research and Technology AIR 931K Washington, D.C. 20360	1